STUDIES ON FABRICATION OF CERMET FUELS AND INTERACTION WITH T91 CLADDING

By

SUDHIR MISHRA

ENGG01201004018

Bhabha Atomic Research Centre, Mumbai

A thesis submitted to the
Board of Studies in Engineering Sciences
In partial fulfillment of requirements
for the Degree of
DOCTOR OF PHILOSOPHY
of
HOMI BHABHA NATIONAL INSTITUTE

August, 2018

Homi Bhabha National Institute

Recommendations of the Viva Voce Committee

As members of the Viva Voce Committee, we certify that we have read the dissertation prepared by Sudhir Mishra entitled " Studies on Fabrication of Cermet Fuels and interaction with T91 cladding" and recommend that it may be accepted as fulfilling the thesis requirement for the award of Degree of Doctor of Philosophy.

Chairman - **Dr. Raghvendra Tewari** **Date:** 03/07/19

Guide / Convener – **Dr. Gautam Kumar Dey** Gautam Kumar Dey **Date:** 03/07/19

Co-guide - <Name> (if any) ----------------- **Date:**

Examiner – **Prof. Parag Bhargava** Parag Bhargava **Date:** 03/07/19

Member 1- **Dr. Ashok Arya** **Date:** 03/07/2019

Member 2- **Dr. Rajeev Kapoor** Rajeev Kapoor **Date:** 03/7/2019

Member 3- **Dr. Sanjib Majumdar** Sanjib Majumdar **Date:** 03/07/2019

Final approval and acceptance of this thesis is contingent upon the candidate's submission of the final copies of the thesis to HBNI.

I/We hereby certify that I/we have read this thesis prepared under my/our direction and recommend that it may be accepted as fulfilling the thesis requirement.

Date: 03/07/2019

Place: Mumbai

Gautam Kumar Dey

(Dr. Gautam Kumar Dey)

Guide

STATEMENT BY AUTHOR

This dissertation has been submitted in partial fulfillment of requirements for an advanced degree at Homi Bhabha National Institute (HBNI) and is deposited in the Library to be made available to borrowers under rules of the HBNI.

Brief quotations from this dissertation are allowable without special permission, provided that accurate acknowledgement of source is made. Requests for permission for extended quotation from or reproduction of this manuscript in whole or in part may be granted by the Competent Authority of HBNI when in his or her judgment the proposed use of the material is in the interests of scholarship. In all other instances, however, permission must be obtained from the author.

Sudhir Mishra

DECLARATION

I, hereby declare that the investigation presented in the thesis has been carried out by me. The work is original and has not been submitted earlier as a whole or in part for a degree / diploma at this or any other Institution / University.

Sudhir Mishra

List of Publications arising from the thesis

Journals

1. Cermet Fuel for fast reactor–Fabrication and Characterization, **Sudhir Mishra**, P.S. Kutty, T.R.G. Kutty, Shantanu Das, G.K. Dey, Arun Kumar, Journal of Nuclear Materials, **2013,** 442, 400-407.
2. Compatibility study between U-UO_2 Cermet fuel and T91 cladding, **Sudhir Mishra**, Santu Kaity, K.B. Khan, Pranesh Sengupta, G.K. Dey, Journal of Nuclear Materials, **2016**, 481, 1-12.
3. U-PuO_2, U-PuC, U-PuN Cermet Fuel for Fast Reactor, **Sudhir Mishra**, Santu Kaity, Joydipta Banerjee, Chiranjeet Nandi, G.K.Dey and K B Khan, Journal of Nuclear Materials, **2018,** 499, 272-283.

Conferences

1. Fabrication and Characterisation of Cermet Fuel for Fast Reactor , **Sudhir Mishra**, P.S. Kutty, T.R.G. Kutty, Rakesh Kumar, G.K. Dey & Arun Kumar, Published in proceedings of International conference on characterization and quality control of nuclear fuels, CQCNF-2012; Hyderabad (India); Feb 27-29 **2012**.
2. Studies on stability of U-UO_2/PuO_2 Cermet fuel for fast reactor and its interaction with T91 cladding, **Sudhir Mishra**, Santu Kaity, P.S. Kutty, G.K. Dey, Arun Kumar, G.J. Prasad, Published in the proceedings of Fast Reactor Fuel Cycle Conference, FR13; organised by IAEA in Paris, France, March 4-11, **2013.**

Sudhir Mishra

DEDICATIONS

To

All my Noble Gurus & Lord Krishna

Your right is to work only and never to the fruits thereof. Let not fruits
of actions motivate you to act Nor let your attachment be to inaction

Verse 2.47 from Bhagvad Gita

ACKNOWLEDGEMENTS

I sincerely thank my guide Prof. Gautam Kumar Dey, former Director Materials Group for his constant guidance and encouragement throughout this work. I am obliged to his whole hearted support and constructive suggestions. He has always given due priority to this Ph.D work despite his hectic schedule. He always kept a keen eye on the progress and quality of the work. I am deeply grateful to him for the discussions that helped me to sort out the technical details of my work.

I am extremely thankful to Shri H S Kamath, former Director of Nuclear Fuels Group for his valuable guidance and technical discussions at several occasions and his sincere involvement in reviewing the technical results of this work.

I would like to sincerely thank Shri Arun Kumar, former Director, Nuclear Fuels Group for providing consistent support for this work during his stay and constantly encouraging me to complete the work.

I would also like to express my sincere thanks to Shri Vivek Bhasin, Director Nuclear Fuels Group for his constant encouragement and extending help whenever required to his full capacity.

I extend my thanks and acknowledge the help and support of Dr. (Mrs) S.B. Roy, former Associate Director, Chemical Engineering Group for enabling the supply of uranium metal powder to carry out this research work

I am grateful to Dr. Deep Prakash, Head, Materials Characterization Section, Powder Metallurgy Division, for his painstaking effort in reviewing this thesis and for rendering valuable help. Technical discussions with him were highly beneficial in value addition of the thesis.

I am grateful to my doctoral committee, Chairman-Dr. Raghvendra Tewari and members- for their valuable suggestions for the progress of the research work at various Doctoral

Committee meetings. My sincere thanks are due to Dr Ashok Arya and Dr K B Khan for their valuable discussions and critical comments during course of this work.

I am truly thankful to all my team members of FBTR fuel fabrication section (FD&MS), PC&NS, QC&IS and FPES, Radiometallurgy Division for providing invaluable support during fabrication and property evaluation of fuel pellets. I sincerely acknowledge Mr. R.S. Prasad, ED&DD for providing me the necessary help and support of workshop. I also acknowledge the help extended by S/Shri Shailesh Katwankar and V P Jathar from Post Irradiation Examination Division for metallographic sample preparation.

It would be unjust if I merely acknowledge Mr. Santu Kaity, Dr. Joydipta Banerjee, Shri Chiranjit Nandi, Dr. Anupam Sarswat and Dr Pranesh Sengupta. They were always there and ready to help me whenever help was needed. I thank them from the bottom of my heart for providing me invaluable support during the entire course of this work.

I owe my sincere gratitude to my parents, Mrs Amarawati Devi and Late Shri Shyam Lagan Mishra for their constant encouragement to look forward and achieve set goal in life. It is because of them I could rise to this stage of life. They have always tried to inculcate noble virtues in me. I am thankful to my in-laws Shri J P Mishra and Mrs Lilawati Mishra for their constant encouragement during course of this work.

Last but not the least I owe a special distinction to my wife Mrs Prerna Mishra and my daughters Sudiksha and Riddhi. They stood behind me during my most difficult times and sacrificed many pleasurable moments. They had always been a source of happiness during course of writing this dissertation. I would like to place on record fruitful discussion I had with Prerna during course work which was a pre-requisite for PhD to start. Also thanks are due to her for valuable help in preparation of manuscript of the thesis. Thanks to all my family members for their best wishes.

CONTENTS

Page No.

ABSTRACT

Cermet is an emerging fuel concept for the fast nuclear reactor system and is ideally designed to combine beneficial properties of both ceramic and metal. (U, Pu)O_2 ceramic fuel is the well-established fuel for the fast reactors and (U, Pu, Zr) metallic fuel is the future fuel. Both the fuels have their own merits and demerits. Optimal solution may lie in opting for a cermet fuel which combines the favorable features of both fuel systems. Different cermet fuels which can be chosen for fast reactor application may be either Nat U- enriched UO_2 or Nat U- PuO_2, Nat U-PuC and Nat U-PuN. The above said cermet fuel is proposed to be encapsulated in Zr lined T91 steel cladding. T91 is ferritic martensitic steel comprising primarily of 9% Cr, 1% Mo and rest Fe.

The focus of the research has been to see (i) the feasibility of fabrication of U-UO_2/ U-PuO_2/U-PuC/U-PuN cermet by classical powder pellet route involving cold compaction & sintering and to study different thermo physical properties of the fuel (ii) to understand interaction between U-UO_2 fuel and T91 cladding with & without Zr lining and to evaluate performance of Zr as barrier layer between fuel & cladding.

U-UO_2 cermet has highest solidus temperature amongst all the cermets studied. Higher the solidus temperature more is the margin for safe operation of fuel. Out of the three cermets containing Pu bearing compound the U-PuN is found to be most stable and has higher solidus temperature. The thermal conductivity of the U-PuC cermet is monitored to be maximum because of presence of Pu_2C_3 besides PuC in ceramic phase .

In the compatibilty study it has been concluded that a Zr layer between fuel and cladding is a very safe option to protect fuel from clad interaction. Nevertheless without Zr, the fuel and cladding interaction is sluggish up to 923 K temperature which is very close to eutectic temperature. The slow reaction is because of presence of ceramic particle in the fuel matrix. The reaction becomes significant at a temperture 993 K and above.

SYNOPSIS

Cermet is an emerging fuel concept for the fast nuclear reactor system and is ideally designed to combine beneficial properties of both ceramic and metal. UO_2 & $(U,Pu)O_2$ mixed oxide (MOX) ceramic fuels have been used in various fast nuclear reactors world over and metallic (U,Pu,Zr) fuel is considered as the promising high breeding proliferation resistant fuel for the future fast nuclear reactors. The fuel cycle of MOX is well established. The advantages of the oxide fuel are its easy fabricability, good performance in the reactor and a well-established reprocessing technology. The drawbacks of MOX fuel are its low thermal conductivity and low heavy metal density resulting in a lower breeding ratio and higher doubling time. On the other hand, metallic fuel has been recognized as one of the candidate driver fuel for liquid-metal cooled fast reactor because of its inherently safe in-reactor performance and fuel cycle economics. In Fast Breeder Reactor (FBR), the basic thermal and neutronic performance of metallic fuels is better than oxide ceramic fuels. The harder spectrum in the metallic fuelled core results in high breeding ratio. Metallic fuel is considered for future FBRs due to its high thermal conductivity, high fissile and fertile atom densities, low doubling time etc. However, a few shortcomings of metallic fuels such as, low solidus temperature, high swelling rate and susceptibility to chemical and mechanical interaction with cladding materials prevent it from achieving its full potential. Metallic fuels possess some other set of challenges in the process of fabrication. Current method of fabrication of the fuel involves melting and casting technologies that are challenged by volatile loss of the material and low yield during production. Injection casting has been the preferred method for metal fuel fabrication for fast reactor fuels such as the driver fuel for Experimental Breeder Reactor (EBR-II) and the demonstration Integral Fast Reactor (IFR) fuel pins. There are material losses and alloy contamination issues that are inherent in the injection casting process, especially when the higher actinides such as Am are involved in the fuel system.

Some techniques are being developed which may overcome volatilization losses and injection casting may be effectively accomplished, but alternative processes are still under development.

At this juncture, cermet fuel combines advantages of both ceramics and metal. Cermet fuel is a type of dispersion fuel consisting of particles of ceramic fuel uniformly distributed in a metal matrix. Cermet nuclear fuels have significant potential to enhance fuel performance because of low internal fuel temperatures and low stored energy. A cermet fuel combines the optimal properties of a ceramic, such as high temperature resistance and high hardness, and those of a metal, which improves the composite's thermal conductivity and mechanical properties. Therefore, the optimal solution might be to design a novel cermet fuel which combines favorable features of both metallic and ceramic fuels.

Different types of cermet fuels which have been developed or used all over the world may be classified into three categories. They are (i) Cermets for use in research reactors containing matrices of either Al or Zirconium/Zircaloy. (ii) Inert matrix cermet for burning plutonium having matrix of Al or Zr suitable for light water reactors or Cr/Mo/W matrix for fast reactor application. (iii) U matrix U-PuO_2 cermet for use in fast reactors for power generation and breeding.

As a cermet fuel, UO_2 has been used primarily in stainless steel matrices and to a lesser extent in refractory metal. The higher oxides U_3O_8 has been tested exclusively in aluminum and has been used in various research reactors. Zirconium and Zircaloy based UO_2 cermet fuel is being used in naval reactors. Haertling etal have reviewed UO_2 dispersed in refractory metals. The most studied cermet has been W-UO_2 system. Other cermet system includes Mo-UO_2, W/Mo/Re alloys-UO_2 and Re-UO_2. Cermet fuel has been considered as advanced fuel for the light water reactors (LWRs). Vatulin etal. have worked extensively for the fabrication of this type of fuel. UO_2-Zr and UO_2-Al cermet fuel fabricated by traditional powder metallurgy route have been successfully tested in MIR research reactor in Russia. In order to dispose plutonium through inert matrix fuel (IMF), the development of cermet fuel with PuO_2-Zr composite was carried out in Russia. It was concluded that PuO_2-Zr cermet system could be considered as a possible variant of new cermet fuel for Pu burning in LWRs. The sub critical accelerator driven system (ADS) is now being considered as a potential means to burn long lived trans uranium nuclides. In European Commission, JRC, Germany, the proposed fuel for ADS is Mo-92 cermet where plutonium and minor actinides will be dispersed in molybdenum matrix. To improve the neutronic characteristics, enriched Mo-92 will be required.

Studies have been carried out on mono nitride fuel development for UN-Al and UN-Zr cermet systems by CERCA- France and the Institute for Transuranium Elements (ITU) Germany between 1985 and 1994. Stability of UN-Al and UN-Zr compounds was confirmed by thermodynamic calculations and out of pile experiments. UN-Al has high thermodynamic stability up to 500^{o}C and UN-Zr at temperatures up to 800^{o}C. UN interacts with matrix (Al or Zr) at higher temperature accompanied by phase transformations and swelling. It was concluded from the results of out-of-pile investigations that the compounds UN-Al and UN-Zr can be considered as candidates for cermet fuels for the use in research reactors. Cermet fuel rods with an inert metal matrix are now considered as a potential solution for plutonium burning. Cermet of the PuO_2-M type (where M stands for Al or Zr) and the PuN-M type (where M stands for V, Cr, and Mo, W) are the most attractive option for Pu utilization in LWRs and FRs, respectively. Al or Zr as matrix is suitable for LWR fuels because of their low thermal neutron absorption cross-sections. The eutectic temperatures are decisive parameters for the selection of the matrix metal or alloy. Cermet fuel is especially promising for reactor designs that require rapid power changes because of its anticipated capability to withstand thermal shock. Molybdenum-metal matrix, UN-fueled cermet has been studied as a fuel candidate for space reactor systems which has to produce variable power as per demand. A strong, relatively ductile, high thermal conductivity metal matrix is more likely to withstand the thermal shocks and stresses.

For British Proto type fast reactor (PFR) whose design began in year 1962 initially it was thought to have a rugged core of high burn up which would serve as test bed for advanced fuel elements. So the initial choice was cermet - a dispersion of $(U,Pu)O_2$, particles in stainless steel. Savchenko etal discuss about a new concept of Pu and minor actinides (MA) containing fuel for fast reactor. The U-PuO_2 fuel proposed is based on dispersion of PuO_2 particles in U or U alloy matrix. The high Uranium content fuel meat is metallurgically bonded to cladding and forms a heat conducting frame work.

As mentioned above, reports are available in literature regarding fabrication and irradiation of different cermet fuel all over the world. However, literature on cermet fuel, which will be useful for power generation as well as breeding in fast reactor, is available only in few numbers in the open literature and hence work regarding such fuel needs further investigation and development.

Different cermet fuels which can be chosen for fast reactor application may be either Nat U-enriched UO_2 or Nat U- PuO_2, Nat U-PuC and Nat U-PuN. The purpose of choosing U metal as matrix is to develop a fuel possessing high breeding ratio besides other beneficial properties of the metal.

The above said cermet fuel is proposed to be encapsulated in Zr lined T91 steel cladding. T91 is ferritic martensitic steel comprising primarily of 9% Cr, 1% Mo and rest Fe. T91 grade steel used in this study was in the standard normalized and tempered condition. Its hardness, measured using Vicker's hardness tester at a test load of 200g was 220 kg/mm^2. The heat treatment of T91 involves austenization at 1323 K and air quenching, followed by tempering at 1023 K for 1 h. The structural integrity of the fuel element is of paramount importance during operation of the nuclear reactors. During reactor operation, fuel comes in contact with the cladding which may result in interdiffusion of fuel and cladding components. A strength reducing zone may develop subsequently, leading to premature breach of the fuel element. Additionally low melting layers can form due to interdiffusion and affect the structural integrity of the fuel element.

So the focus of the research has been to see (i) the feasibility of fabrication of U-UO_2/ U-PuO_2/U-PuC/U-PuN cermet by classical powder pellet route which involves cold compaction followed by sintering & to establish a flow sheet for fuel fabrication and to study different thermo physical properties of the fuel (ii) to understand interaction between U-UO_2 fuel and T91 cladding with & without Zr lining and to evaluate performance of Zr as barrier layer between fuel & cladding.

The diffusion reaction at the interface was studied with the help of Scanning electron microscopy (SEM), Energy dispersive spectroscopy (EDS) and Electron probe microanalysis. From the composition profiles reaction zone thickness was calculated. The activation energy for growth of reaction layer was determined.

To fabricate different types of cermet fuels following steps were carried out.

1. Production of U metal powder

U metal powder produced by calciothermic reduction of UO_2 was used for fuel fabrication. This powder was received from one of the laboratories of Bhabha Atomic research Centre (BARC).

2. Production of ceramic powders viz. UO_2, PuO_2, PuC and PuN

Green UO_2 powder was received from Nuclear Fuel Complex (NFC), Hyderabad. Raw PuO_2 powder obtained through PUREX process and oxalate route was received from the fuel reprocessing plant, BARC. Sintered UO_2, PuO_2, PuC and PuN powders were produced from green UO_2 and PuO_2 powder by suitable processing. A brief description of the production process for cermet and different parameters maintained during production are mentioned below.

Uranium metal powder taken for the study was in the size range of 1 to 15 μm and was regular in morphology. UO_2 powder was prepared from UO_2 pellets which were sintered at 1650°C. These pellets were crushed in a jaw crusher and milled in an attritor. The powder was then sieved and powder of size < 75 microns were used for this study. The UO_2 powder obtained was irregular in shape. The O/M ratio of the UO_2 powder was found to be in the range of 2-2.015. Two compositions, namely U-15wt%UO_2 and U-30wt%UO_2 were made out of these powders. Uniform mixing of the powders was ensured by using a blender. Compaction was done at different pressure varying from 500 MPa to 1050 MPa using a double action hydraulic press at room temperature. Green pellets were sintered at 1348K for 8 hrs in argon atmosphere. One important concern in the handling of U metal powder is its pyrophorocity and oxidation when in contact with air. The oxidation of the powder could change the sintering behavior of the compact. Hence handling of the powder was carried out in protective atmosphere. Dynamic flow of the argon gas was maintained inside the glove-box during the entire process of fabrication. O_2 and H_2O level in the glove box was maintained below 10 ppm.

Sintered PuO_2 powder was produced by suitable heat treatment of green PuO_2 powder. PuC powder was prepared by carbothermic reduction of PuO_2 by C. During preparation of PuC powder Pu_2C_3 phase was also formed as seen from the XRD pattern. However for simplicity we have mentioned this powder as PuC throughout the manuscript.

PuN was prepared by carbonitridation method. A charge combining PuO_2 and C was homogenized in a stirred ball mill. The proportion of the PuO_2 and C was decided by following chemical equation

$$PuO_2 + 2C + 0.5\ N_2 \leftrightarrow PuN + 2CO\uparrow \qquad (2)$$

The quantity of C was taken 1.1 times the stoichiometric value to ensure complete reduction of PuO_2. The compacts prepared out of the mixed powder were heated at 1773 K in presence of N_2 atmosphere for 15 h, followed by 4 h soak in presence of N_2+H_2 atmosphere. Nitrogen plays the dual role of a reactant and carrier gas for removal of CO. The clinkers obtained were crushed and milled. The milled powder was sieved to obtain powder particle size below 75 μm. XRD on powder was carried out to understand different phases present.

PuC, PuN powders are very much prone to oxidation and pyrophoric in nature. Hence handling of the powder was carried out in dry boxes filled with protective Ar atmosphere. PuO_2, PuC and PuN powders were mixed with U in three different proportions namely 15, 20 and 25 wt. %. Uniform mixing of the powders was ensured using a blender. Compaction was done at different pressures varying from 500 MPa to 1050 MPa using a double action hydraulic press. Sintering of the green pellets was carried out in high purity argon atmosphere at 1223 K for 8 hrs. Characterisations of all the fuels have been carried out using Dilatometer, Differential Thermal Analyser, X-ray diffractometer, and Scanning Electron microscopy.

Next part of the work was to study compatibility between cermet fuel and T91 cladding. The compacts of U-15%UO_2 (hereafter referred as U-15%UO_2) were cut into 5 mm thick discs. The typical diameter of the sintered cermet compact was about 6.80 mm. T91 steel rod of the same diameter was also cut into discs of about 0.5 mm thickness. The surfaces of all these discs were metallographically polished to 1 μm surface finish. Two types of diffusion couples were prepared as described below:

a) Couples between U-UO_2 and T91 discs with a Zr foil of thickness ~100 μm in between them, referred to as U-UO_2/Zr/T91 couples, and

b) Couples between U-UO_2 and T91 discs without a Zr foil in between, referred to as U-UO_2/T91 couples.

The components of the diffusion couples were kept in fixtures made of Inconel 600, to ensure intimate contact during annealing. A Ta foil was used to prevent any chemical reaction between couples and fixture. The fixtures containing these couples were encapsulated in quartz tubes. Each quartz capsule was evacuated and flushed with helium several times before it was sealed and then annealed in a resistance heating furnace. U-UO_2/T91 couples were maintained at temperatures 923K, 973K, 993K, 1023K , 1073K for 1000 h and at temperature 1223 K for 50 h. U-UO_2/Zr/T91 couples were annealed in a resistance heating furnace maintained at 1023 K and 1073 K for durations up to 1000 h and at temperature 1248K for 50 h. Subsequently their microstructures were examined using Scanning electron microscope (SEM), X-ray, Energy dispersive spectroscope (EDS) and Electron probe microanalyser (EPMA).

Uranium metal powders have poor compressibility and sinterability. The metal powder used in the present study had a narrow size distribution (1-15μm). The narrow size distribution, higher inter-particle friction and work hardening of the metal powder results in the necessity of high compaction pressure for obtaining good quality green pellets. Oleic acid was used as die wall lubricant to take care of friction between die wall and powder particles. It has been reported that the Uranium compact requires about 85% of the melting temperature for densification to start. In comparison to the densification temperature of U, metals like Zr, Ni start shrinking at a temperature around 45% of their melting temperatures while Th begins to shrink at temperature 65% of its melting temperature. It was observed in the present study that the shrinkage of cermet initiates above 1125 K, which is about 80% of the solidus temperature of the cermet. This is high sintering temperature when compared to melting temperature of the U metal. This may be because of phase changes associated with U metal in the fuel matrix. Solidus temperature of the U-15wt%UO_2 cermet fuel is around 1370 K, as observed from the DTA experiment. This shows that the fuel has high solidus temperature which is favourable for higher in-reactor operating temperature of the fuel.

Thermal conductivity for U-UO_2 cermet was measured by Transient Plane Source (TPS) method. It is observed that thermal conductivity increases with increase in temperature. With increase in temperature the thermal conductivity of UO_2 falls downwards whereas that of Uranium, increases. In the present case increase in themal conductivity of cermet is due to the higher contribution of U to the overall thermal conductivity at higher temperatures.

The interaction between U and UO_2 interface is not revealed in SEM examination. This may be due to the presence of sintered UO_2 particle having O/M ratio near 2.0 and heat treatment in an inert argon atmosphere which probably rules out the possibility of formation of UO_2 oxides with higher O/M ratios. Decrease in the O/M ratio below 2.0 and release of oxygen may happen at a higher temperature like 1900K in vacuum but that condition does not exist in the present case. Porosities are observed inside UO_2 phase as well as in the inter particle region between U and UO_2 phase. The available porosities in the fuel matrix act as site for the entrapment of fission products, resulting in lower damage of the fuel matrix by fission products accumulation and lower swelling as compared to metallic fuel.

In case of U-PuO_2/PuC/PuN cermet it is observed that for the same compaction pressure, green density in terms of %TD is maximum for U matrix PuN cermet. This is because density of PuN is higher compared to other Pu compounds. Further the sintered density in terms of %TD of U-PuN cermet is also observed high. On the other side green density (%TD) as well as sintered density (%TD) of U-PuO_2 is minimum amongst all. On investigation it was established that during heat treatment of PuO_2 powder, Pu_4O_7 phase has formed. After sintering of U-20wt%PuO_2 cermet presence of Pu_2O_3 and PuO_{2-X} phases are observed as confirmed from the XRD pattern. Pu_2O_3 compound has lower density as compared to PuO_2 and its (Pu_2O_3) presence along with the latter results in higher overall volume of the pellet leading to lowering of final density of the compact. In ΔG° vs. T diagram UO_2 line lies below PuO_2 formation line which means UO_2 is more stable compared to PuO_2. So the formation of more stable UO_2 by U after accepting O_2 from Pu compound further results in volume increase. Since UO_2 is less dense compared to PuO_2 it will subsequently decrease the density of U-PuO_2 cermet. This could be the reason for lower density observed for U-PuO_2 cermet as compared to the other two compositions.

It is observed from the DTA studies that there is drop in phase transformation (α to β and β to γ) temperature of U based cermet fuel compared to pure U metal. The explanation for this change is mentioned in subsequent sentences. Compounds of Uranium namely UO_2, UC, UN are more stable than compounds of Plutonium like PuO_2, PuC, PuN. Hence, thermodynamically, it is possible that Pu compounds may get reduced by U to form metallic Pu at high temperature. Subsequently, combination of free Pu, thus formed, with surrounding U may result in formation of (U,Pu) alloy at locations where ceramic particles are present. Thus formation of alloy will lead to a drop in phase transformation temperature as well as a reduction in solidus temperature of the fuel.

It is monitored form DTA studies that phase transformation of cermets shifts towards lower value with increase of % Pu in dispersoids. This could be because Pu dispersoids containing high % of Pu may release more Pu after reduction alloying with U resulting in lower solidus temperature. However when we compare for solidus and other phase transformation temperatures of U-PuO_2, U-PuC and U-PuN of similar composition, it is observed that maximum decrease is in case of PuC dispersed cermet and is least for PuN dispersed cermet. Thermodynamically, PuN is the most stable compound amongst the three Pu compounds studied. Solidus temperature of the U-20wt%PuN is highest amongst the three type of cermet studied. It is around 1350K, as observed from the DTA plot. The designers prefer a fuel that has the highest solidus temperature and therefore U-20%PuN is attractive.

Thermal conductivity of U-20%PuC and U-20% PuO_2 are the highest and lowest respectively among the cermets investigated in this study. One of the important factors for higher contribution of U-20%PuC cermet towards thermal conductivity is the presence of almost 50 % Pu_2C_3 in the ceramic phase. The specific heat of Pu_2C_3 is more than double that of PuC which effectively increases overall thermal conductivity of U-20%PuC cermet. PuO_2 has poor thermal conductivity as compared to PuC and PuN for all temperature range and also it decreases with increase in temperature. Therefore U matrix PuO_2 cermet shows the lowest thermal conductivity. Thermal conductivity values of U-PuO_2, U-PuC, U-PuN as determined in this study are 9 W/m K, 18 W/m K and 25 W/m K respectively. Thermal conductivity of PuC and PuN is almost same at 873 K being 13 W/m K where as thermal conductivity of PuO_2 is 2.47 W/m K at the same temperature, which is very low compared to PuC and PuN .On the other hand thermal conductivity of pure U is 38 W/m K at the same temperature. The addition of PuO_2 in U matrix results in lowering of thermal conductivity of cermet. However it is observed that thermal conductivity of U-20 wt.% PuO_2 increases with increase in temperature. This is due to contribution of U to the overall thermal conductivity at higher temperatures. Higher thermal conductivity is beneficial as it results in a low centerline operating temperature of the fuel at a higher linear power rating.

In the compatibility studies, the results of U-15%UO_2/T91 diffusion couple annealed at 923 K and 973 K indicate that there is discrete development of $U(Fe,Cr)_2$ intermetallic phase along the interface after 1000 h of annealing. A maximum of 3 μm width of diffusion layer is observed at 923 K. However the thickness of the dffusion layer increased up to 5 and 9 μm with increase in annealing tempertaure to 973 K and 993 K respectively. No distinct reaction zone was observed for the couples annealed up to 993 K .

For the diffusion couple annealed at 1023 K development of a distinct reaction zone is observed at the interface. Further it is also observed that there is removal of U from the region close to the fuel leading to a U lean zone along the interface. However, U metal away from the interface has not taken part in the diffusion reaction. This may be due to the reduced area of contact between U and Fe in the U-UO_2/T91 diffusion couple and sluggish diffusion reaction between U and Fe in presence of UO_2. The thickness of reaction zone is around 30 μm. From microstructural analysis by SEM and elemental analysis by EDS it was estimated that two different type of phases are present in the reaction zone. The results are in agreement with existence of phases acoording to U-Fe phase diagram .

The thickness of the reaction layer at fuel-T91 interface increased significantly when the annealing temperature is increased from 1023 K to 1073 K for the same annealing time. It can be infered that rate of interdiffusion is very much dependent on temperature and increases effectively with the rise in temperature. The higher rate of diffusion at the interface at 1073 K may also be attributed to formation of solid solution between U and Fe over a wide range of composition. The microstrucure of the diffusion couple shows development of a distinct bright reaction zone of 300 μm. U apparently diffuses out from the fuel and reacts with the constituents of T91. In general, the diffusion layers formed in the couples correspond to those dictated mainly by the interaction of U with Fe.

When the annealing temperature is increased to 1223 K eutectic microstructure is observed and it is different from the microstructure formed at lower temperature. At higher temperature, the kinetics of interdiffusion of both U and Fe becomes higher, leading to eutectic melting in lesser time.

The microstructural analysis of U-15%UO_2/Zr/T91diffusion couples revealed an excellent bond formation at both the U-15%UO2/Zr and Zr/T91 interfaces after annealing at 1023 K. The microstructure of U-15%UO2/Zr/T91 diffusion couple shows that there is no significant diffusion of U into 100 μm thick Zr barrier layer. Further, no eutectic melting between U-15%UO2/Zr and Zr/T91 interface is observed. The formation of any intermetallic compound is not observed at the Zr/T91 interface. It is also evident from U, Zr, Fe and Cr , X-ray mapping that, there is no penetration of U in Zr metal as well as that of Zr in T91. Similar results were observed at 1073 K. At 1248 K eutectic microstructure was observed.

To summerise it can be noted that feasibility of fabrication of cermet by powder pellet route has been established. Uranium sinterability was observed to be poor. Maximum density of the sintered pellet that could be achieved was 80% TD. Nevertheless this density is acceptable for fast reactor application as the smear density required for such use is around 70-75% TD. U-UO_2 cermet has highest solidus temperature amongst all the cermets studied. Higher the solidus temperature more is the margin for safe operation of fuel. Out of the three cermets containing Pu bearing compound the U-PuN is found to be most stable and has higher solidus temperature. The thermal conductivity of the U-PuC cermet is monitored to be maximum because of presence of Pu_2C_3 besides PuC in ceramic phase . The fuel with higher thermal conductvity turns out to be the designer's choice for use in the reactor. The coffecient of thermal expansion is high for all the cermets studied and comparable to U-20%Pu-10%Zr metallic fuel which makes the fuel inherently safe because of negative reactivity coefficient.

In the compatibilty study it has been concluded that a Zr layer between fuel and cladding is a very safe option to protect fuel from clad interaction. Nevertheless without Zr the fuel and cladding reaction is sluggish up to 993 K temperature which is very close to eutectic because of presence of ceramic particle in the fuel matrix. The reaction becomes significant at temperture above 993 K.

LIST OF FIGURES

Page No.

LIST OF TABLES

Page No.

LIST OF SYMBOLS & ABBREVIATIONS

α decay	Alpha decay
β-decay	Beta decay
γ-decay	Gamma decay
α-uranium	Allotrope of uranium from Room Temperature to 668°C
β-uranium	Allotrope of uranium from 668 °C to 775 °C
γ- **uranium**	High temperature allotrope of uranium from775°C to 1132°0C
ADS	Accelerator Driven System
Al	Aluminium
BSE	Back Scattered Electron
C	Carbon
Cr	Chromium
DAC	Derived Air Concentration
DFMF	Demonstration Facility for Metallic Fuel
DTA	Differential Thermal Analyser
EDS	Energy Dispersive Spectroscopy
EPMA	Electron Probe Microanalyser
EBR	Experimental Breeder Reactor
FBR	Fast Breeder Reactor
FBTR	Fast Breeder Test Reactor
Fe	Iron
FR	Fast Reactor
ΔG°	Standard Free Energy Change
h	Hour

% ha	Percentage Heavy Atom
H	Hydrogen
IFR	Integral Fast Rector
IMF	Inert Matrix Fuel
LWR	Light Water Reactor
MA	Minor Actinides
MC	Mixed Carbide
MeV	Mega Electron Volt
MN	Mixed Nitride
µm	Micron Meter
MOX	Mixed Oxide
MPa	Mega Pascal
MWth	Megawatt thermal
MWe	Megawatt electrical
N	Nitrogen
Ni	Nickel
NFC	Nuclear Fuel Complex
PHWR	Pressurised Heavy Water Reactor
PPM	Parts per million
PFR	Proto type Fast Reactor
O/M	Oxygen to Metal ratio
Pu	Plutonium
PuO_2	Plutonium Oxide
Pu_2O_3	Di Plutonium trioxide
PuC	Plutonium Carbide

Pu_2C_3	Di Plutonium tricarbide
PuN	Plutonium Nitride
PUREX	Plutonium Uranium Redox Extraction
SEM	Scanning Electron Microscopy
TD	Theoretical Density
U	Uranium
UO_2	Uranium Oxide
UC	Uranium Carbide
UN	Uranium Nitride
V	Vanadium
W	Tungsten
W/m	Watt per meter
Wt.%	Weight percent
XRD	Xray Diffraction
Zr	Zirconium

1. CHAPTER 1. INTRODUCTION

1.1 Nuclear Reactor

A nuclear reactor is source of energy produced by sustained fission chain reaction of elements like uranium and plutonium. The first sustained fission chain reaction was demonstrated by Enrico Fermi and his team in year 1942 in the world's first nuclear reactor Chicago Pile-1 [1]. Uranium was used as fuel, graphite as moderator and Cadmium metal rods were used to control the reaction. Thus the world entered the nuclear age on December 2, 1942 [1, 2]. A single atom of U^{235} produces 200 MeV of energy under fission. The energy produced by one kg of Uranium is about 20 tera joules (2×10^{13} joules), which is equivalent to as much energy as $1.5x10^{3}$ tons of coal [3]. However fertile isotopes like U^{238} present in natural uranium and Th^{232} alone cannot sustain chain reaction. They need to be converted to fissile isotopes by neutron absorption. On December 20, 1951 the first reactor to produce power was Experimental Breeder Reactor-1(EBR-1) at IDAHO, USA [4]. But the nuclear power on commercial scale could be produced from Shipping Port Reactor at Pennsylvania in year 1957 [5]. The nuclear reactors are also used for production of radio isotopes, testing of nuclear fuel and structural materials, nuclear physics studies etc. Such reactors are known as Research reactors. Broadly nuclear reactors are classified in to two categories namely Power reactors and Research reactors. Power reactors are further classified into Fast neutron reactors and Thermal neutron reactors. They are popularly known as fast reactor and thermal reactors.

1.1.1 Fast reactor

A fast reactor is a nuclear reactor which uses fast neutrons to sustain fission chain reaction. Fast neutrons of energy nearly 1 MeV are responsible for sustained fission reaction in such reactors. Liquid metal is used as coolant but moderator is undesirable. Excess of fast neutrons are produced in fast reactor unlike thermal reactors. The fuel used in the fast reactor has high enrichment compared to that needed for the thermal reactor [6]. They have compact core and high power density. When fast reactors are designed to generate more fissile material than they consume, they are known as Fast breeder reactors (FBRs). Fast rectors also act as burner for actinides produced from conventional thermal reactors [7].

The share of nuclear power generation in total power produced can be significant only when breeding of fissile material takes place. This is possible in the fast reactors. This would extend the uranium resource appreciably. To begin with the purpose of the fast reactor deployment was to burn Uranium more efficiently and extend the U resources. Natural U containing 0.7% U^{235} is being used by light water reactors. Rest 99.3% of natural U mostly contains U^{238} which can be used by fast breeder reactors to produce fissile material Pu^{239}. In thermal reactors U is utilized less than 1% for production of power. The generation of radioactive waste reduces in fast reactor because not only minor actinides are produced in lower rate due to lower capture to fission but are also consumed through fission [8]. In fast reactor with thorium loaded as blanket material, U^{233} along with low U^{232} is produced as compared to thermal reactor. However during operation of fast reactors several technical and material problems were encountered and also conclusion was drawn from the geological exploration that Uranium scarcity may not be an issue in future for a long time. Because of these reasons Fast reactors could not compete with the existing light water reactors. All over the world operating experiences for fast reactor exists for more than 400 reactor years. Table 1.1 and 1.2 show details of different fast reactor operating currently in different parts of world and planned for future operation respectively.

Table 1.1 . Fast neutron reactors in operation/ going to start in near future [9]

Reactor	Type	Coolant	Power (MW) thermal/electrical	Fuel	Country	Year
BOR-60	Experimental loop	Sodium	55/10	Oxide	Russia	1969
BN-600	Prototype pool	Sodium	1470/600	Oxide	Russia	1980
BN-800	Experimental pool	Sodium	2100/864	Oxide	Russia	2014
FBTR	Experimental pool	Sodium	40/18	Oxide, carbide, (Metal)-Future Fuel	India	1985
PFBR	Prototype pool	Sodium	1250/500	Oxide	India	2021
CEFR	Experimental pool	Sodium	65/20	Oxide	China	2010
JOYO	Experimental loop	Sodium	140/-	Oxide	Japan	1978-2007 May restart 2021

Table 1.2. Planned fast neutron reactors [9]

Reactor	Type	Coolant	Power (MW) thermal/electrical	Fuel	Country	Year
PRISM	Prototype pool	Sodium	840/311	Metal	USA	From 2020
ACR-100	Prototype pool	Sodium	260/100	Metal	USA	Working with GEH
Astrid	Prototype pool	Sodium	1500/600	Oxide	France with Japan	About 2030
Allegro	Experimental loop	Gas	50	Oxide	France	About 2025
MYRRHA	Experimental	Lead-Bismuth	57	Oxide	Belgium with China	Early 2020s
AlFRED	Prototype	Lead	300/120	Oxide	Romania with Italy and EU	From 2025
BN-1200	Commercial Pool	Sodium	2800/1220	Oxide/Nitride	Russia	From mid 2020s
Breast-300	Prototype loop	Lead	700/300	Nitride	Russia	From 2020
SVBR-100	Prototype Pool	Lead-Bismuth	280/100	Oxide	Russia	From 2019
MBIR	Experimental loop	Sodium (Lead-Bismuth)	150	Oxide	Russia	From 2019
CDFR-1000	Prototype Pool	Sodium	/1000	Oxide	China	From 2023
CDFBR-1200	Commercial, Pool	Sodium	/1200	Metal	China	From 2028
PGSFR	Prototype Pool	Sodium	/150	Metal	South Korea	From 2028
FBR	Prototype Pool	Sodium	/600	Oxide	India	Beyond2025

1.1.2 Importance of Fast reactor in India

Nuclear energy has a significant role to play in the contribution of the ever growing power requirement of our country. Department of Atomic Energy has the mandate for contributing in providing energy security to the nation. India is pursuing the three stage nuclear power programme based on its scantily available Uranium and abundantly present Thorium[10].

The first stage of programme envisaged to use natural Uranium has been realised by operating Pressurised Heavy Water reactors (PHWRs) [11]. The second stage of the programme is to deploy fast reactors where Pu obtained from reprocessing plant [12] will be used as fuel along with U^{238} for power production besides breeding Pu in the reactor and conversion of thorium into U^{233}. Eventually when enough of U^{233} is generated the reactor can operate with the U^{233}–thorium MOX fuel in the third stage of India's nuclear programme [13]. India embarked on its second stage programme with the successful operation of a research reactor named Fast Breeder Test Reactor (FBTR) [14]. The successful operation of FBTR for all these years has given impetus to design Prototype Fast Breeder Reactor (PFBR) [15]. This has been possible because of development of enabling technologies in India. Now PFBR is in advance stage of commissioning [16]. The construction of 6 FBRs of 600 MWe capacity (FBR 1 to 6) will be launched in the next 15 years [17]. Life extension of the existing test reactor (FBTR), design and construction of another test reactor, FBTR-II fuelled by oxide/metallic fuel is also proposed. The fresh metallic fuel for FBTR-II will be fabricated by expanding Demonstration Facility for Metallic Fuel (DFMF) at Kalpakkam. The studies for development of high breeding fuels i.e. metallic fuels, cermet fuels for future fast reactors and establishment of the optimum reprocessing route e.g. pyro-chemical/aqueous route will be carried out.

1.2 Different types of Fuel for Fast reactor

Different types of fuel considered for use in fast reactor are as follows

- Enriched UO_2 (Oxide fuel)/ $(U,Pu)O_2$ (Mixed Oxide fuel or MOX fuel)
- (U,Pu)C ,(Mixed Carbide or MC)/ (U,Pu)N ,(Mixed Nitride, MN)
- Metallic fuel

1.2.1 Oxide /Mixed Oxide fuel

Oxide fuels are one of the most popular choices for fast reactor fuel systems [18]. Oxide fuel which have been used in fast reactors include enriched UO_2 and $(U, Pu)O_2$ mixed oxide. These fuel have excellent burn up potential and high melting points [19]. The fabrication flow sheet of these fuels is easy to follow and their reprocessing is also well established. Thus a proven fuel cycle option and large experience of fuel irradiation for power production makes this fuel very attractive.

The first recorded use of Oxide fuel in fast reactor was in Soviet BR-5 reactor [20]. The core was loaded with PuO_2 fuel and the reactor was made critical in year 1959. The reactor saw burn up of 5 % ha. There were numerous element failures. Rapsodie, a 20 MWt reactor built in France used $(U, Pu)O_2$ fuel as its driver fuel. The reactor was made critical with oxide fuel in year 1966. Though the first choice of this reactor was metal fuel but it was rejected because of inherent swelling issues associated with metal fuel. Mixed carbide fuel was also considered for use in this reactor but because of unavailability of sufficient irradiation experience of this fuel this choice also could not be finalized. US built 20 MWth reactor, SEFOR was operated with MOX fuel. BOR-60 a test bed for large reactors, developed by former USSR used 90% enriched UO_2 pellets as its fuel. The reactor started operating in year 1969. The other facilities where MOX fuel has been used are Fast Flux Test Facility (FFTF) USA [21], PHENIX reactor in France and Proto type fast reactor (PFR) in UK etc.

In the seventies development of MOX fuel for the FBTR (Fast Breeder Test Reactor), was initiated in India. The initial fuel considered for the FBTR was MOX fuel. The composition of the fuel was (0.3Pu, 0.7U)O_2 where UO_2 was enriched to 85%. Natural UO_2 with PuO_2 was used for developing the fabrication flow-sheet for this fuel. Subsequently due to non-availability of enriched UO_2 this fuel composition was abandoned. Afterwards, development of a new fuel with composition 76% PuO_2 with natural UO_2 was taken up. However, this fuel composition was also not pursued intensely because initial results showed incompatibility with the liquid coolant sodium and low thermal conductivity. Later with compatibility studies it was established that PuO_2 up to 44% composition in MOX has no compatibility issue with sodium [22]. Indian Prototype Fast Breeder reactor (PFBR) is supposed to be loaded with MOX fuel with two composition namely $(U_{0.79},Pu_{0.21})O_2$ and $(U_{0.72},Pu_{0.28})O_2$ [23].

1.2.2 Mixed Carbide/Mixed Nitride

Mixed uranium plutonium monocarbide (MC) and mononitride (MN) are considered as advance fuel for fast reactor [18, 24]. These fuels possess high heavy metal density, high breeding ratio, low doubling time, high thermal conductivity and excellent chemical compatibility with sodium coolant [25, 26]. Their crystal structure is closed packed NaCl type. They can be operated at higher linear power rating and high specific power compared to oxide fuel. The use of carbide and nitride fuel is not very common like oxide fuel in fast reactor. The first recorded use of carbide fuel was in BR-5 fast reactor in Soviet in the year 1965 [20]. The fuel was UC in the Na bonded SS pin. Large number of helium and Na bonded MC and MN pins were irradiated in Experimental Breeder reactor (EBR-II) [27], USA, the Dounreay Fast Reactor (DFR) [28] UK, Rapsodie, France [29] ,BOR-60, U.S.S.R [30] and JMTR, Japan [31]. In these reactors MC and MN fuel with different cladding materials have been satisfactorily tested for more than 10% ha. Fission gas release was observed to be around 30% for this burn up but at higher burn ups (>15% ha) the release exceeded 50%. The swelling rate remains high in case of MC and MN fuel because of their closed packed NaCl type of structure. So these fuels demand enough porosities /pellet clad gap to accommodate swelling. However this leads to decrease in thermal conductivity and hence Na bonded MC and MN fuel element is better choice for utilizing the full potential of the fuel.

The nitride fuel has its own advantages over carbide fuel. It is less susceptible to oxidation & hydrolysis and added advantage of easy dissolution [32]. Russians have planned to use nitride fuel in their fast reactor BN-1200 with sodium coolant and in BREST-300 with lead coolant. Mixed (U, Pu) C is being used as driver fuel for fast Breeder test Reactor (FBTR) in India. It is the only reactor in the world which uses Plutonium rich mixed carbide fuel as driver fuel and is operating since 1985 [23, 24]. Post irradiation examination of FBTR fuel pins has been carried out at burn ups 2.5, 5.0, 10 & 15.5 % ha. The peak power before discharge at these burn ups was 320, 320, 400 & 400 W/cm respectively. After 2.5 & 5.0 % ha burn up it was observed that there was no fuel clad mechanical interaction (FCMI), negligible wrapper and cladding strain and lower fuel swelling rate [33]. At 10% ha burn up it was observed that FCMI has initiated, significant increase in dimension of cladding and wrapper has occurred but margin was available for wrapper dilation for fuel handling. Sufficient strength and residual ductility was measured in the cladding and wrapper material. After 15.5 % ha burn up it was observed that the gap between pellet and clad has closed throughout the length of the pin [34]. Higher rate of increase in cladding and wrapper dimension has occurred besides substantial decrease in strength and ductility.

1.2.3 Metallic Fuel

The metallic fuel was the first choice for the fast reactor. Initial fast reactors were constructed during 1945-1960 time period and these reactors were operated with metallic fuel. In US early reactors which operated with metal fuel include Clementine, LAMPRE-I, and LAMPRE-II developed by Los Alamos Scientific Laboratory, EBR-I and EBR-II developed by Argonne National Laboratory, and Fermi, originally developed by Atomic Power

Development Associates [4]. Dounreay fast reactor (DFR) was developed in UK by United Kingdom Atomic Energy Authority during the same period [20, 35]. Work on metallic fuel was also performed to some extent in Russian Federation.

The metal fuel has the advantages of high thermal conductivity, higher metal density and higher breeding potential. The higher coefficient of linear expansion has big advantage from the safety consideration [36, 37]**.** Because of higher metal density it offers highest breeding ratio and shortest doubling time. Cast delta stabilised plutonium alloy clad in mild steel was used as fuel in the first fast reactor Clementine. The LAMPRE-I (1961–1963) reactor was fueled with molten Pu–Fe alloy. The Enrico Fermi Reactor (Fermi I) in Michigan (1963–1972) was fueled with a U–Mo alloy [38]. Metal fuels used in EBR-I consisted of unalloyed U and U–Zr and Pu–Al alloys .The first core of EBR-1 was fueled with stainless-steel-clad highly enriched (93%) U and breeding was demonstrated in this reactor [39]. U-Fissium alloy fuel was first used as driver fuel in EBR-II [38, 40]. Fissium is an alloy which approximates equilibrium mixture of metallic fission product elements left over by pyro metallurgical recycling designed for EBR-II. It consists of 2.5 wt.% Molybdenum, 1.9 wt.% Ruthenium, 0.3 wt.% Rhodium, 0.2 wt.% Palladium, 0.1 wt. % Zirconium, and 0.01 wt. % Niobium. The first metallic fuel U-5% Fissium alloy which was loaded in the EBR-II reactor had high smear density (85 to 100%) and no plenum to collect fission gas. This fuel failed at very low burn up of 3 ha% because of high swelling of the fuel due to fission product accumulation. Later U-Zr binary alloys and U–Pu–Zr ternary alloys were also used as driver fuel or proposed for driver fuel use and irradiated in EBR-II. More than 120000 fuel rods have been irradiated in EBR-II.[41, 42]. The metal fuel was developed for the BN-350 reactor in Russian Federation. The alloy U-1.5 wt. % Mo + 0.1 wt. % Sn + 0.1 wt. % Al was used as fuel. The burn up of U core was up to 1.5% ha [43]. Under irradiation the metal fuel behaves like a plastic material and the fission gases directly exert pressure on the cladding if there is no free volume to accommodate the swelling. This was the cause of the failure for high smear density fuel initially loaded in the EBR-II reactor. Smear density is calculated by dividing the mass of fuel (including any non-gaseous fission products) in a unit length of pin by the theoretical mass of a unit length of void less fuel of the same composition, with diameter equal to the inside diameter of the cladding. So this was not chosen as the main line fuel as ability of clad material to withstand high burn up conditions could not be demonstrated [44]. The research programme to improve the performance of the metallic fuel was mainly carried out in USA. The aim was to design for the optimum fuel clad gap so that fuel gets sufficient space for swelling and becomes porous for the fission gases to get out of the fuel by inter connecting porosity. Accordingly fuel pin with smear density of 75% and sufficient plenum space was fabricated and loaded as driver fuel in EBR-II reactor, the composition remaining exactly same. This time the fuel could be operated up to 8% ha [35]. The swelling accommodation was also tried by introducing central hole in the fuel rod. The tests containing U-20%Pu-10 %Zr alloy fuel could start only in year 1985 for the Integrated Fast Reactor (IFR). The addition of Zirconium results in better chemical compatibility of fuel and the clad by reducing the inter diffusion of clad and fuel components. Irradiation testing of U-Pu-Zr alloy has been done in USA in EBR-II whose first driver fuel was U-Fissium alloy [45].

Reprocessing of the metallic fuel can be done by PUREX process or by pyro metallurgical method which involves electro-refining [46]. Pu, U, minor actinides and residual fission products get deposited on the cathode. This product on cathode can be used for fuel fabrication. This route of fabrication has its own advantages. As pure fissile material is not freely available so it makes fuel proliferation resistant. Because of the recycling of minor actinides the waste decay period to background reduces to 100 years compared to million years otherwise. Development of pyro metallurgical process is continuing in countries like Japan [47], USA, and Russia etc. India has also started study of this process.

Recently metallic fuel has been chosen by India for further development and intensive investigation [23]. Plutonium bearing fuel is considered to be the best fuel for the fast reactor. India has scanty resources of uranium so sustenance of its fast reactor programme to breed more plutonium and in turn generate more power becomes necessity. At present fast reactors have been planned to run on mixed oxide fuel but in long run the shift towards metallic fuel is desirable. In this regard already work on development of metallic fuel has been started. Option is to go for either mechanically bonded binary U-Pu alloy with Zr lined T91 cladding or Na bonded U-Pu-Zr ternary alloy [17].

1.3 Issues related to different fuels

The oxide fuel has lower thermal conductivity that leads to fuel restructuring and enhanced swelling [48]. It has low fissile atom density, two moderating atoms for each metal atom and reduced compatibility with sodium [49]. This results in a lower breeding ratio and higher doubling time.

There are several issues associated with fabrication of (U, Pu),C and (U, Pu) N fuel. The cost of fabrication is high and also large numbers of fabrication steps are needed. They are pyrophoric in nature and highly susceptible to hydrolysis, hence fabrication of these fuels requires inert gas environment with oxygen and moisture maintained below 25 ppm inside glove-box [24, 50]. Stringent control of carbon stoichiometry has to done to avoid formation of metallic phase and keep higher carbides within tolerable limit. Carbide fuels are generally fabricated with M_2C_3 content in the range of 10-20 % in order to avoid presence of metallic phase during fabrication and to take care of burn up related metal phase generation. Unlike oxide fuel where O/M ratio increases with burn up, in carbide fuel C/M reduces with burn up and thus there is likely hood of metal phase formation. The presence of metal phase may lead to low temperature eutectic formation with clad constituents causing clad failure. Higher limit of M_2C_3 is kept to avoid clad carburization and to avoid making the fuel more creep resistant [51].

Large scale reprocessing of the irradiated carbide and nitride fuels has not been well established. The disadvantage of MN fuel is presence of N^{14} content in the fuel which has a high parasitic neutron absorption cross-section. C^{14} gets generated during irradiation which emits β radiation and therefore not acceptable for release in natural environment. This problem may be avoided by using nitrogen as N^{15} which makes the fuel superior to MC in all respects [25].

Shortcomings of metallic fuels include, low solidus temperature, high swelling rate and susceptibility to chemical and mechanical interaction with cladding materials which prevent it from achieving its full potential. Current method of fabrication of the fuel involves melting and casting technologies that are challenged by volatile loss of the material and low yield during production. Injection casting has been the preferred method for metal fuel fabrication for previous fast reactor fuels such as the driver fuel for EBR-II and the demonstration IFR fuel pins [35]. There are material losses and alloy contamination issues that are inherent in the injection casting process, especially when the higher actinides such as Am are involved in the fuel system. Some techniques are being developed which may overcome volatilization losses and injection casting may be effectively accomplished, but alternative processes are still under development [52].

1.4 Cermet Fuel

Cermet fuel is a type of dispersion fuel consisting of particles of ceramic fuel uniformly distributed in a metal matrix. Cermet nuclear fuels have significant potential to enhance fuel performance because of low internal fuel temperatures and low stored energy [53]. A cermet fuel is ideally designed to have the optimal properties of a ceramic, such as high temperature resistance and high hardness, and those of a metal, which improves the composite's thermal conductivity and mechanical properties. Therefore the optimal solution might be to design a novel cermet fuel which combines favorable features of both metallic and ceramic fuels. Experience with cermet fuels in test reactors and in the US naval reactors program had shown an ability to achieve very high burn ups without failure [54]. For British Proto type fast reactor (PFR) whose design began in year 1962 initially it was thought to have a rugged core of high burn up which would serve as test bed for advanced fuel elements. So the initial choice was cermet - a dispersion of $(U,Pu)O_2$, particles in stainless steel [20]. Cermet fuel was fabricated and loaded in Dounreay Fast Reactor (DFR) and other thermal test reactor for irradiation testing. The cermets could achieve high burn ups. But breeding gain with SS matrix was an issue with cermet fuels so the programme for use of cermet in PFR was abandoned. Studies have been carried out with U-PuO_2 cermet fuel in Russian federation where it is possible to tap power from the fuel and also achieve high burnups [55].

1.5 Aim of the work

The aim of present investigation was to study the feasibility of fabrication of cermet with dispersoids of UO_2 and Pu compounds in U metal matrix by powder metallurgy route. The basic knowhow for nuclear fuel fabrication by classical powder pellet route exists in Bhabha Atomic Research Centre (BARC). UO_2, $(U,Pu)O_2$, $(U,Pu)C$ fuel pellet fabrication for thermal and fast reactors has been carried out in large scale at BARC and Nuclear Fuels Complex(NFC), Hyderabad [56, 57]. Thus the part of motivation was derived from success of classical powder pellet route for fabrication of nuclear fuel pellets for different reactors in our country. India is going in a big way to adopt fast reactor programme to meet per capita power requirement for the future generation with nuclear energy besides other sources of energy. The operation of fast reactors would require lot of Pu bearing fuel to run efficiently and also produce more Pu as fissile material to feed new fast reactors. The generation of fissile material in form of Pu is possible in maximum amount only in fast reactor system of fuel cycle using metal based fuel as initial feed material [58]. Different types of fuels like carbide, oxide have been used in FBTR either as driver fuel or in form of experimental pin. Metal fuel like Na bonded ternary alloy fuel (U-19%Pu-65Zr) or mechanically bonded binary alloy fuel (U-15%Pu) are being studied [59, 60]. Motivation for present work also came from the fact that there is a need to develop a fuel for fast reactor which would have easy fabricability with high yield through existing powder pellet route and also easy reprocessibility to complete the closed fuel cycle. Cermet fuel consisting of dispersion of fissile ceramic like enriched UO_2, PuO_2, PuC, PuN in U metal matrix have the potential to be used for high burn ups with low stored energy. Therefore the aim of the present work was to develop the process for fabrication of cermet fuel and establish the feasibility for large scale production.

1.6 Scope and objective of the present work

The different ceramic particles chosen for development of cermet fuel were UO_2, PuO_2, PuC, and PuN. Different cermet fuels suitable for fast reactor application may be either Nat U-enriched UO_2, Nat U-PuO_2, Nat U-PuC, or Nat U-PuN. One of the objectives of the investigation was to find out the stability of the dispersoid in the U metal matrix. The purpose of choosing U metal as matrix was to develop a fuel possessing high breeding ratio besides other advantageous properties of the metal.

The focus of the research has been to see the feasibility of fabrication of U-UO_2/ U-PuO_2/U-PuC/U-PuN cermet by classical powder pellet route which involves cold compaction followed by sintering, to establish a flow sheet for fuel fabrication and to study different thermo physical properties of the fuel.

The above said cermet fuel is proposed to be encapsulated in Zr lined T91 steel cladding. The structural integrity of the fuel element is of paramount importance during operation of the nuclear reactors. During reactor operation, fuel comes in contact with the cladding which may result in interdiffusion of fuel and cladding components. A strength reducing zone may develop subsequently, leading to premature breach of the fuel element. Additionally low melting layers can form due to interdiffusion and affect the structural integrity of the fuel element. So another objective of the study was to understand interaction between U-UO_2 fuel and T91 clad with and without Zr lining and to evaluate performance of Zr as barrier layer between fuel and cladding. Interdiffusion experiments were carried out with the help of diffusion couples at annealing temperatures in range of 923 to 1223 K. The diffusion reaction at the interface was studied with the help of scanning electron microscopy (SEM), energy dispersive spectroscopy (EDS) and Electron probe microanalysis. From the composition profiles reaction zone thickness was calculated.

1.7 Outline of the Thesis

The structure of this thesis is as follows

Chapter 1 contains introduction to nuclear reactor, different type of fuel used in fast reactor with their merits & demerits and objective of the present research.

Chapter 2 reviews the current literature on different type of cermet fuel fabricated and irradiated in different reactors throughout the world and identifies the gap area and formulates the problem for investigation.

Chapter 3 provides details of the equipment & procedures used during and post experimental characterisation.

Chapter 4 introduces U-UO_2 cermet fuel fabrication steps involving production of U, sintered UO_2 powder, mixing, milling of the powders, cold compaction, sintering and characterization of the fuel.

In chapter 5 details of preparation of heat treated PuO_2, PuC, PuN powders and fabrication of U-PuO_2, U-PuC, U-PuN cermet by cold compaction & sintering route and characterization of the fuels has been presented.

Chapter 6 contains results of compatibility study of U-UO_2 cermet with T91 cladding with and without Zr layer in between them, by diffusion couple experiments to evaluate performance of Zr as a barrier layer.

Chapter 7 provides discussion on major findings & lists the summary from the work and suggests some topics where further work could be useful.

2. CHAPTER 2. LITERATURE SURVEY

2.1 Introduction

Cermet fuel is a type of dispersion fuel consisting of particles of ceramic fuel uniformly distributed in a metal matrix. Presence of high density U metal in the fuel matrix gives the advantage of high breeding ratio of the fuel. A cermet fuel is ideally designed to have the optimal properties of a ceramic, such as high temperature resistance and high hardness, and those of a metal, which improves the composite's thermal conductivity and mechanical properties. Cermet nuclear fuels have significant potential to enhance fuel performance because of low internal fuel temperatures and low stored energy. Hence the use of cermet fuel consequently leads to decrease of the energy stored in the reactor core [61-64]. In cermet fuel element the cladding is often metallurgically bonded to the metal matrix and this improves fuel to coolant heat transfer and lowers fuel centerline temperature [64]. A large amount of work was performed on cermet fuels in the late 1950's and early 1960's as an alternative to oxide pellet fuel in fast and light water reactors [54]. The most common example of cermet fuel is UO_2 in stainless steel studied for military reactor. As a cermet fuel constituent, UO_2 has been used primarily in stainless steel matrices and to a lesser extent in refractory metal. Such a fuel has poor breeding characteristics as the steel matrix absorbs a lot of neutrons. Cermet nuclear fuel was considered seriously for Prototype Fast Reactor (PFR), Dounreay UK and Fast Flux Test Facility (FFTF) Hanford USA, but the idea was abandoned when it was realized about poor breeding characteristics of the fuel [36].

Zirconium and Zircaloy based UO_2 cermet fuel is being used in naval reactors [54]. The higher oxides U_3O_8 has been tested exclusively in aluminum and has been used in various research reactors. Aluminium matrix cermet fuels remain the choice for research and test reactors. The fuel rods with UO_2 dispersed in an Al and Zr matrix have been designed [30, 65] and full size experimental fuel rods for VVER-440 with UO_2-Zr and UO_2-Al cermet fuels have been successfully tested in the research reactor MIR, in Russia.

Studies have been carried out on nitride based cermet with the development of UN-Al and UN-Zr cermet systems by CERCA- France and the Institute for Transuranium Elements (ITU) Germany between 1985 and 1994. Stability of UN-Al and UN-Zr compounds was confirmed by thermodynamic calculations and out of pile experiments.UN-Al has high thermodynamic stability up to $500^{\circ}C$ and UN-Zr up to $800^{\circ}C$. UN interacts with matrix (Al or Zr) at higher temperature accompanied by phase transformations and swelling. It was concluded from the results of out-of-pile investigations that the compounds UN-Al and UN-Zr can be considered as candidates fuels for the use in research reactors [66].

Haertling etal. [67] have reviewed UO_2 dispersed in refractory metals. The most studied cermet has been W-UO_2 system. Other cermet system includes Mo-UO_2, W/Mo/Re alloys-UO_2 and Re-UO_2. Data are available primarily for W- UO_2 fuel. Failure mechanism of the cermet is typically degradation of mechanical integrity and loss of fuel. Techniques found to aid in retaining fuel include the use of coating around UO_2 fuel particles, use of oxide stabilizers in UO_2, minimizing grain size in metal matrix, controlling the cermet sintering atmosphere etc.

Cermet fuel has been considered as advanced fuel for the light water reactors (LWRs). Vatulin etal. [65] from Russia have worked extensively for the fabrication of this type of fuel. UO_2-Zr and UO_2-Al cermet fuel fabricated by traditional powder metallurgy route have been successfully tested in MIR research reactor in Russia. Their work reveals that in order to increase the stability of above mentioned fuel, oxygen to metal ratio of the fuel should be in the range of 2.15-2.25. With such oxygen to metal ratio, intensity of the reaction between matrix and ceramic material reduces. X- ray analysis shows that bi-phase of UO_2-U_4O_9 forms in the fuel granules. Presence of U_4O_9 gives thermodynamic stability to the cermet fuel. Two basic methods namely low temperature impregnation and capillary impregnation have been developed by them to provide metallurgical coupling between fuel particle and matrix material [68, 69].

Cermet fuel rods with an inert metal matrix are now considered as a potential solution for plutonium burning. Cermet of the PuO_2-M type (where M stands for Al or Zr) and the PuN-M type (where M stands for V, Cr, Mo, W) are the most attractive option for Pu utilization in Light Water Reactors (LWRs) and Fast Reactors (FRs), respectively. Al or Zr as matrix is suitable for LWR fuels because of their low thermal neutron absorption cross-sections. The decisive parameter for the selection of the metal matrices or alloys is their eutectic temperatures [66, 70, 71]

Cermet fuel of composition UO_2-64 wt.% Mo was irradiated in the TANOX device in the Siloes experimental reactor, France [72]. Tests demonstrated good behavior of the cermet fuel in terms of enhanced thermal conductivity and fission gas retention during high temperature post irradiation annealing.

In order to dispose plutonium through inert matrix fuel (IMF), the development of cermet fuel with PuO_2-Zr composite was carried out in Russia. It was concluded that PuO_2-Zr cermet system could be considered as a possible variant of new cermet fuel for Pu burning in LWRs [73]. The sub critical accelerator driven system (ADS) is now being considered as a potential means to burn long lived trans uranium nuclides. In European Commission, JRC, Germany, the proposed fuel for ADS is Mo-92 cermet where plutonium and minor actinides will be dispersed in molybdenum matrix. To improve the neutronic characteristics, enriched Mo-92 will be required [74]. In order to address the issues (swelling, stability under irradiation, gas retention and release) related to use of Mo as matrix two irradiation experiments have been conducted at the High Flux Reactor (HFR) Petten, Netherlands. The behaviour of molybdenum looks satisfactory up to 1000°C [75, 76]. Cermet fuel is especially promising for reactor designs that require rapid power changes because of its anticipated capability to withstand thermal shock. Molybdenum-metal matrix, UN-fueled cermet has been studied as a candidate fuel for space reactor systems which has to produce variable power as per demand. A strong, relatively ductile, high thermal conductivity metal matrix is more likely to withstand the thermal shocks and stresses [77].

Savchenko etal. [55], discuss about a new concept of Pu and minor actinides (MA) containing fuel for fast reactor. The U-PuO_2 fuel proposed is based on dispersion of PuO_2 particles in U or U alloy matrix. The study has been done using high density U alloys like U-Mo, U-Zr, and U-Zr-Nb. In the new fuel element design, a frame work fuel element having porous uranium alloy meat is filled with PuO_2 powder of < 50 µm size. The high Uranium content fuel meat is metallurgically bonded to cladding and forms a heat conducting frame work.

Plutonium oxide as the dispersed 'fuel' phase could be used with particle loading in the range of 6–12 vol % [78] in a system utilizing a burnable poison to control the reactivity for plutonium burning applications.

Sinha etal. [79] have discussed fabrication of U-UO_2 cermet fuel system for fast reactor and their characterization in terms of phase analysis and lattice parameter determination by X-ray diffraction technique.

As mentioned above, reports are available in literature regarding fabrication and irradiation of different cermet fuel all over the world. However, literature on cermet fuel, which will be useful for power generation as well as breeding in fast reactor, is available only in few numbers in the open literature and hence work regarding such fuel needs further investigation and development.

The structural integrity of the fuel element is of paramount importance during operation of the nuclear reactors [80-82]. During reactor operation, fuel comes in contact with the cladding which may result in interdiffusion of fuel and cladding components. A strength reducing zone may develop subsequently, leading to premature breach of the fuel element. Additionally low melting layers can form due to interdiffusion and affect the structural integrity of the fuel element.

One of the important cladding material to be used for encapsulating cermet fuel is T91 steel . T91 grade steel is a 9Cr–1MoVNb type steel. This steel being ferritic has the advantage of a higher resistance to void swelling. However, a rise of the ductile-brittle transition temperature (DBTT) due to fast neutron irradiation is a matter of concern. The above mentioned steel exhibits a high mechanical strength and combines low thermal expansion with high heat conductivity [83] . For reliable operation of a fast breeder reactor, the fuel elements must be resistant to breach even in case of overpower transients [80]. To determine this resistance capability of fuel elements, extended overpower transient tests over a range of element design and operating conditions are usually being conducted. In off- normal reactor events, such as loss of coolant flow, elevation of fuel temperature may lead to formation of the liquid phase at the interface, which promotes cladding wastage and degrades cladding integrity [27, 84-89].

From the standpoint of accident transients, the most important factor is the accelerated rate of cladding attack, once eutectic liquefaction forms at the interface. The chemical compatibility between the fuel and clad material is of prime importance because of the formation of low melting eutectics which may often limit the life of the fuel pin in a reactor. The temperature of the eutectic reaction between the fuel and the cladding is considered as a critical parameter for the design of the metallic fuel pin [90] .

The selection of cladding materials are important from their resistance to interaction with U or U–Pu based alloy fuels. Pu forms low melting eutectic with stainless steel [91]. Some studies have reported that the interdiffusion behavior appeared to be dependent on the composition of the cladding materials. Ogata et al. [92] reported that the additives like Cr and Mo in the HT9 steel do not significantly affect the potential for the liquefaction in the peripheral region of the slug. For reliable operation of a fast breeder reactor, the fuel elements must be resistant to breach during operational overpower transients.

Reports are available in literature regarding fuel clad interdiffusion involving U-10Zr, U-Pu-10Zr, U-Pu alloy fuel and Fe, Fe-Cr, Fe-Cr-Ni, SS316, D9 type of clad material [93-95] . Higher swelling associated with D9 steel renders it being unacceptable for use at high burn-up. HT9 [95] and T91 grade steels are suitable for high burn-up operation because of low-swelling behavior. Therefore, study of FCCI is more important in these types of steels. The interdiffusion between U–10Zr alloy and HT9 at 973 K was studied by Lee et al [96] . The diffusion behavior between U–10Zr with T91 was investigated by Ryu et al [97] . The fuel-clad chemical compatibility between U–Zr alloys and ferritic/martensitic steels have been reported in the literature, with emphasis on the U–10Zr alloy fuel and HT9 cladding. However, the work on fuel–clad chemical interaction between U-UO_2 cermet and T91 steel is not available in open literature and requires investigation. Hence, in order to assess the fuel cladding compatibility of cermet fuel, the relative interdiffusion behaviour of various elements in the fuel & cladding and type of intermetallic phases that can develop in the fuel cladding interface must be studied.

2.2 Phase system

U has been used as the matrix material and U and Pu based ceramic as dispersed phase in cermet fuel fabrication. A brief account of different phase system is given below.

2.2.1 Uranium

Uranium exhibits three polymorphic forms namely, orthorhombic α phase up to 661ºC, β phase up to 769ºC and γ phase up to 1130ºC. The crystal structure of U was first described by Jacob and Warner in year 1937 [98]. Orthorhombic crystal of uranium shows anisotropic behaviour. Details of different phases of U with temperature, crystal structures, lattice parameter etc are provided in table 2.1. Cycling uranium material at elevated temperature causes growth in crystal. The orthorhombic crystals elongate in one direction and shrink in other direction. Thermal cycling and irradiation growth lead to internal stresses which in turn lead to grain boundary cracking and this have been a major problem in operation of U metal as a fuel. Internal stresses also cause creep rate of uranium to increase under irradiation. Alloying in small amount helps to resist growth in fuel. Adjusted Uranium has been used in UK Magnox reactor. It contains 400 ppm of Fe and 1000 ppm of Al [36].

2.2.1 UO_2

UO_2 at high temperature forms mixed phases of U_3O_8 and UO_2 (Fig.2.1). In the oxidation sequence U_4O_9 phase is also present. During oxidation of UO_{2+x}, when x exceeds 2.25 and temperature greater than 1400K, a mixed phase of UO_2 and U_3O_8 results. A pure form of hexagonal U_3O_8 structure is formed when O/M ratio is 2.6. When UO_2 is oxidised to this phase its structural properties change significantly and it becomes powder.

2.2.2 PuO_2

PuO_2 is a limited oxide which does not have a stable super stoichiometric form according to the phase diagrams of plutonium–oxygen [99]. Plutonium monoxide (PuO) is also unstable. Apparently it exists only under the conditions of specific oxygen equilibrium, produced on the surfaces of plutonium compounds or in a vapour state. Plutonium sesquioxide Pu_2O_3 occupies a special place in the phase diagram (Fig.2.2). This compound can exist in two crystallographic modifications. In the α phase it possesses a crystal lattice in the form of a body-centered cube, and in the high-temperature β phase its crystal lattice is hexagonal [100]. The theoretical density of PuO_2 is 11.46 g/cm^3. The melting temperature of plutonium dioxide is 2667 K, while the melting temperature of the sesquioxide is 2358 K.

Table 2.1. Allotropic transformation of Uranium metal [101]

	Alpha-phase	Beta-phase	Gamma-phase	Liquid
Temp. Range of stability (^{o}C)	Up to 660	660-775	775-1132	>1132
Crystal Structure	Base Centered orthorhombic	Tetragonal	BCC	
Atoms/cell	4	30	2	

Lattice parameters (A^{o})	a = 2.8536;
	b = 5.8698;
	c = 4.9555
		a = 10.759
		c = 5.656
			a =3.52	

Density (gm/cm^{3})	19.07	18.11	18.06	

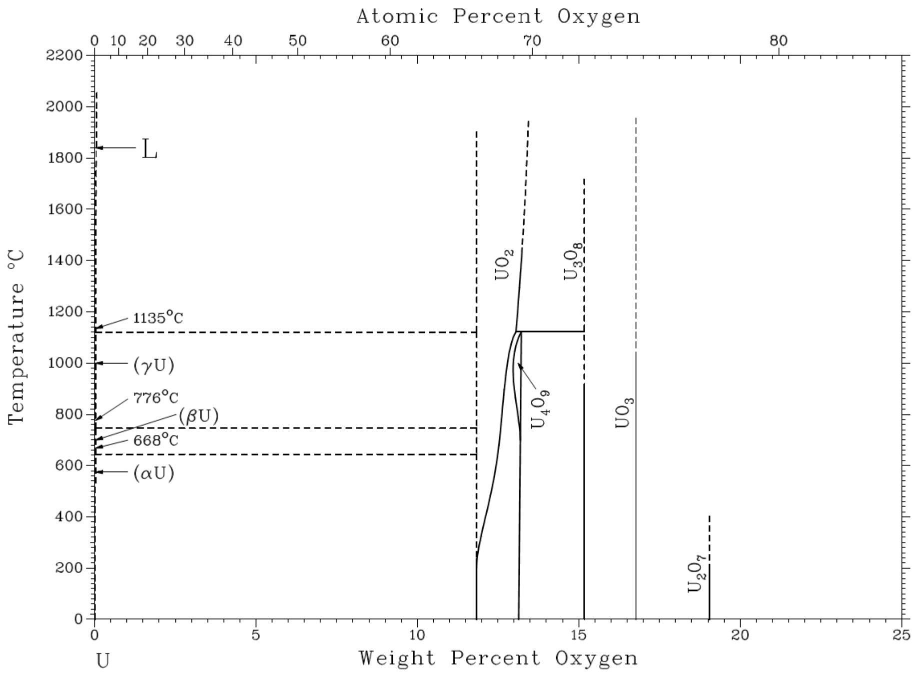

Fig. 2.1.U-O phase diagram showing different phases with variation of temperature and composition [102]

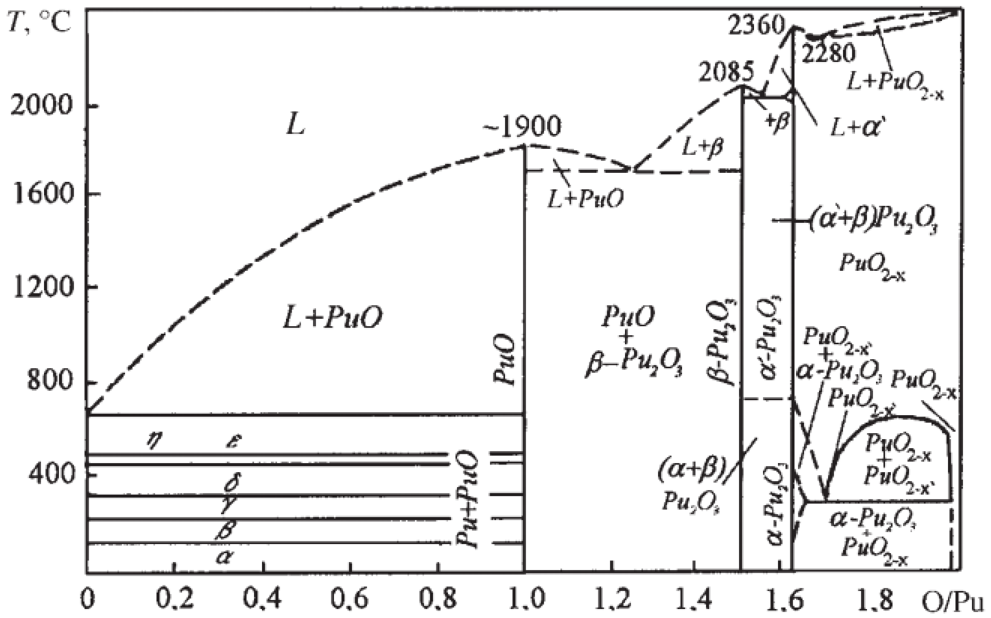

Fig. 2.2. Pu-O phase diagram showing different phases with variation of temperature and composition [100]

2.2.3 UC and PuC system

Storms [103] studied UC first and established the phase diagram (Fig.2.3). Uranium forms three different compounds with C namely UC, U_2C_3, and UC_2. At room temperature UC has a line compound.

It is stable and does not undergo any phase change from room temperature to its melting point i.e. 2780 K. U_2C_3 is a line compound and it decomposes into UC and UC_2 between 2096 K and 2110 K. The β transition in UC_2 occurs at 2041 K when carbon is present and at 2051 K when U_2C_3 is present.

Mulford [104] was first to study PuC system critically and establish the general form of the binary phase diagram (Fig.2.4). Pu forms four compounds with carbon namely PuC, Pu_2C_3, PuC_2 and Pu_3C_2 (zeta phase). The crystal structure and melting point of these compounds are given in table 2.2. At room temperature plutonium monocarbide has appreciable homogeneity range. It is always a hypo stoichiometric compound with respect to C. PuC is stable and does not undergo any phase transformation from room temperature to its melting point 1875 K. Pu_2C_3 has a composition range and melts peritectically at 2285 K to form PuC_2 and liquid. PuC_2 is stable only at high temperatures and is assumed to melt peritectically. The melting point and crystal structures of different carbides and nitrides of uranium and plutonium are in given in table 2.2.

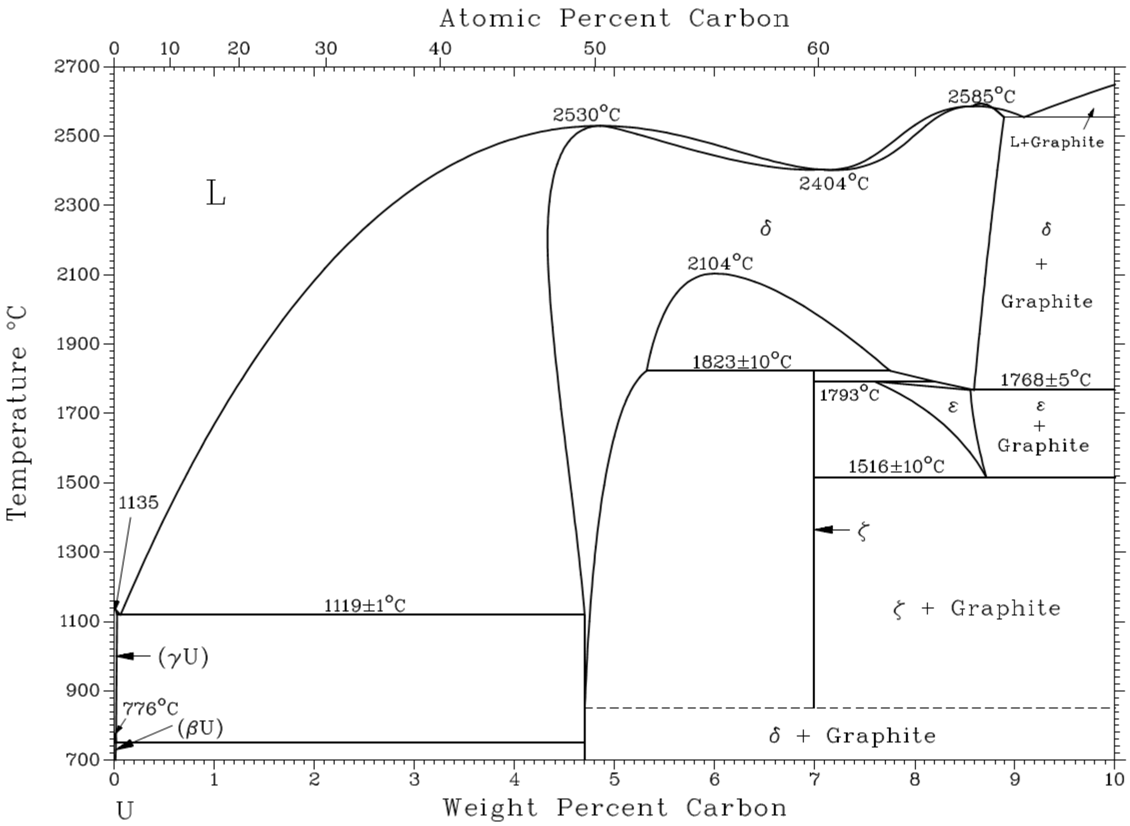

Fig. 2.3. U-C phase diagram showing different phases with variation of temperature and composition [105].

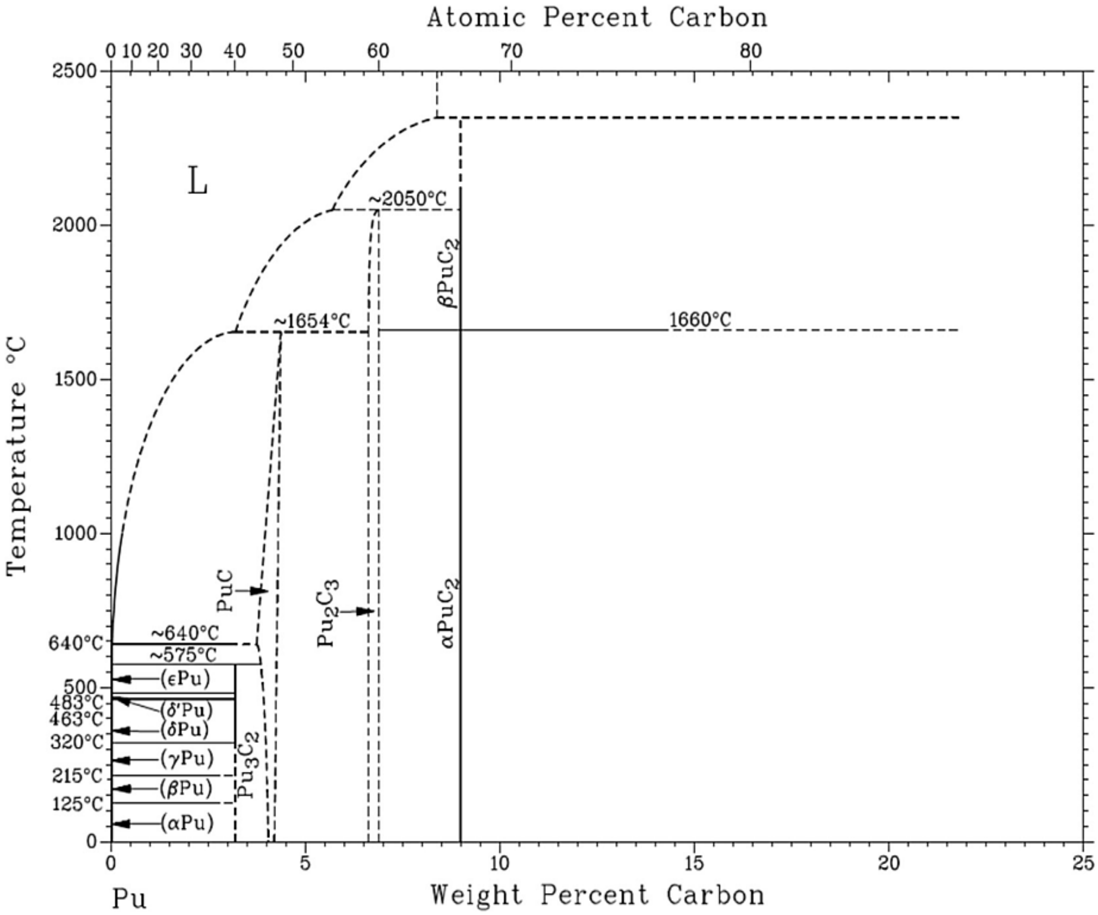

Fig. 2.4. Pu-C phase diagram showing different phases with variation of temperature and composition[105]

2.2.4 U-N and Pu-N system

The U-N system is characterised by four compounds namely UN, α U_2N_3, βU_2N_3 and a nitrogen deficient UN_2 (Fig.2.5). PuN system has only one compound, the mononitride (Fig.2.6). It exists over a small range of composition up to the melting point. Under 0.1 MPa of nitrogen, PuN decomposes on heating to give Plutonium (liquid) at 2483±30K. The details regarding these compounds are given in the table 2.2. Both UN and PuN form a complete range of solid solution.

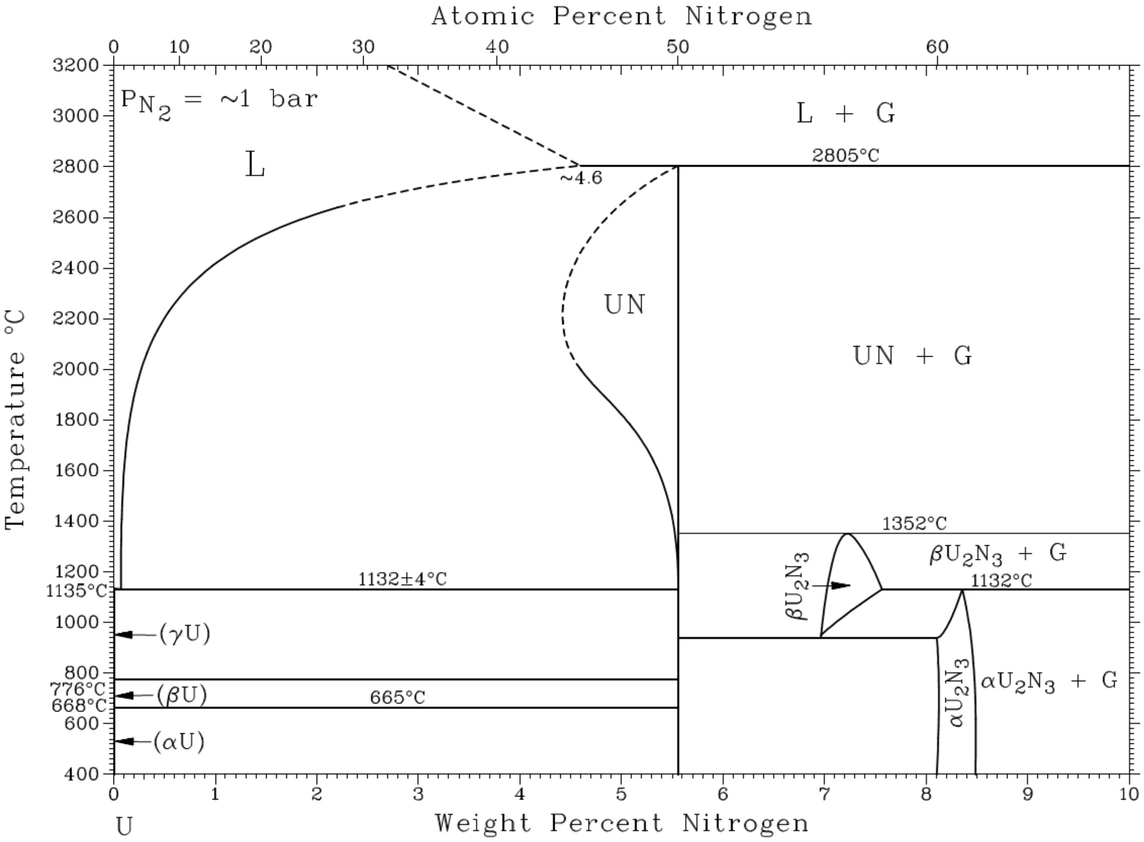

Fig. 2.5.U-N phase diagram showing different phases with variation of temperature and composition [106]

Table 2.2. Melting point and Crystal structure of Carbides and Nitrides of Uranium and Plutonium [106]

Properties	Monocarbides		Sesquicarbides		Dicarbide		Mononitride		Sesquinitride		Dinitride
	UC	PuC	U_2C_3	Pu_2C_3	UC_2	PuC_2	UN	PuN	U_2N_3	Pu_2N_3	UN_2
Crystal Structure	FCC NaCl type	FCC NaCl type	BCC	BCC	Tetragonal CaC_2 type	Tetragonal CaC_2 type	FCC NaCl type	FCC NaCl type	BCC Mn_2O_3	Hexagonal Pu_2O_3 type	FCC CaF_2 type
Lattice Parameter(nm)	0.49605	0.49728	0.80880	0.81313	a=0.35190 c=0.59790	a=0.3630 c=0.6094	0.48892	0.490476	1.0685	a=0.3696 b=0.5840	0.5210
Melting Point (K)	2780	1875	2100	2285	2720	2620	3123 at 0.25MPa	2843	–	–	–

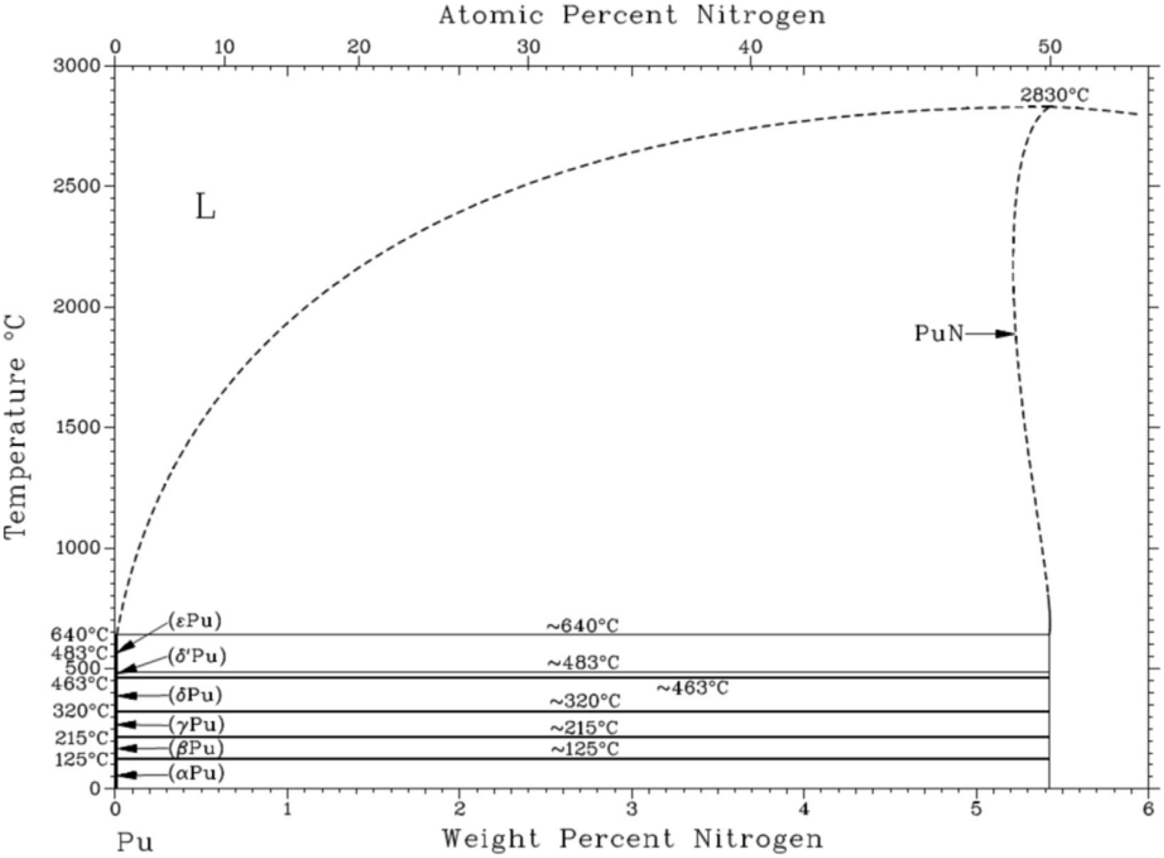

Fig. 2.6. Pu-N phase diagram showing different phases with variation of temperature and composition [107].

2.3 Fabrication of different components of cermet

2.3.1 Uranium

Different methods by which U metal powder can be produced are

- Electrolytic method
- Mechanical grinding
- Cryogenic milling
- Hydriding and Dehydriding
- Atomisation
- Calciothermic reduction of UO_2

2.3.1.1 Electrolytic Preparation of Uranium Metal Powder.

Uranium powder could be produced by electrolysis of fused salt bath [108]. The apparatus used for this method of production is a graphite crucible which acts as anode. Sodium chloride and calcium chloride are taken in equal parts by weight in the graphite crucible and green salt of potassium uranous fluoride (KUF_5) is added to it. The cathode consists of a molybdenum strip suspended in the center of the crucible. During electrolysis gray spongy mass interspersed with solidified salt gets adhered to the surface of the molybdenum cathode. The interspersed solidified salt serves to protect the metal from oxidation while it is cooled. After cooling, the mass is broken off the cathode and dissolved in water. As the density of U metal is high, traces of calcium fluoride or other insoluble salts, as well as the finer grained portions of the powder is washed away leaving fairly pure, coarse gray product. Further washing is done using 5% acetic acid to remove traces of calcium carbonate and oxide. Finally it is washed with alcohol & ether and dried.

2.3.1.2 Mechanical grinding

It is a simple and one of the oldest methods to produce metal powder [109]. It uses equipment of low cost, simple operation and fast equipment procurement time. The target alloy from which metal powder is to be produced is subjected to grinding using a lathe machine containing rotating bit. The bit grinds the alloy material and produces chips. The chips are sieved to produce necessary powder size. The size of the powder obtained in the process is generally larger than desired size and this leads to high rate of rejection. The size of the powder could be reduced by increasing the speed of the lathe but process is not suitable for large scale production. The other disadvantages of the process are high degree of contamination from the grinding bit, slow processing time and mechanical working of the resulting powder. The cold work also imparts a high degree of strain into the ground powder.

2.3.1.3 Cryogenic milling

The principle of cryogenic milling is to expose the material to low temperature which makes most of the material brittle [110]. The bulk material or the mechanically ground powder are placed in a steel vial with steel grinding ball. The vial contents are then chilled with liquid Argon and agitated in a high energy ball mill. The bulk material grinding results only in trace amount of powder. The mechanically ground powder however gets reduced to smaller size but with more number of operation in the ball mill. The overall impurities pick up of the powder from the steel vial and ball is high. Because of this reason this method is not followed.

2.3.1.4 Hydriding and Dehydriding

In this process small uranium metal pieces are heated in presence of H_2 gas [111]. The gas reacts with metal at temperature as low as 273 K to 323 K. The reaction rate becomes quite rapid at approximately 498 K. High purity H_2 is used for the reaction. H_2 pressure also affects the rate of reaction, higher the pressure faster is the rate of reaction. The reaction is exothermic but at temperature above temperature 498 K the rate of reaction decreases. The fine hydride powder is then decomposed in vacuum at temperature of 498 K or above. The dissociation pressure of UH_3 increases with increase of temperature. The powder obtained by this process is very fine (~3.5µm) and starts to burn; soon it comes in contact with air. Because of very fine nature of the particles, the powder produced is not considered suitable for fuel fabrication.

2.3.1.5 Atomisation

In this method of powder production the molten metal is turned into fine droplets which form the powder [112]. There are different methods of atomization commercially available. The most common atomization type is two fluid method. In this method the falling stream of molten metal is impinged with high pressure jet of gas or water. Centrifugal method is also common where a rotating consumable electrode or molten metal stream is allowed to fall on a rotating disc. The homogenisation of melt for two component system is very important because the alloys often preferentially melt leading to non-homogeneous powder formation. Out of the commercially common atomization methods, inert gas atomization was chosen to be the most promising since its operating parameters are well understood as it has been used in the past to produce uranium powder. The main disadvantage of atomization (aside from the cost) is the resulting spherical shape of the powders that easily segregate and are difficult to compact.

2.3.1.6 Calciothermic Reduction of UO_2

Metallothermic reduction of UO_2 powder is one of the prominent routes for production of U metal powder [113]. In this process U metal is produced by using Ca as the reducing agent. UO_2 and Ca powder are blended together and heated to high temperature. Ca present in the powder mixture reacts with UO_2 and reduces it to metal forming the CaO slag. The removal of the slag is carried out by leaching the product with acetic acid. The left over mass is then crushed and milled to produce metal powder. The different process parameters play important role in deciding the particle size and their distribution. One of the important parameter is O/M ratio of UO_2 powder. With high O/M ratio the enthalpy of the reaction is high which raises the final temperature of the reaction causing an increase in the particle size of the powder.

2.3.2 UO_2 powder

Uranium from refining mills is generally available as Uranyl Nitrate Solution. UO_2 powder is manufactured by following methods.

1. Ammonium-Di-Uranate (ADU) route
2. Ammonium-Uranium-Carbonate (AUC) route
3. Integrated Dry or wet route (IDR)

2.3.2.1 Ammonium-Di-Uranate (ADU) route

ADU powder is produced from Unary Nitrate Solution by passing NH_3 gas in to the solution which results in precipitation of the powder [114]. The ADU is subjected to calcination at temperature between 873 – 973 K and reduction at around 923 K to get sinterable grade powder. The freshly prepared UO_2 powder is pyrophoric and difficult to handle. Therefore, it is stabilized at room temperature by controlled oxidation in CO_2 .The stabilized UO_{2+x} powder, is easy to handle. The powder produced by ADU route is non-free flowing. India follows the ADU route for production of natural UO_2 powder for PHWR fuel manufacture.

2.3.2.2 Ammonium-Uranium-Carbonate (AUC) route

AUC process starts with either UF_6 or Uranium nitrate hexahydrate (UNH) as the starting material [115]. Cylinder containing UF_6 are heated with steam for evaporation. CO_2 and NH_3 are injected into the system containing UF_6. This results in formation of Uranyl Ammonium carbonate which precipitates as yellow crystal in slurry form. The slurry is dried to produce AUC powder. The powder is relatively coarse having size in range of 10-20 µm compared to 3 - 4 µm obtained from ADU route. Because of coarse nature of the powder the steps like precompaction and granulation are not required during fuel pellet fabrication.

2.3.2.3 Integrated Dry or wet route (IDR)

Enriched UO_2 (U^{235}>0.7wt %), powder is produced from UF_6 obtained from enrichment plant either by dry route e.g. IDR (Integrated Dry Route) or wet route. In IDR route [116] UF_6 gas from enrichment plant is first treated with steam and then followed by hydrogen treatment at around 923-973 K to get UO_2 powder.

In the wet route, UF_6 is hydrolysed to oxyflouride and then treated with ammonia to get ADU followed by calcination, reduction and stabilization to get UO_2 powder. The feed powder for manufacture of enriched UO_2 fuel for Indian BWR is produced by the wet route

2.3.3 PuO_2 powder

The most commonly used method for separation and purification of Pu from the irradiated fuel is Plutonium, Uranium, Reduction, Extraction (PUREX) process [117]. Large amount of Pu roughly more than 500 metric tons has been separated by this method till date. In this method of extraction selective removal of U (VI) and Pu (IV) from a nitric acid solution of dissolved irradiated fuel is carried out using hydrocarbon solvent containing TBP. The fission products are left behind in the acid solution. The plutonium and uranium are back extracted from the loaded organic solvent in to aqueous phase. Further purification of the uranium and plutonium is done by applying ion exchange process and additional solvent extraction stages with TBP. In India PUREX process is followed with oxalate route to produce PuO_2 powder. The purified solution of PuO_2 is treated with oxalic acid to form plutonium oxalate which is calcined at 500º C to produce fine PuO_2 powder with high specific surface area.

2.3.4 Preparation of PuC powder

Different techniques which are used for production of PuC_{1-x} powder on laboratory scale are described below.

2.3.4.1 Arc melting of Pu-C mixture

Metallic Pu powder and graphite are mixed together and subjected to arc melting[118]. The reaction is carried out in glove-box type containment under inert atmosphere. The arc melted product is subjected to annealing treatment for homogenization.

2.3.4.2 Reaction of PuH with C

PuH is first prepared by reacting metal powder with hydrogen at 473-573 K. PuH on decomposition at around 500º C provides very fine powder which have large surface area and suitable for reaction with graphite [119]. The reaction of PuH and graphite is carried out in vacuum or inert atmosphere between 673 to 873 K inside glove box.

2.3.4.3 Reaction of PuH with propane

Reaction of PuH with propane is carried out between 673 to 873 K. Propane reacts with fine powder of metal hydride forming Pu_2C_3 [120]. Subsequent annealing of the powder is done with PuH_2 to reduce Pu_2C_3 to PuC_{1-x}

2.3.4.4 Carbothermic reduction of PuO_2

PuO_2 powder is mixed with graphite and precompacts are made out of the powder [121]. The precompacts are subjected to carbothermic reduction at temperature between 1373 to 1773 K under vacuum. The product obtained are either Pu_2C_3 or oxygen rich PuC_{1-x}.

2.3.5 Preparation of PuN powder

2.3.5.1 Reaction of PuH with NH_3 or Nitrogen

PuH prepared by hydriding route is subjected to reaction with either Nitrogen or NH_3 at comparatively low temperature [122]. Reaction of nitrogen with Pu hydride powder is facilitated because of surface hydration due to presence of H_2.

2.3.5.2 Carbothermic reduction in presence of Nitrogen

PuO_2 is mixed with graphite in stoichiometric proportion. The precompacts are prepared and subjected to carbothermic reduction under nitrogen atmosphere at 1773 K [123]. The soak is maintained for 15 hrs at this temperature. Initially formation of PuC takes place followed by removal of C with nitrogen. The product thus converts to PuN with some amount of oxygen. To take care of oxygen, product is exposed to N_2+H_2 atmosphere at 1773 K for 4 hrs followed by cooling.

2.4 Nuclear properties of U and Pu

Uranium is the naturally occurring element which contains 0.72% of the fissile nuclide U^{235}, 0.006% U^{234} the rest being the fertile nuclide U^{238}. Density of U is 19.1 g/cc. The powder form of U is highly pyrophoric and it is handled inside a glove-box with inert gas cover. It decays mostly by alpha. When inhaled inside body it gives internal dose till it gets completely removed. The biological half-life of the Uranium is around 150 days. Biological half life is defined as the time period in which the mass of radionuclide inside human body reduces to half its original mass.

Plutonium element does not exist in nature. It is a man-made element. In nuclear reactor it is produced from U^{238} by neutron capture reaction. Different major isotopes of Pu are Pu^{238}, Pu^{239}, Pu ^{240}, Pu^{241} and Pu^{242} [124].The higher isotopes of Pu are produced by successive neutron capture reaction. Pu^{238} isotope of plutonium is used as a power source because of its high specific power (560W/kg) and low half-life [99]. This isotope of Pu is produced by (n, 2n) reaction. The production of different isotopes of Pu is shown in fig.2.7.

Plutonium is a highly radiotoxic material. Its specific activity is high because of lower half-life compared to Uranium. It decays mostly by α mode. It is a hazardous material from health point of view. Once it enters our body through inhalation it takes long time to come out of the body. Its biological half-life is around 50 years. Its allowable concentration in air is limited to 1 Bq/m^3 which is known as derived air concentration (DAC). For all the aforesaid reasons Pu is handled inside well ventilated leak tight glove-box [125] maintained at 3 to 4 air changes per hour.

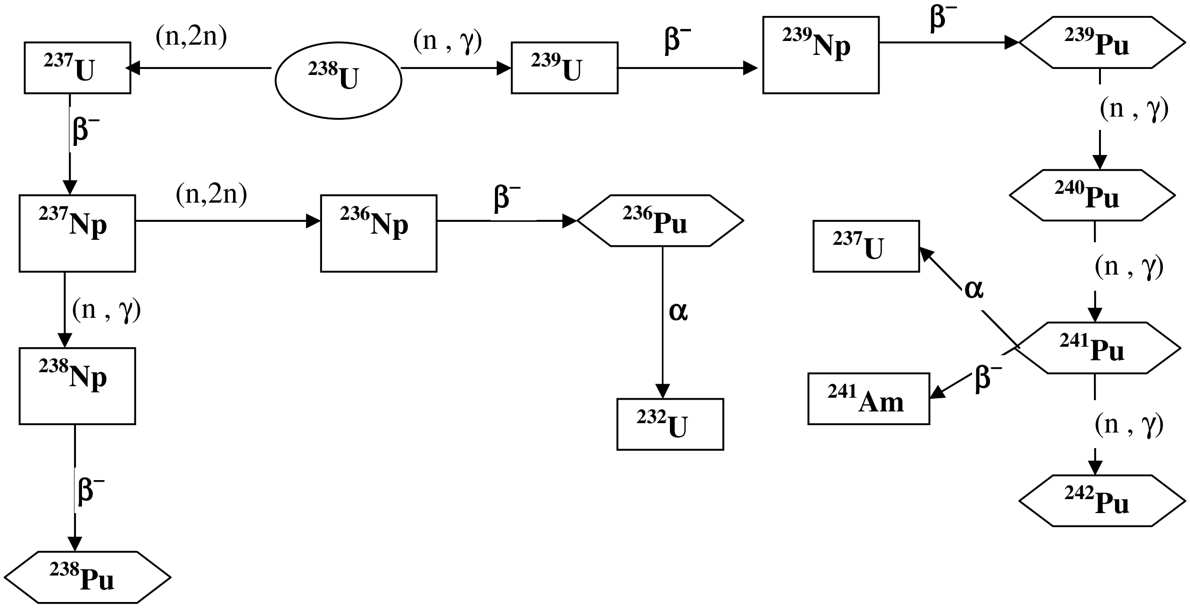

Fig.2.7. Production of different isotopes of Plutonium [99]

The lab where the glove-boxes are installed is also maintained at 7 to 8 air changes per hour to take care of Pu release and maintain DAC. Table 2.3 provides different properties of Pu isotopes which affect its handling inside glove-box. The half-life of Pu^{241} is 14.4 years. It converts to Am^{241} by β decay. Am^{241} is alpha active and decays to Np^{237} with γ emission of 60 KeV energy. It generates heat about 114w/kg. It emits low energy γ with high intensity. This creates man-rem problem during handling of Pu inside glove-box. It demands proper shielding in front of glove-box. Therefore the time between processing of Pu from burnt uranium till its use for fuel fabrication needs to be kept minimum to avoid built-up of Am^{241}. Even mass numbered isotopes of Pu like Pu^{238}, Pu ^{240} and Pu^{242} emit spontaneous neutrons. The neutrons are also emitted by (α, n) reaction with light mass numbered elements present either as impurities or constituent of Pu compounds e.g. oxygen in PuO_2. Hence depending upon percentage of these isotopes present in the Pu, shielding from neutron also needs to be provided during fuel fabrication work.

Table 2.3. Different properties of Pu isotopes [99]

Isotope	Half-life(yrs.)	Decay mode	Alpha energy in MeV	Specific Activity (10^9Bq/g)	Spontaneous fission neutron rate (n/g.s)	Heat Generation (W/Kg)	Product Isotope
^{236}Pu	2.85	α	5.763	1.96 X 10^4	-	-	U^{232}
^{238}Pu	87.7	α	5.49	6 X 10^2	2.6 X 10^3	560	U^{234}
^{239}Pu	2.41 X 10^4	α	5.096	2	0.03	1.9	^{235}U
^{240}Pu	6.6 X 10^3	α	5.162	8	1.02 X 10^3	6.8	U^{236}
^{241}Pu	14.4	β	-	3.7 X 10^3	-	4.2	^{241}Am
		α(0.002%)	4.893	-	-	-	^{237}U
^{242}Pu	3.8 X 10^5	α	4.898	0.1	1.7 X 10^3	0.1	U^{238}
^{241}Am	4.3 X 10^2	α	5.48	1.2 X 10^2	1.1	114	Np^{237}

High burn up Pu contains isotope Pu^{236} [126] in ppm level whose daughter products are Thalium(Tl) and Bismuth(Bi).The presence of these elements increases the dose level during handling of Pu as they are hard γ emitter.

2.4.1 Properties of plutonium as a nuclear fuel

Different fission parameters of Pu are provided in the table 2.4. It is evident from the table that extra nos. of neutrons (η-1) required to sustain fission chain reaction is maximum in case of Pu in fast spectrum. However it is not a good fuel material for thermal spectrum because of its high capture cross-section. The ratio of capture to fission cross section ($\alpha=\sigma c/\sigma f$) for Pu is high in thermal spectrum compared to fast spectrum.

Table 2.4. Fission parameters in fast and thermal spectrums[127]

Parameter	U^{235}		Pu^{239}		Pu^{241}		U^{233}	
n-spectrum	fast	thermal	fast	thermal	fast	thermal	fast	thermal
σf barns	1.78	580	1.91	740	2.54	1000	2.69	530
σc barns	0.435	100	0.438	270	0.29	400	0.29	50
$\alpha=(\sigma c/\sigma f)$	0.244	0.172	0.231	0.365	0.114	0.400	0.108	0.094
η-1	1.01	1.06	1.40	1.12	1.73	1.13	1.32	1.28

σf - Fission cross-section, σc - Neutron capture cross section, η - number of neutrons produced per neutron absorbed. η-1 gives the extra number of neutrons available after fulfilling the fission chain reaction requirement.

Higher η-1 value means higher availability of neutrons for conversion of fertile nuclides to fissile nuclides apart from taking care of leakage losses and capture in structural materials.

All the isotopes of Pu are fissionable in fast reactor in contrast to thermal reactor where Pu^{239} and Pu^{241} only undergo fission. Pu^{239} and Pu^{241} are associated with low delayed neutron fraction which creates an impact on the reactor core behavior. Pu^{239} has lower delayed neutron fraction compared to Pu^{241}. Lower the delayed neutron fraction difficult it becomes to control the reactivity. The research reactor grade Pu contains higher Pu^{239}. This type of plutonium requires special attention during its use in the reactor.

2.4.2 Criticality considerations during handling of plutonium

Criticality is an issue during handling of Pu material [128]. Following measures are adopted to address this issue

- Control of mass of the material so that critical mass limit is not crossed
- Storage of the material in a cylindrical vessel with specified dimensions

- Control on neutrons by use of neutron absorbing material like Boron
- Moderating materials like water should be avoided
- Exercising administrative control

In fast reactor fuel fabrication facility higher percentage of fissile material is handled compared to thermal reactor fuel fabrication facility. This restricts the throughput of the fast reactor fuel fabrication line as the criticality consideration becomes an important parameter for deciding the amount of Pu to be handled at one location.

2.5 Fabrication Techniques

The different fabrication techniques[65, 129] used for cermet fuel fabrication are as described below.

2.5.1 Vibropacking of fuel

In this method of fabrication, fuel (UO_2 particles), matrix material ((Al,Si) alloy or (Zr-Fe-Be) alloy) and cladding material with one end plug welded are made ready. The fuel is first vibropacked in one end welded cladding tube followed by degassing of vibropacked fuel pin. The second step is filling of the pin by molten matrix material till saturation in a special furnace. The third step is to weld the top end of the fuel cladding. The volume share of fissile material (UO_2) is around 60 %.

Vibratory compaction method for fabrication of nuclear fuel was first reported in year 1955 [130]. Gradually various types of pneumatic and electrodynamics vibratory compaction equipment have been developed to achieve high compaction efficiency. In the initial period lot of pins of MO_2 (mixed oxide) for fast and thermal reactor were fabricated by vibratory compaction method.

The first step for preparation of pins by this method is production of granules to desired size distribution. This is followed by blending of the particles of various size fractions. Then simultaneous loading and compaction of blended particles in one end welded tube is done with frequencies varying over a range of kilohertz. The rate of infiltration, settling of the fine particles in the voids formed by packing of coarse particles depends on frequency of vibration, particle shape and size and internal geometry of cladding tube. The packing density can vary in the range of 60-90% of TD by controlling granule particles in one ,two or three sizes [131]. By packing spheres of one size in a tube diameter larger than ten times the microsphere diameter, a density of around 60%TD. can easily be obtained. By mixing coarse and medium size spheres (7-10 times smaller than coarse fraction) in ratio of 3:1 , a packing density of 80% TD can be achieved. The highest density of 90% TD can be achieved by mixing coarse, medium and fine fraction(10 times smaller than the medium) in volume ratio of 7:2:1

2.5.2 Hot pressing of fuel pellets

In this method of fabrication initial materials are fuel particles (UO_2), inert matrix material (Zr-l%Nb alloy), and the fuel cladding. The fuel particles are coated with inert matrix material by powder metallurgy technique. The fuel particles are then subjected to hot pressing to fabricate fuel pellets. The pellets are then loaded inside cladding tube, followed by vacuuming, inert gas filling and top end welding. The volume share of fissile material (UO_2) is up 60-70%.

In hot pressing, pressure and temperature are applied simultaneously on the compact. The use of hot uniaxial as well as hot isostatic pressing has been reported mainly for the consolidation of UN, PuN and (UPu)N powders [132]. The tantalum lining is used as a barrier to carbon diffusion from the graphite die into the compact. Tungsten or molybdenum lined graphite die, has also been used to hot press carbide powders to high density (95%TD) [133]. For fabricating fuel rods with high length to diameter ratios, hot isostatic pressing (HIP) has to be used in place of hot uniaxial pressing [132]. In this technique UN, or (U,Pu)N powders are first cold pressed in the form of rods. These rods are then wrapped in tantalum foils and inserted in graphite lined niobium or tantalum cans. The composites are then heated to temperatures in the range 1643-1843K in an autoclave containing an inert gas (usually argon) at a pressure of around 70 MPa. The metal tubing collapses and compresses the nitride compacts and thus rapid densification is achieved by simultaneous action of temperature and pressure. One issue related to hot pressing is that it is uneconomical and unsuitable for large scale production.

2.5.3 Fabrication by the zone melting process using powder mixture

To begin with fuel particles (UO_2), inert matrix powder of (Al,Si) alloy and one end welded cladding material is made ready. The two types of the powder are mixed and filled inside cladding tube and vibropacked. The cladding is subjected to degassing followed by zone melting from bottom to top under vibration. The tube is finally welded at the top and subjected to quality control checks. The choice of powder fractions and fabrication regimes allows fabrication of the fuel pins with a wide range of volume fractions of fissile material (in practice 30-70 %) and ensures the monolithic structure of the fuel without chemical interaction between the molten matrix and the cladding material within wide range of pin length.

2.5.4 Fabrication by the zone melting of pre-pressed fuel pellets

The starting materials are fuel particles (UO_2), the inert matrix (Al,Si) alloy powder and one end welded cladding material. The two powders are mixed uniformly followed by pre-pressing of the powders at room temperature. The pre pressed pellets are placed in the cladding tube and exposed to zone melting arrangement from bottom to top with simultaneous column pressing. This is followed by upper end plug welding and inspection for quality checks.

2.5.5 Cermet fuel fabrication by powder metallurgy together with extrusion

This fabrication process [65] involves following steps

- Fuel granules production
- Fuel compact manufacturing
- Fuel meat manufacturing
- Fuel element manufacturing

2.5.5.1 Fuel granules production

The fuel granules are produced by powder metallurgy method where the ceramic powder is first prcompacted and then the pellets produced are crushed and allowed to pass through a particular sieve. This yields granules in a particular range of size which is used to disperse in the metal powder.

2.5.5.2 Fuel compact manufacturing

Both the metal and ceramic powders are blended uniformly. Suitable binder is added in the blend. The purpose is to avoid the density stratification and friction between the particles. The binder also provides necessary porosity. The mixed powders are then compacted to get required green density. This is followed by sintering of the pellets at high temperature.

2.5.5.3 Fuel meat manufacturing

The sintered compact is put in a barrel (Al alloy or Zirconium based alloy) and plug is inserted in one of its end. The assembly is then deformed for 2-5%. Subsequently an open butt end of the barrel is rolled and assembly is extruded at temperature around 773 K to 873 K for 80 to 100 % deformation.

2.5.5.4 Fuel element manufacturing

The fuel meat is degassed and inserted into a cladding tube. The joint rolling of fuel meat and cladding tube is performed. The end plugs are inserted at both the ends of the tube and butt welding is carried out. The state of the cladding surface and the weld is examined.

2.5.6 Cermet fuel fabrication by powder metallurgy together with impregnation

The methods of impregnation are used when requirement is to have fuel with high thermal conductivity [65]. There are two basic methods.

- Low temperature Impregnation
- Capillary impregnation

2.5.6.1 Low temperature Impregnation

This method of fuel fabrication includes

- Preparation of Porous UO_2 granules and matrix alloy
- Filling with UO_2 granules
- Impregnation with matrix alloy

The fuel granules of UO_2 are uniformly mixed with the Al matrix alloy powder. An aqueous solution of polyvinyl alcohol (PVA) is used as binding material. The mixing of the powders is carried out in a blender. The mixed powder is compacted to make billet. The compact is comminuted and sieved to obtain particle in a particular size range. The particles are spherodised in a cone drum type mill. The particles are sintered at temperature of 1823 K. The particles are filled in cladding tube, vibrocompacted and impregnated with Al alloy. The impregnation is carried out in the vertical furnace.

2.5.6.2 Capillary Impregnation

In capillary impregnation first filling of cladding tube is done with fuel and matrix granules. This is followed by vacuum annealing at temperature higher than the melting point of the matrix material. It coats the fuel granules and the cladding under action of capillary forces forming connection between fuel granules itself and between the fuel granules and cladding. The connecting bridges increase the heat conductivity of the fuel meat. The capillary impregnation is carried out either by heating a fuel element in vacuum resistance furnace or by pulling it via an inductor. After impregnation the end of the tubes are welded and subjected to quality control checks.

2.5.7 Cold compaction, Sintering and Encapsulation

This is the conventional powder metallurgical technique to produce green pellets followed by sintering at high temperature. The two types of powder are first blended to achieve the homogeneity. The green compacts are then fabricated following steps like precompaction, granulation and final compaction. The green pellets are then sintered and encapsulated in cladding material by suitable welding process [23]. During fabrication of green pellets the shape, size range of the powder particles are important. The powder particles having irregular shape are easier to compact as this type of shape facilitates locking of the powder particles. For metal powder having spherical shape, compaction and fabrication of green pellets becomes difficult [129]. Amongst all the existing methods of consolidation of the powder, the conventional powder metallurgical technique of cold pressing and sintering is the simplest, the most well established and the most widely accepted all over the world for large scale production. In the cold pressing and sintering route, small as well as large diameter pellets of controlled densities and phase contents can easily be fabricated on a large scale by proper powder characterization and optimisation of the sintering parameters. The degree of densification and the microstructural features of sintered pellets depend, besides sintering ternperature and time, on the average particle size or surface area of the powder, the binder , the sintering aids (if any). The different sintering atmosphere like vacuum, Ar, Ar+H2 etc are used during sintering process. The sintering atmosphere is found to affect the sinterability to some extent. One important disadvantage of this process is maximum numbers of process steps which may cause impurity pick up and more radiation exposure during pellet fabrication. Pellet-pin performance is considered superior than vibrocompacted pin. The particles in vibrocompacted fuel pin are in direct contact with the inside surface of the cladding tube from the start of the reactor. So the probability of the fuel clad chemical interaction is facilitated however the mechanical interaction is lower. This is because of loose nature of the particles which results in relocation reducing the net axial and radial expansion. Further in case of accidental breach of the cladding tube of vibrocompacted pin, more fuel is released in the coolant circuit compared to pellet-pin. This causes a gross contamination and increase of radiation level of the primary coolant. In a vibrocompacted pin the fission gas release is higher because gas has to travel shorter distance to come to surface of the small size of individual particles. However the fission gas release is not an issue in case of fast reactor as enough plenum space is provided to accommodate the gases [134]. The irradiation experience of vibrocompacted pin is not as extensive as the case of pellet-pin. Considering all factors, it may be concluded that the cold pressing and sintering route is still the best available method of consolidation of fuel pins. Nevertheless, the vibratory compaction technique has also a number of strong points.

3. CHAPTER 3. EXPERIMENTAL DETAILS

This chapter provides brief description about the equipment used for fabricating cermet, experimental procedure and techniques employed for characterization and evaluation of different thermo physical properties. The experimental procedure for preparation of samples for compatibility study between fuel and cladding has also been described. The fuel has been characterized by using techniques like X-ray Diffraction (XRD), Differential Thermal Analyser (DTA) Scanning Electron Microscopy (SEM) , Energy Dispersive X-ray Spectroscopy (EDS) and Alpha auto radiography. The thermal conductivity of the fuel samples have been evaluated using thermal plane transient method (TPT) and thermal diffusivity by laser flash technique. The working principle of these techniques is also briefly discussed in this chapter.

3.1 Starting Powders

Starting materials used for the present study were powders of U, UO_2, graphite and PuO_2. U and PuO_2 powders were received from two different laboratories of Bhabha Atomic Research Centre (BARC).. U was produced by calcothermic reduction of UO_2 with Ca followed by leaching and vacuum drying of the powder in inert atmosphere. UO_2 powder was received from Nuclear Fuel Complex (NFC) , Hyderabad. This powder was produced by calcinations of ADU (Ammonium diuranate) at 1000 K followed by reduction with H_2 at 900 K. PuO_2 powder was obtained through PUREX [117] process and Oxalate route in the reprocessing plant. The PuO_2 powder was calcined at 800 K . Calcination at this temperature yields powder of fine particle size and high specific surface area. During this process step there is evolution of CO_2 from the PuC_2O_4 leaving behind PuO_2 powder with pores. The presence of pores in the powder particles increases the specific surface area.This characteristics of the powder facilitates carbothermic reduction under vacuum at lower temperature which is desirable to avoid volatilisation losses during calciothermic reduction of

PuO_2 by C. However disadvantage of high specifc surface area is absorption of moisture by the PuO_2 powder as it is hygroscopic in nature. If it is not used after its production for some times then a heat treatment at temperature around 200°C is carried out to get rid of moisture. The different characteristics of these powders are given in the table 3.1.

Table 3.1.Characteristics of starting powders

Material	Specific Surface Area(m^2/gm)	Particle Size(μ)	Apparent density(g/cm^3)	Tap density(g/cm^3)	Total Impurities (wt %)
PuO_2	15-20	3-5	1.6-1.8	2.5-2.7	0.25
UO_2	3-4	2-4	1.5-1.7	2.2-2.5	0.3
U	2-3	5-15	6-6.5	7.2-8	0.05
Graphite	5.5	8-10	0.43-0.47	0.50-0.60	0.05

3.2 Equipment

Uranium metal powder is pyrophoric in nature. Plutonium [135], is a highly hazardous and radiotoxic element because of its high specific activity (.0625curi/gm) and longer biological half-life (50 years). Compounds of Pu namely PuC and PuN are also pyrophoric in nature. Therefore these materials are handled in special glove boxes [136] under inert gas cover with the aid of alpha tight neoprene gloves. The glove boxes are maintained under negative pressure by elaborate arrangement of ventilation system. A once through circulation of protective atmosphere like N_2 is maintained inside the glove box to avoid oxidation of the metal and carbide powder. The O_2 and moisture level in the N_2 atmosphere is maintained below 25 ppm [24]. This is required to take care of pyrophoric hazard from metal and carbide powder. The purity of protective atmosphere is continuously monitored by oxygen and moisture sensor. High purity Ar (IOLAR-1, maximum 2 ppm each O_2 and H_2O) gas was used as sintering atmosphere in the high temperature furnace. Most of the equipment used in the present investigation was housed inside glove boxes. A list of the equipment which was used for the study is given in the table 3.2. The equipment listed for processing of powder to pellet and sintering are normally used in conventional powder metallurgy industries. However the furnace used in present study was different from the conventional furnaces. A brief description of some of the equipment is mentioned as below.

3.3 All metal Resistance Furnace

In all metal resistance furnace as the name indicates all parts of the furnace consist of metal. Tungsten mesh heater cylindrical in shape is used to raise the temperature up to 1973 K. A cylindrical shield surrounds the heater. The purpose of the shield is to insulate heat from dissipation as it consists of layers of thin tungsten and molybednm sheets with gap of few mm in between. The combination of heater and shield remains covered with bell shaped vessel made of stainless steel. The vessal has capability of water circulation to facilitate regulation of the temperature of the furnace. The furnace has the provision of operation in both vacuum and inert gas atmosphere. The furnace vacuum could be maintained up to 0.2 pascal. The vacuum was utilized for carbothermic reduction of the powder. Tungsten trays were used for loading charge in case of carbothermic reduction in vacuum. Ytria coated molybednm trays were used for sintering of cermet pellets in argon atmosphere. The glove box housing the furnace was also maintained in Ar atmosphere. The trays supported by Moly rods were kept one over other with suitable gap in between them. This arrangement of trays was placed in the centre of heater. The temperature of the furnace was measured by a W-5%Re/W-25%Re thermocouple. The maximum heating rate maintained during heating of the furnace was 6°C/min. A sketch of the furnace is shown in fig.3.1.

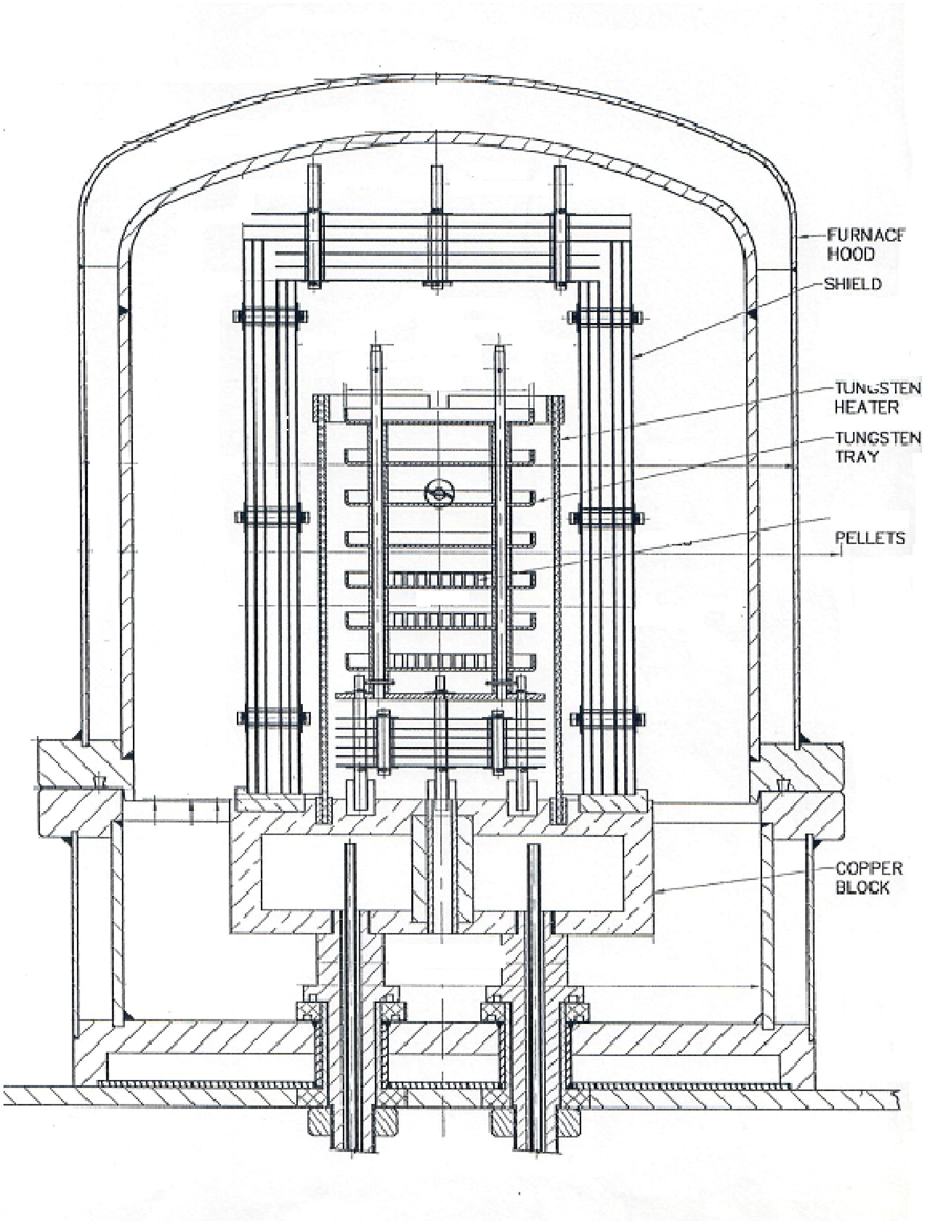

Fig. 3.1. All Metal Furnace

3.4 Equipment for measurement of thermo physical properties

It is very important to evaluate different thermo-physical properties of the fuel to utilize them for the fuel pin design, understand in pile behaviour of the fuel and to prepare computer code for accidental analysis. The thermo-physical properties like thermal expansion, thermal conductivity, phase changes and solidus temperature were measured and reported in thesis.

Table 3.2. List of equipment inside glove box

Name of the Equipment	Notable features	Purpose
Balance	Capacity-300g, Resolution 0.001 g	Weighing of the powders
Attritor	Small vessel 1 ltr capacity, Grinding media-WC balls	Mixing of PuO_2 powder with C and milling of sintered UO_2, PuC, PuN powder
Powder compaction press	Hydraulic press, Double bore, Double compaction 10ton capacity	To make precompacts and final cermet compacts
High temperature all metal furnace	Resistance furnace, capacity up to 1kg charge. Heating element W mesh heater	For carbothermic reduction under vacuum and sintering under protective atmosphere
BET surface area measurement system	Works on low temperature nitrogen adsorption principle	Measurement of specific s/c area of crushed milled clinkers of PuC, PuN etc
Sieve shaker	Motorised arrangement to shake sieves	To separate different range of particle size.
Differential Thermal Analysis (DTA)	Combined TG/DTA/DSC; Make: M/s SETARAM Instrumentation, France	To measure the phase transition temperature of different powders and cermet fuel
Dilatometry	Make: M/s SETARAM Instrumentation, France	To measure thermal expansion of the cermet fuel
Thermal conductivity (TPS technique)	Hot Disk Thermal Constant Analyser (Hot Disk TPS 2500).	To measure thermal conductivity of U-UO_2 cermet from room temperature to 923 K
Thermal diffusivity (laser flash technique)		Measurement of thermal diffusivity of Pu bearing cermet from 723 K to 1323 K
X-ray diffractrometry		To determine different phases and phase contents in cermet
Alpha autoradiography	Use of Cellulose nitrate film	To see the homogeneity of Pu distribution in Pu bearing cermet

3.4.1 Differential Thermal Analysis (DTA)

The phase transition temperatures of U metal powder and U-15wt% UO_2 sintered cermet were determined using DTA (Model no. Setsys Evoluation 24 combined TG/DTA/DSC; Make: M/s SETARAM Instrumentation, France). Sample weighing 200mg was loaded into an alumina crucible. The crucible was then loaded in a furnace which was purged with high purity argon gas flowing at 2dm^3/h. To avoid oxidation of the sample, commercially available oxygen trap was used. The heating and cooling rates could be programmed. The temperature calibration was done by measuring the melting points of high purity metals, such as Zn, Al and Ag. The resulting thermogram was recorded. The instrument was evacuated with a standard mechanical pump and backfilled with argon several times prior to the tests. For the cermet sample heating and cooling rate were programmed at 5 K min^{-1}. The phase transition temperatures of U metal powder and sintered cermets comprising UO_2 dispersed in U metal matrix and compounds of Pu dispersed in U metal matrix, were determined from the heating and cooling curve.

3.4.2 Dilatometry

Dilatometer was used to measure the change in dimension of the sample either because of expansion or contraction during heating. The thermal expansion of a material refers to change in its dimension as a function of temperature under normal pressure. When the dimension changes are measured for the bulk material it is called as bulk thermal expansion. The change in dimension measured in atomic level is called lattice thermal expansion. The concept of thermal expansion is explained from the nature of inter atomic potential well between two atoms [137]. With increase in temperature the average inter atomic distances between the atoms increases. This is because of asymmetric nature of potential energy well. The symmetry of the potential energy well depends upon bond strength. Stronger the bond strength more symmetric is the potential energy well resulting in less expansion of the lattice.

The coefficient of thermal expansion gives quantitative idea about the thermal expansion of solids. Literatures on different techniques for measurement of thermal expansion have been reviewed by James etal. [138] in a very lucid way. In the present study bulk thermal expansion of the fuel has been measured by Dilatometry technique.

The shrinkage behavior of the green cermet compact and expansion behaviour of sintered cermet fuel was studied using a high temperature vertical dilatometer (Model no. Setsys Evoluation 24, combined TG/DTA/DSC; make: M/s SETARAM Instrumentation, France).

For conducting the experiment the sample was loaded inside a sample holder made of Al_2O_3 and it was heated to desired temperature. The change in the length of the sample is transmitted through a frictionless push rod to LVDT transducer. A nominal load of 5 g was applied by the push rod over the sample. A calibrated thermocouple was placed to record the sample temperature. The heating rate could be programmed. The dilatometric experiments were carried out in high purity argon atmosphere at a dynamic gas flow rate of 2 dm^3/h.

For U-UO_2 cermet both shrinkage and expansion behaviour were studied. To understand the shrinkage behaviour of the compact, green pellets of both the compositions were heated from ambient temperature to 1350 K. The heating rate used for the study was 5 K/min. Expansion behaviour was studied by heating sintered pellet continuously from ambient temperature to a maximum of 1223 K. A plot of $\Delta L/L$ vs. temperature was obtained. The coefficient of linear thermal expansion from 473 K to 923 K was estimated from change in length.

Thermal expansion behaviour of cermet containing 20 wt% PuO_2, PuC and PuN each in U metal matrix was studied using dilatometer. The plot of percentage thermal expansion vs. temperature was obtained from experimental thermal expansion data. The coefficient of linear thermal expansion (CTE) from 373 K to 823 K was estimated from the measured change in length.

3.4.3 Thermal conductivity by Transient Plane Source (TPS) technique

Thermal conductivity is the property of material from which its ability to conduct heat is known. The Fourier equation related to thermal conductivity term is mentioned as below

$$Q= -k\ A\ dt/dx$$

where Q is heat flux, k is thermal conductivity; A is area of the sample surface conducting heat

The thermal conductivity is measured either in steady state or transient state using different techniques [139]. Thermal conductivity of U-15wt%UO_2 and U-30wt%UO_2 sintered cermets was determined by Transient Plane Source (TPS) technique [140, 141] using Hot Disk Thermal Constant Analyser (Hot Disk TPS 2500). Its principle is based on a specially designed wheatstone bridge with TPS sensor as one of the arms. The TPS unit is calibrated using an Inconel 600 standard sample from room temperature to 923K.

Two identical cylindrical cermet samples of both the composition and having a diameter 20 mm and height 10 mm were specially prepared for this experiment. The sintered density of the cermet sample compact was 80% TD. The surfaces of the samples were polished to have a good thermal contact with the TPS sensor and to minimize the contact resistance. The sensor was sandwiched between two halves of the sample. Mica sensor of radius 3.189 mm was used for measurement. The samples were heated in high purity argon atmosphere to avoid oxidation. Further to avoid temperature drift inside, the samples were maintained for 30 minutes at the set temperatures. Two measurements were carried out at each set temperature. A source meter supplied a constant voltage across the bridge. Before the measurement, the bridge remains automatically balanced and as the resistance of the sensor increases the bridge becomes increasingly un-balanced. A digital voltmeter equipped with a scanner or multiplex card records the un-balanced voltage. From these recorded voltages, it was possible to determine the temperature increase of the sensor and consequently the thermal conductivity of the sample.

3.4.4 Thermal diffusivity by laser flash technique

The most popular method used for measuring thermal conductivity from thermal diffusivity is the flash method which is the transient method and was developed by Parker et.al.[142]. It is a fast method and provides values with accuracy and reproducibility. Different advantages of this method are as listed below.

- Small size sample is required (around 10 mm dia and 2 mm thickness). Hence favorable for radioactive material where availability of bulk amount is difficult.
- A single experiment gives number of data. The measurement takes few seconds only.
- Thermal diffusivity data in wide range (10^{-3} to 10 $cm^{2}\cdot s^{-1}$) is obtained
- Sample evaluation can be done for high temperatures.

Thermal conductivity (λ) data was determined from the thermal diffusivity (α, cm^2/s), specific heat (Cp, J/kg/K) and density (ρ, g/cm3) using the following relation:

$$\lambda = \alpha \times \rho \times Cp \quad (3)$$

For the measurement of thermal diffusivity, the sintered pellet was sliced into thin discs of about 10 mm in diameter and 2 mm thick using a low speed cut off wheel. The top and bottom surface of the discs were coated with thin graphite layer by spraying [143]. The sample was loaded horizontally inside the sample holder, placed in the constant temperature zone of the furnace and heated to different temperatures in vacuum of the order 10^{-6} mbar. The sample was maintained under adiabatic condition at the measurement temperature before the laser irradiation. All measurements were carried out in flowing argon atmosphere. The Nd-YAG laser [144, 145] was used as a heat source and the laser was fired on the bottom surface of the pellet and the temperature rise on the opposite side of the pellet was recorded as a transient signal using indium antimony (In-Sb) as the infrared detector (fig.3.2). The recorded thermal response curve gives $t_{1/2}$ value which is the time taken for half the maximum temperature rise on the opposite side of the sample. This was used to calculate the thermal diffusivity. Thermal diffusivity was experimentally measured between 723 K and 1323 K by laser flash method. The density of the samples was measured and specific heat values were taken from the literature.

The thermal diffusivity (‘a’, $cm^{2\cdot}s^{-1}$) was calculated from the following relationship:

$$a = W.\, L^2 / \pi.t_x$$

L: sample thickness in cm,

t_x: time elapse in seconds for ‘x’ fraction rise in temperature of the rear surface of the sample

W: a dimensionless parameter which is a function of the relative heat loss from the sample during the measurement

$t_{1/2}$ is the time required in seconds to reach half of the maximum temperature rise at the rear surface of the sample and W= 0.1388 for $t_x = t_{1/2}$

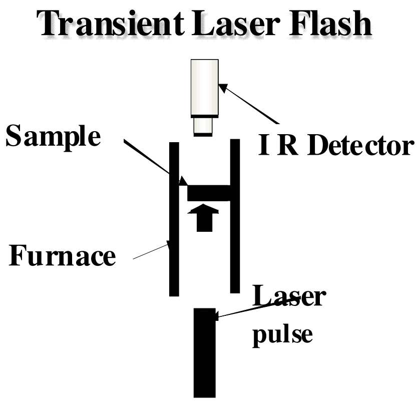

Fig. 3.2. Arrangement in flash method for diffusivity measurement

3.4.5 X-ray Diffractometer

X-ray diffraction is one of the important techniques to extract information about the crystal structure and lattice parameter [146, 147] of any material. The identification and characterisation of the material is carried out by obtaining their diffraction pattern. The diffraction takes place when the wavelength of X- ray is of the same orders as that of inter planar spacing of the crystal. X-rays generally used for characterisation have wavelength in the range of 0.6 to 2.3 A°. The monochromatic X-rays are utilised for diffraction studies. When monochromatic beam of X- rays falls on the sample it interacts mainly with electrons of the material and scatters. The scattered X-rays combine to result in constructive and destructive interference. This is called as diffraction. When the material has periodic arrangement of the atoms the diffraction patterns shows sharp maxima at certain angles. These angles are called Bragg angles and they follow relation known as Bragg's law. This law is as mentioned below

$$n \lambda = 2 d_{hkl} \sin\theta$$

where θ is Bragg angle, d= interplanar spacing for plane (h k l), λ= wavelength of X–rays

The size and arrangement of the atoms decide the intensity of the diffracted beam. Generally we come across polycrystalline materials which contain number of crystallites oriented in different directions. When X-ray beam falls on a poly crystalline material all the crystallites having different interplanar spacing of the atoms take part in the diffraction. By changing the scattering angle all the diffraction peaks from the powder sample can be detected. This detection of the X-ray peak is done by x-ray diffractometer. This equipment consists of a source of monochromatic X-ray beam and a detector which receives the diffracted beam after scattering. The angle of diffraction of the beam and intensity of diffracted beam are recorded in the electronic system of the machine. From these data intensity vs. 2θ graph is plotted which is called as diffraction pattern. The identification of the material is achieved from its powder diffraction pattern. The diffraction pattern of different elements, mixtures etc are available in Powder diffraction file (PDF). This file is maintained by Joint committee of powder diffraction standards (JCPDS). The other uses of XRD includes identification of solid solution in alloy, strain developed in crystallite etc.

For present study to understand the formation of phases in the fuel material STOE- theta-theta X ray diffractometer was used. The diffractometer produced Cu K_α radiation (λ=1.5406 A°) with help of graphite monochromator. The function of graphite monochromator is to eliminate K_β component of Cu-X-ray radiation. NaI (Tl) was used as detector. The sample preparation for powder was done by mixing the sample powder with Zinc-behenate binder followed by compaction with a manual hydraulic press. For XRD of sintered pellets mounting of pellets in bakelite was carried out followed by fine polishing. The samples were scanned in the range of 20-70° with an interval of 0.02 and counting time of 1 sec.

3.5 Microstructural examination

Microstructural analysis on the sintered cermet pellet was carried using a Scanning Electron Microscope (SEM) and optical microscope.

3.5.1 Metallographic Examination of the Pellets

Metallographic examination of the sintered cermet pellets using optical microscope was carried out for identification of phases, observation of pores, inclusions, cracks etc.

3.5.2 Scanning Electron Microscopy (SEM)

SEM is used to study the topography, morphology and phases present in a sample. When the surface of the sample is scanned with a beam of electrons produced during operation of SEM, its image is formed. The beam of electrons interacts with surface of the sample to produce more electrons and X rays of wide range of energy besides heat and light. The electrons produced after interaction of primary electrons with sample are called secondary electrons (SE), back scattered electrons (BSE) and X-rays are called as characteristic X-rays. Secondary electrons and back scattered electrons are used to generate the image which shows the morphology and topography of the sample surface. The back scattered electrons generate the contrast in the phases in a multicomponent sample. The composition of phases are analysed from characteristic X-rays. Energy dispersive X-ray analysis (EDS) generally remains a part of SEM and it is used for compositional analysis. The SEM which was used for present study worked at 20 KV acceleration potential. The surface of the sample was sputter coated with gold before placing on the sample holder for characterisation. Everhart-Thronley detector recorded image during SE mode operation and solid state detector was used for receiving image during BSE mode. The elemental analysis was done using Energy Dispersive Spectroscopy.

3.6 Alpha Autoradiography of the Pellets

This method is used to check the distribution of plutonium across the cross-section of the sample. It is based on spontaneous emission of α particle from plutonium. The impressions of α particles are obtained on a cellulose nitrate film. The sample is first polished to create smooth surface. Cellulose nitrate film (CN-85) is wrapped with mylar film of 4μ thickness and kept in intimate contact with the sample for 10 to 15 seconds. The film is afterwards decontaminated and etched in 2.5 (N) NaOH solution for 30 minutes. The treatment with etchant reveals the tracks created by attack of α particles on the cellulose film. These are observed under microscope and photographed. The observation of distribution of track across the cross-section of the sample is used to conclude for the homogeneity of the Pu distribution. Samples from Pu bearing cermet were exposed to alpha autoradiography to understand the distriution of Pu across the cross-section of the pellet.

3.7 Sample Preparation for Metallography, Autoradioglphy and X-ray Diffractometry

Bakelite was used to hot mount the sintered pellet at 25 MPa pressure and 400 K

temperature for 15 minutes duration. A rotary grinder was used to carry out successive grinding of the sintered pellet with SiC paper of different grades (240, 320, 400 and 600 grits). Kerosene oil was used as lubricant during grinding operation. The polishing of the samples was carried out by using micro cloth mounted on a polishing wheel, Diamond paste abrasive of 4-8 μ size and < 2 μwas used for coarse and fine polishing respectively. Kerosene oil was used for intermittent cleaning of sample. The polished sample was finally cleaned ultrasonically in carbon tetrachloride bath. The samples were dried and examined under microscope to see pores, inclusion, distribution of fuel particles etc.

3.8 Chemical Analysis

Chemical analysis of metal, oxide, carbide and nitride powders was carried out at different stages of fabrication of fuel pellet for O_2, N, C, U and Pu content. Inert gas fusion method was used for determination of O_2 and N_2.Combustion method was utilised for determination of C. Biamperiometry analysis was employed for determination of Pu and U content in the sample.

3.9 Experimental procedure for compatibility study between U-UO_2 fuel and T91 cladding

Cermet compacts of two different composition namely U-15 wt% UO_2 (hereafter referred as U-15%UO_2) and U-30wt% UO_2 (hereafter referred as U-30%UO_2) were fabricated by a powder pellet route. The details of fabrication procedure is given in Chapter 4 of the thesis. The typical diameter of the sintered cermet compact was about 6.80 mm.

The compacts of two different compositions of U-UO_2 cermet as mentioned above were cut into 5 mm thick discs. T91 steel rod of the same diameter was also cut into discs of about 0.5 mm thickness. The surfaces of all these discs were metallographically polished to 1 μm surface finish. Two types of diffusion couples were prepared as described below:

a) Couples between U-UO_2 and T91 discs with a Zr foil of thickness ~100 μm in between them, referred to as U-UO_2/Zr/T91 couples, and

b) Couples between U-UO_2 and T91 discs without a Zr foil in between, referred to as U-UO_2/T91 couples.

The cermt fuel was sandwiched between two T91 discs and kept inside the Inconel 600 holder to ensure intimate contact during annealing. To ensure the physical contact between the samples appreciable amount of pressure was maintained above the couple by tightening the lid of the Inconel holder. A Ta foil was used to prevent any chemical reaction between couples and fixture. The diffusion couple-fixture assembly is shown schematically in fig.3.3. The fixtures containing these couples were encapsulated in a quartz tube (fig.3.4) in helium atmosphere and annealed in a resistance heating furnace .

Besides above diffusion couple preparation , to investigate the thermal stability of the sintered fuel comapcts of above said compsition, the samples of fuel wrapped in a tantalum foil were encapsulated in a quartz tube under helium atmosphere similar to diffusion couple samples and annealed in resistence furnace.

Before proceeding for annealing experiment it was necessary to determine the phase transistion temperature for U-T91 composite and U-15%UO_2-T91 compsite to fix the annealing temperature.The phase transition temperatures of U-T91 composite and U-15%UO_2 cermet with T91 cladding were determined using DTA. Sample of about 200 mg each consisting of U metal powder + T91 steel & U-15%UO_2 fuel + T91 steel were loaded into an alumina crucible and separate DTA run was taken for each of them. The temperatures of phase transformation were determined from the heating curve. Before proceeding for annealing experiment it was necessary to determine the phase transition temperature for U-T91 composite and U-15%UO_2-T91 composite to fix the annealing temperature.

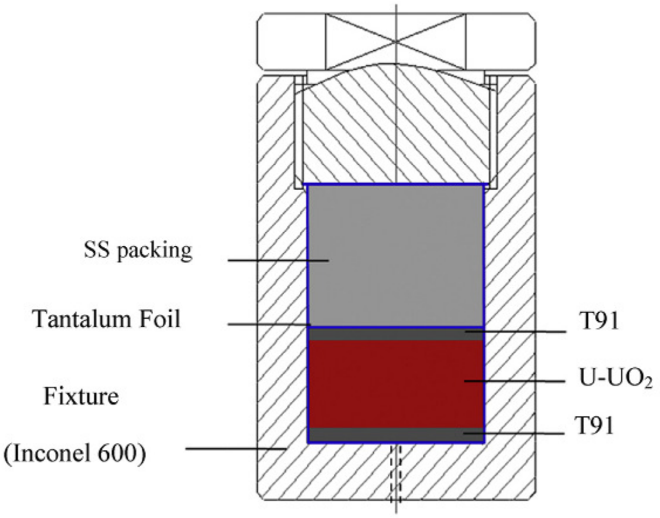

Fig. 3.3. The schematic diagram of the fixture and arrangement of samples inside the fixture

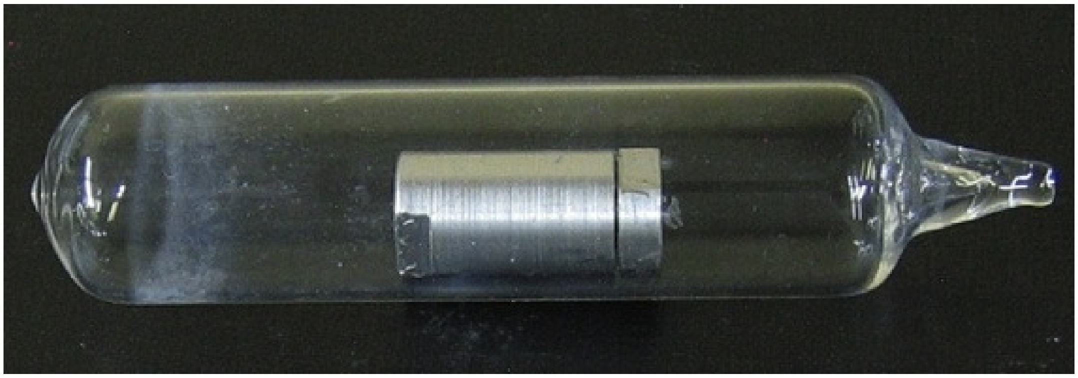

Fig. 3.4 Quartz encapsulated diffusion couple fixture

Subsequent to annealing, the couples were sectioned using a slow speed diamond cutting wheel in presence of kerosene as coolant. The exposed cross sections were metallographically polished to 1 μ surface finish. The extent of reaction and phases formed at the interface were characterised using SEM coupled with an energy dispersive spectrometer (EDS). The X-ray line scans of U, Fe and Cr and O were acquired across the interfaces of the diffusion couples to determine the distribution of each element. EPMA (CAMECA SX 100) was also used to find out the distribution of the different elements across the interface.

.

4. CHAPTER 4. U-UO_2 CERMET FUEL

This chapter deals with fabrication and characterization of U-UO_2 cermet. Fabrication of (Natural U, UO_2) cermet fuel by powder metallurgy route has been carried out. To begin with mixing of uranium metal and UO_2 ceramic powder was done. The mixed powder was compacted at different pressure to obtain different green density. The green pellets were sintered in cover of Ar atmosphere inside the furnace at different temperature to densify. All these steps were carried out in glove-box with inert cover gas. The characterisation of the fuel was carried out using Dilatometer, Differential Thermal Analyser, X-ray diffractometer, and Scanning Electron Microscope. The thermal conductivity of the fuel was also measured.

4.1 Production of U metal powder

U metal powder used for the experiment was produced by calciothermic reduction of UO_2 powder followed by leaching of product by acetic acid. This powder was received from one of the laboratories of BARC Trombay. Uranium metal powder was in the size range of 1 to 15 µm as observed during SEM examination and was regular in morphology (fig.4.1). The chemical composition of U powder is shown in table 4.1.

4.2 Production of heat treated UO_2 powder

The production of sintered UO_2 pellet was carried out following the conventional powder pellet route. The different process steps followed for this route of production are precompaction of fine powder, granulation, final compaction followed by sintering at high temperature. The as received powder from NFC , Hyderabad was first precompacted at 105 MPa and granulated through 30 mesh size sieve to increase the bulk density and flowability of the powder. The granulated powder was admixed with zinc behenate lubricant by blending in attritor at low speed of 100 rpm. This step helps to reduce the friction between die & powder particles and also the inter particle friction is taken care of during final compaction. The final compaction was carried out in a double bore double compaction die at 300 MPa pressure. The green density was obtained around 55% TD (TD of UO_2 is 10.96 gm/cm^3). Sintering of the green pellets was carried out at 1923 K. During sintering intermediate soaking steps were maintained. First soak was performed at 473 K for 2 hrs to remove moisture from the pellets. Subsequent soak was held at 1073 K for 2 hrs followed by final soak at 1923 K for 4 hrs. The soak at 1073 K facilitates stabilisation of O/M ratio near 2. The sintered pellets of density ranging between 94 to 96% TD were obtained by this process. The sintered pellets were crushed in a jaw crusher and powder size ranging from 500 to 1000 µm was obtained. Next step was milling of the crushed powder in an attritor at 250 rpm for 2 hrs. The milling resulted in fine powder below 100 µm. Sieving was performed to obtain UO_2 particle between 75 and 20 µm size by controlled crushing. However the left over particles up to 25% (of the amount taken for dispersion) below 20 µm were also recycled. The UO_2 powder was of irregular shape as shown in fig.4.2. The O/M ratio of the UO_2 powder was in the range of 2- 2.015. Table 4.2 represent the chemical compositions of UO_2 powder.

Table 4.1. Chemical composition of U metal powder (ppm)

Al	B	Ca	Cd	Co	Cr	Cu	Fe	Mg	Mn	Mo	Si	V	W	Zn	Pb	Ni
<20	0.2	20	0.30	<10	25	30	40	35	6	20	<120	10	300	20	10	30

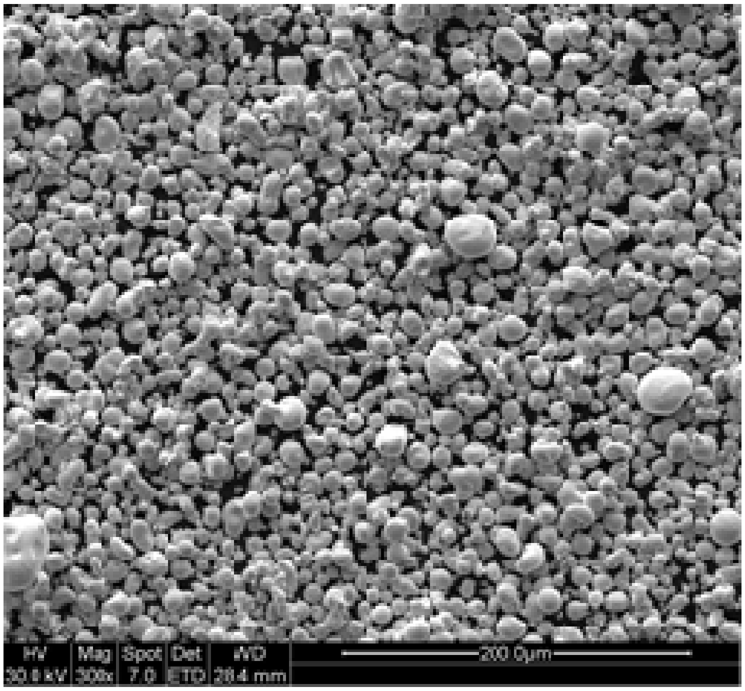

Fig. 4.1.SEM micrograph showing spherical morphology of U metal powder

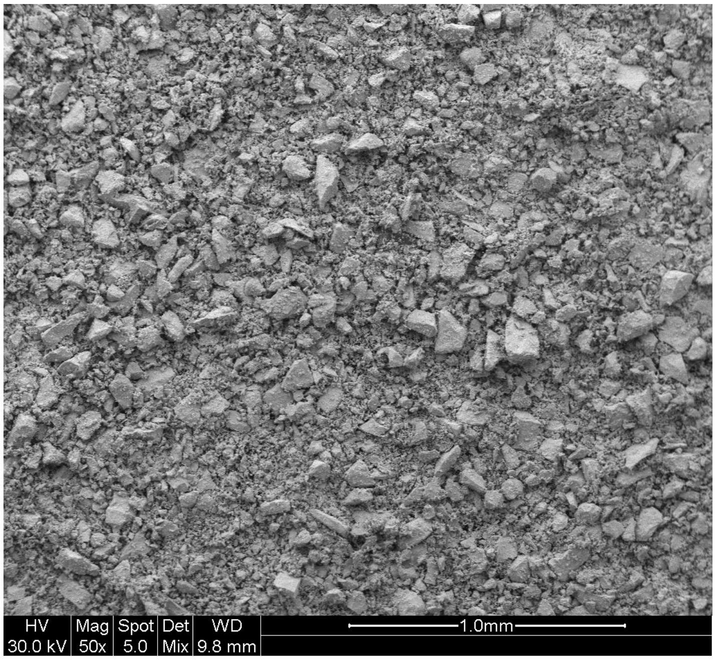

Fig. 4.2. SEM micrograph showing irregular morphology of UO_2 ceramic powder.

Table 4.2 Chemical composition of UO_2 ceramic powder (ppm)

Al	B	Ca	Cd	Co	Cr	Cu	Fe	Mg	Mn	Mo	Si	V	W	Zn	Pb	Ni
14	5	23	0.16	<10	<10	2	14	24	<2	5	67	<10	<10	10	5	5

4.3 Fuel pellet fabrication

Two compositions, namely U-15wt%UO_2 and U-30wt%UO_2 were made from Uranium and UO_2 powders. Uniform mixing of the powders was ensured by using attritor at low speed of 100 rpm. During mixing of the powders liquid binders and lubricants were added in few batches. The liquid binder and lubricant used were namely Polyethylene glycol (0.4 w %) and oleic acid (0.2 w %) respectively. Solid binder Zinc-behenate was also tried as admixed binder during compaction. The effect of admixed lubricant and binder on sintered density was studied. Table.4.3. shows effect of binder & lubricant on sintered density. Compaction was done at different pressure varying from 450 MPa to 1050 MPa using a double action hydraulic press at room temperature. During compaction die wall lubrication with 10% glycerol in ethanol or oleic acid was carried out. The plot of compression ratio (volume of loose powder/volume of the compact) vs. compaction pressure of the mixed powder is shown in fig. 4.3. Sintering of the green pellets was carried out both in argon and vacuum atmosphere at different temperatures. The vacuum level was maintained at 0.2 pascal. During sintering in Ar atmosphere an over presure of 100 mbar was maintained. A plot of variation of sintered density with the temperature and atmosphere is shown in fig.4.4. The pellets were compacted at 750 MPa pressure. The variation in density of the green and sintered pellet with pressure is shown in fig.4.5 and 4.6. The flow sheet developed for the fabrication of the cermet compacts is shown in fig.4.7. One important concern in the handling of U metal powder is its pyrophorocity and oxidation when in contact with air. The oxidation of the powder may change the sintering behavior of the compact. Hence handling of the powder needs dry boxes filled with protective atmosphere like argon or helium. Dynamic flow of the argon gas was maintained inside the glove-box during the entire process of fabrication. O_2 and H_2O level in the glove box was maintained below 10 ppm.

4.4 Preparation of sample for study of thermal stability of sintered pellets

To investigate the thermal stability of the sintered fuel compacts, the samples of fuel wrapped in a tantalum foil were encapsulated in a quartz tube under helium atmosphere similar to diffusion couple samples and annealed in a resistance furnace at temperature 1223 K for 1000 hrs. The detail of encapsulation is mentioned in section 3.4 of chapter 3.

Table 4.3. Effect of binder on the sintered density

Sample No.	Sintered Density (%TD) With Binder	Sintered Density (%TD) Without Binder	Compaction Pressure (MPa)
1	77	79	900
2	74	77	800
3	70	73	750
4	71	74	675
5	69	73	600

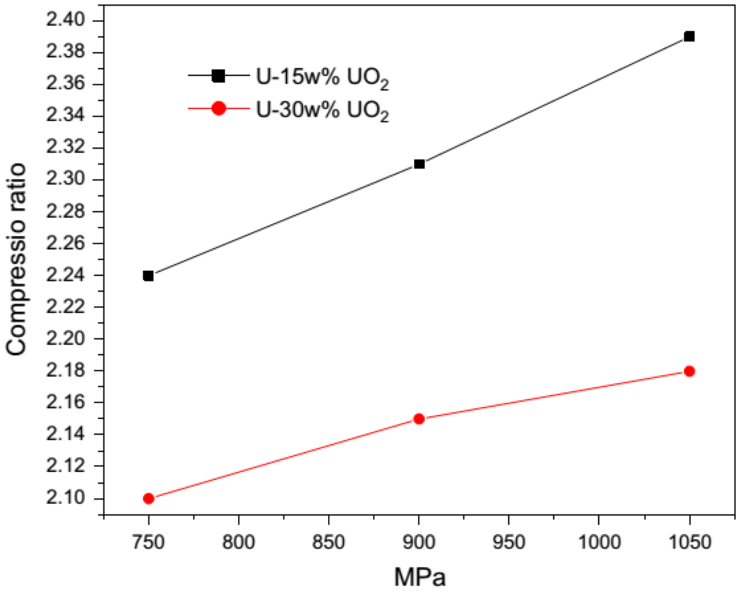

Fig. 4.3. Compression ratio vs. compaction pressure plot for U-15wt% UO2 and U-30 wt%UO2 cermet

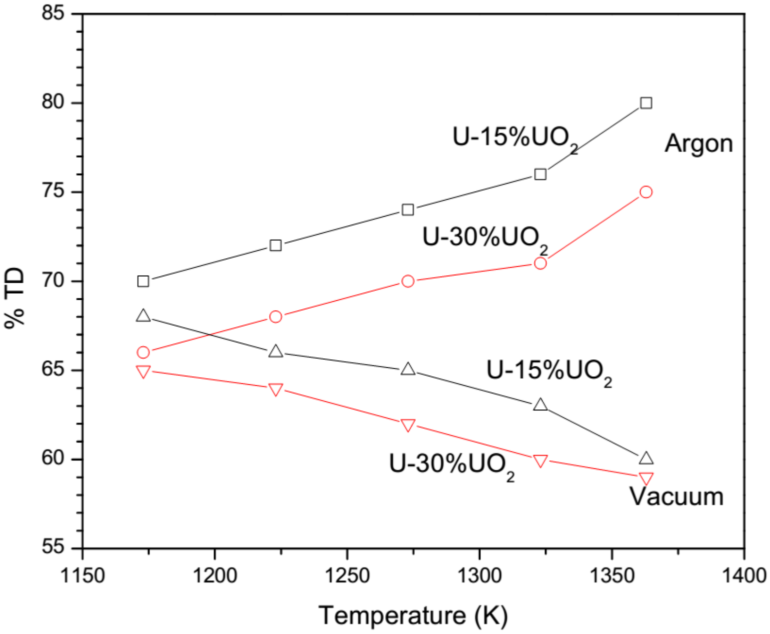

Fig. 4.4. Variation of sintered density of compacts in Argon and Vacuum atmosphere

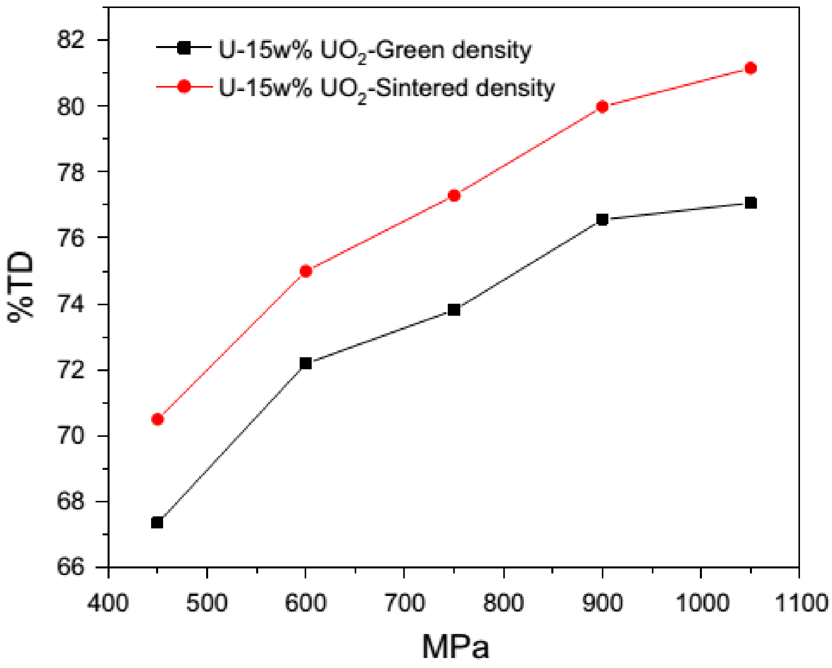

Fig. 4.5. Density vs. compaction pressure plot for U-15wt% UO_2 cermet sintered at 1348K for 8hrs

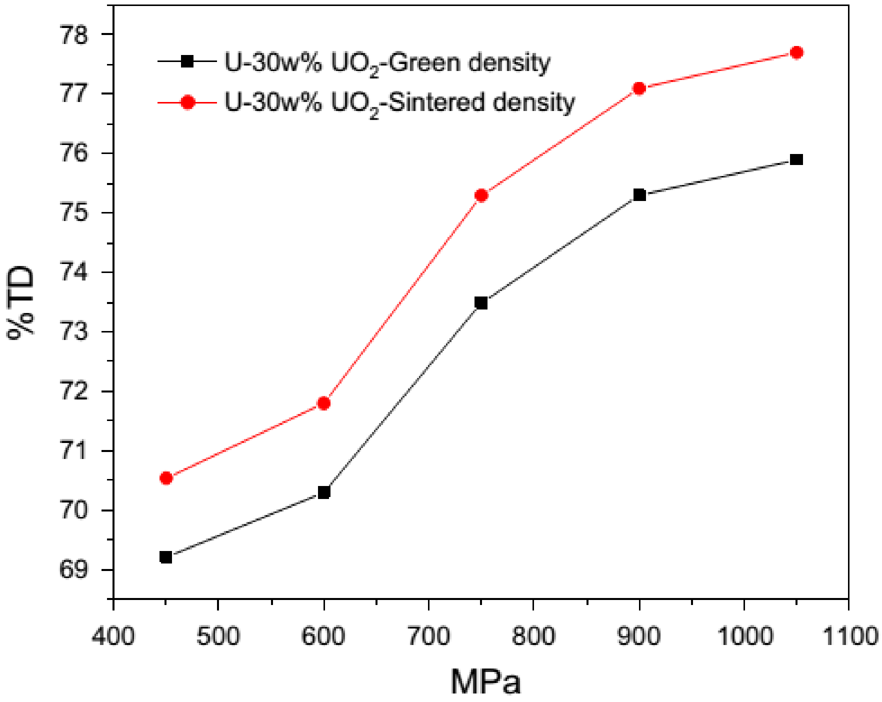

Fig. 4.6. Density vs. compaction pressure plot for U-30wt% UO_2 cermet sintered at 1348 K for 8hrs

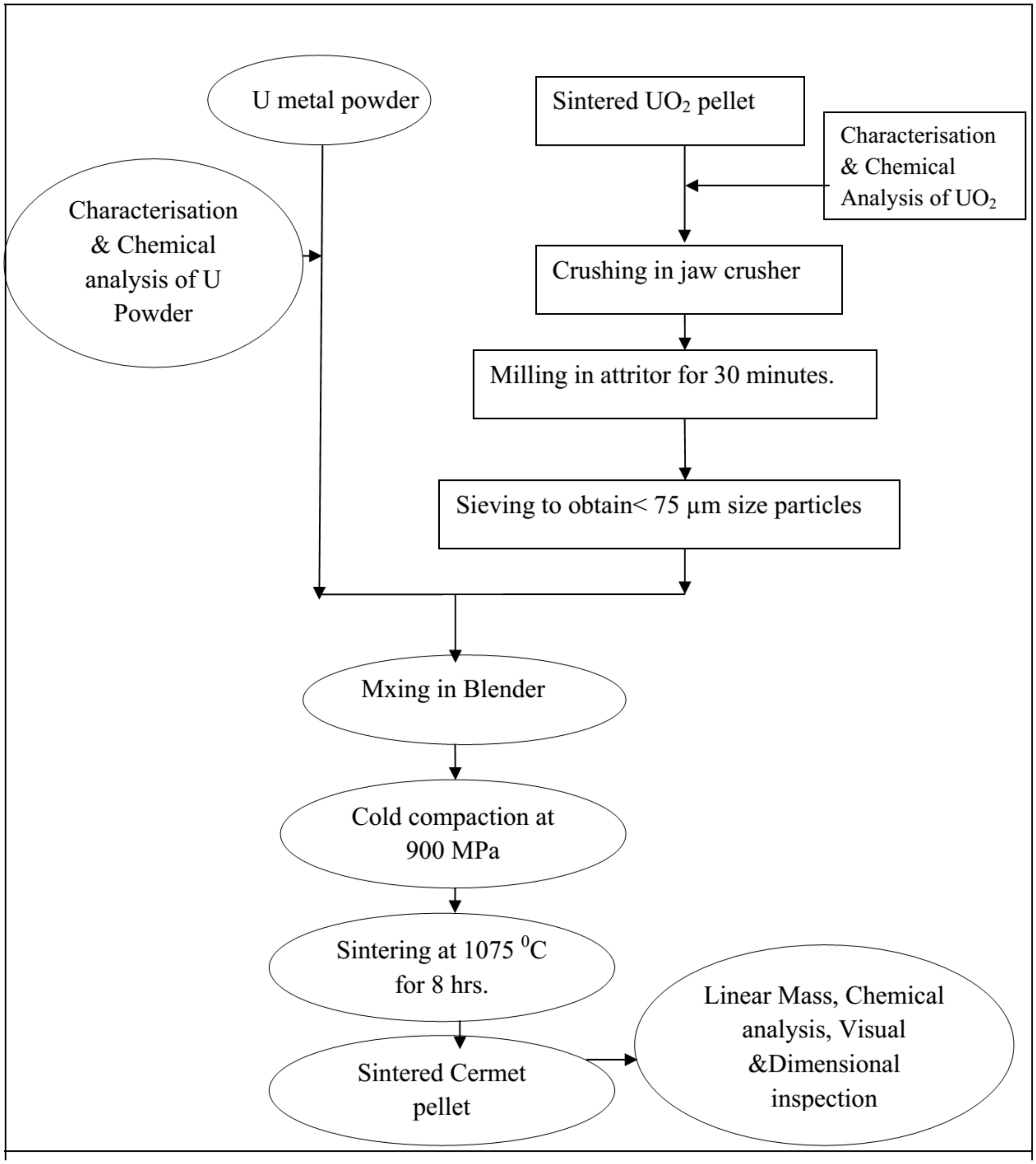

Fig. 4.7. Flow sheet showing different steps of cermet fuel fabrication

4.5 Results

4.5.1 DTA

The DTA curve obtained for U metal powder on heating is shown in fig. 4.8 The phase transition temperatures were determined from this DTA curve. The peak observed at 937 K corresponds to α ↔ β phase transition and the peak at 1040K is due to β ↔γ phase change. The third peak at 1393 K corresponds to the melting point of the metal. The DTA curve for sintered U-15wt% UO_2 cermet is shown in fig. 4.9. In this case also α ↔ β phase transformation peak is observed at 940 K, β ↔γ phase change at 1063 K and solidus temperature is found to be at 1370 K.

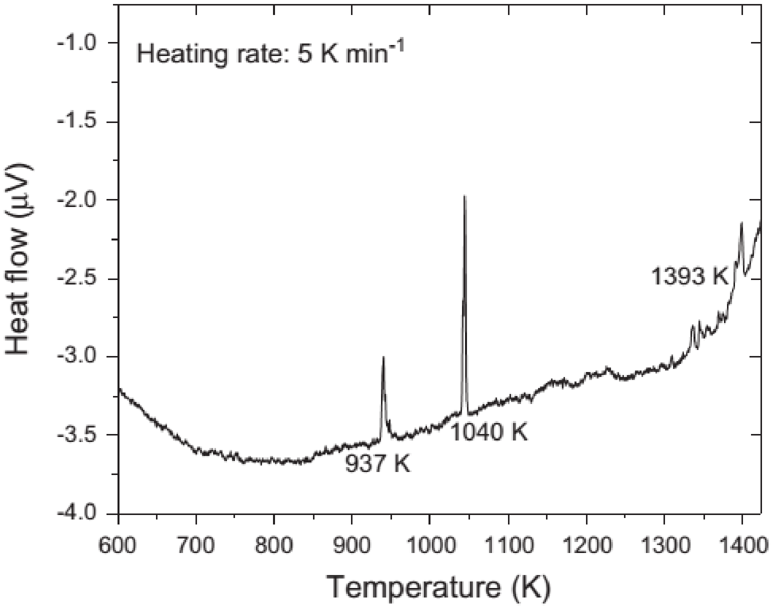

Figure 4.8. DTA curve for Uranium metal powder

4.5.2 Shrinkage and Thermal Expansion

The curve presented in figs.4.10 and 4.11 show the shrinkage behaviour of the green compacts with temperature under isothermal and non-isothermal conditions respectively. Initial increase in the dimension of the compact is because of thermal expansion and phase changes in the metal causing increase in dimension. The shrinkage in the compact is observed above 1125K.

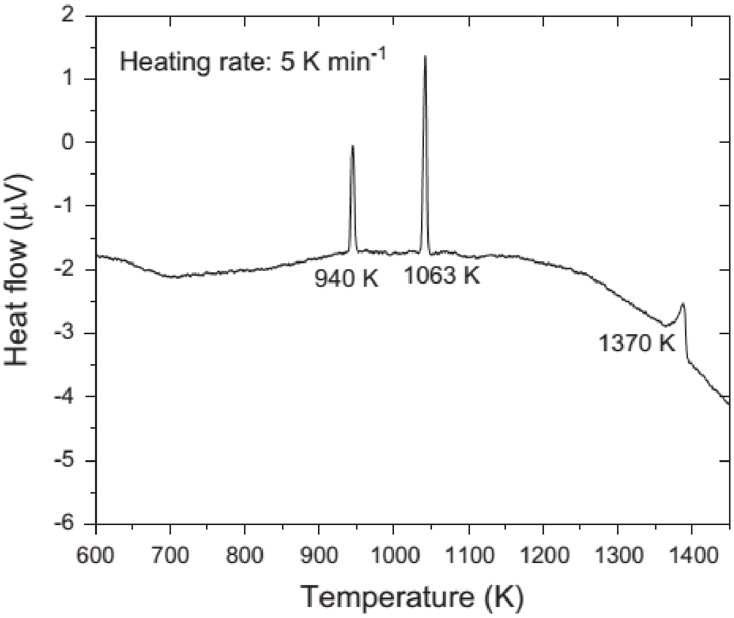

Fig. 4.9. DTA curve for the sintered U-15wt% UO_2 cermet

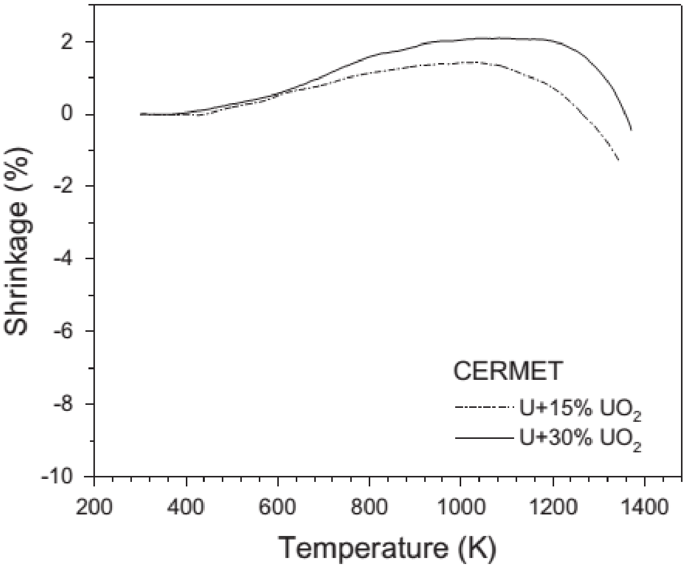

Fig. 4.10. Shrinkage behaviour of U-15wt% UO_2 and U-30 wt% UO_2 green cermet in non isothermal condition

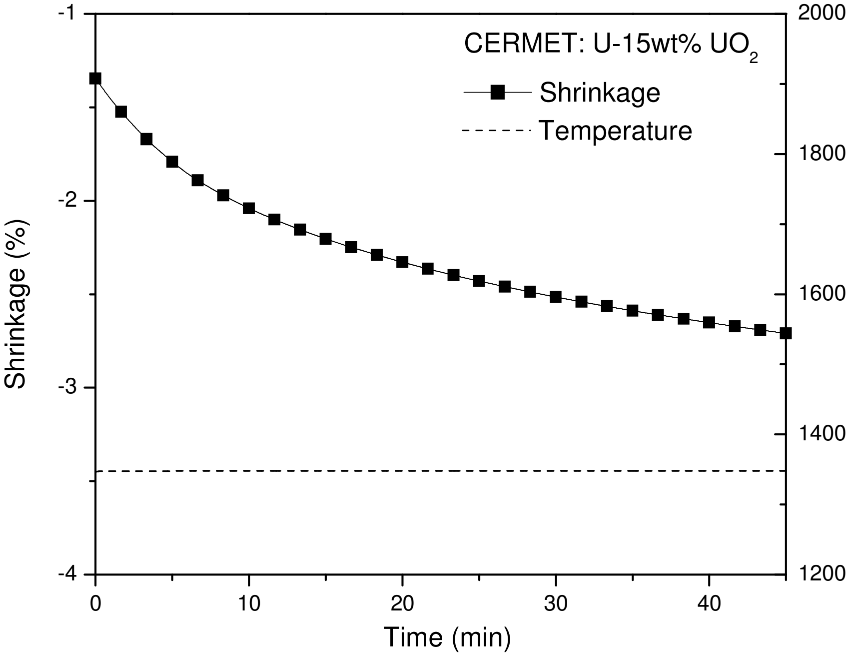

Fig. 4.11. Shrinkage behaviour of U-15wt% UO_2 green cermet compacts observed in dilatometer in isothermal condition

The dilatometric curves for thermal expansion presented in fig. 4.12 show two distinct phase transformations at 973 K and 1040 K for sintered compacts. Coefficient of linear thermal expansion was determined from this plot. The curve in the temperature range 473-923K for U-15wt%UO_2 cermet could be fitted by a third degree polynomial as:

$(\Delta L/Lo)\times100= -0.00905+2.82693\times10^{-4}T+2.94234\times10^{-6}.T^2-1.14348\times10^{-9}.T^3$

where, L_0 is the initial length (at 298 K) and ΔL is the difference between the instantaneous length at any temperature T and L_0 .T is the temperature in K.

Similarly, curve for U-30wt%UO_2 cermet could be fitted (473-923 K) by the following relation:

$(\Delta L/Lo)\times100= 0.05444-8.45788\times10^{-5}T+2.65711\times10^{-6}.T^2-1.05094\times10^{-9}.T^3$

The average coefficient of linear thermal expansion, for the temperature range 473-923K, has been determined and was found to be 17.08 × 10^{-6}/K for U-15wt% UO_2 and 12.8x 10^{-6}/K for U-30 wt%UO_2 cermet.

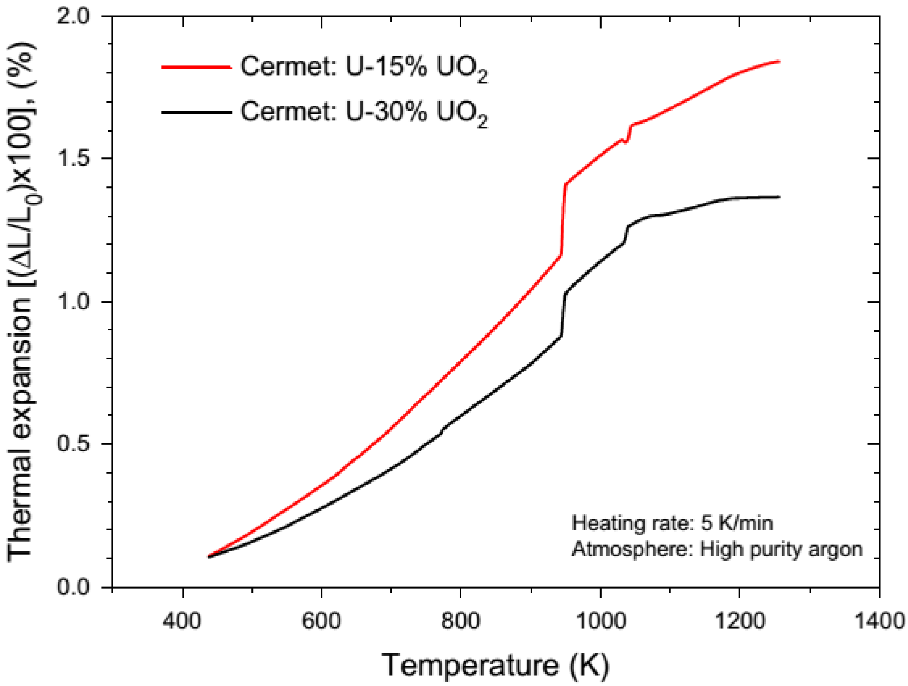

Fig. 4.12. Thermal expansion behaviour of sintered U-15wt% UO_2 and U-30wt% UO_2

4.5.3 Thermal conductivity

The thermal conductivity for the sintered compacts of both the compositions was measured as a function of temperature and is shown in fig.4.13. It is observed that the thermal conductivity of the cermets increases with increase in temperature. The thermal conductivity of U-15wt%UO_2 cermet is higher than U-30wt%UO_2 cermet for the temperatures ranging from 298 to 873 K. The thermal conductivity for U-15wt%UO_2 and U-30wt%UO_2 cermet is 15 W/m K and 8.38 W/m K respectively at 87 K. The temperature dependence of thermal conductivity of both U-15wt%UO_2 and U-30wt%UO_2 cermets could be expressed as a first degree polynomial. In the temperature range of 298-873 K the expression for U-15wt%UO_2 is:

T.C (W/m K) =7.9764+0.0083x T (K)

Similarly the expression for thermal conductivity of U-30wt %UO_2 is:

T.C (W/m K) =6.5057+0.0023 x T (K)

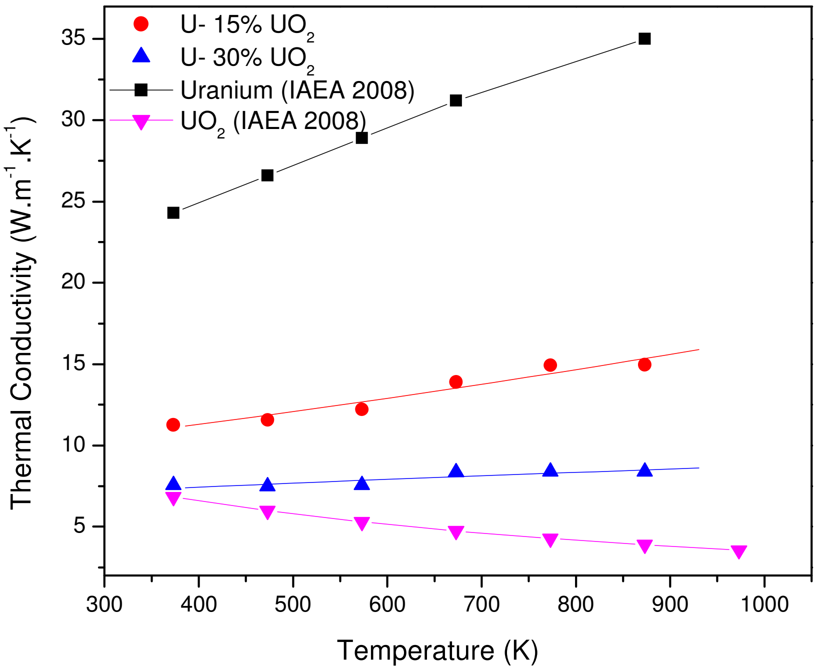

Fig. 4.13. Thermal conductivity plot of U-15% UO_2 and U-30wt% UO_2 cermet

4.5.4 Microstructure

SEM examination of the sintered pellets was carried out to study the microstructural features. Uniform distribution of UO_2 particles in the U matrix was observed for both the compositions as seen in figs 4.14 & 4.15. Small UO_2 particles interspersed in U matrix are observed in SEM micrograph. Presence of porosities in UO_2 phase as well as between U and UO_2 interface is observed in the SEM micrograph shown in figs.4.16 & 4.17. The XRD analyses of the cermets are presented in figs. 4.18 & 4.19. The peaks in the XRD pattern correspond to presence of α U and UO_2 phase. The presence of any other phase is not observed in the fuel matrix, which is the evidence of the fact that there was no impurity pick-up during the fabrication process.

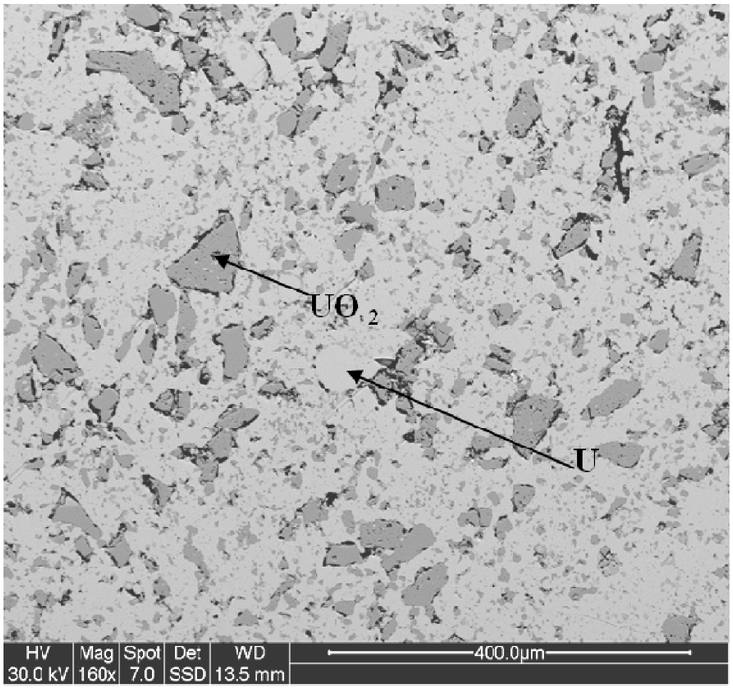

Fig. 4.14. SEM micrograph showing darker UO_2 particles in U metal matrix for U-15wt% UO_2 cermet

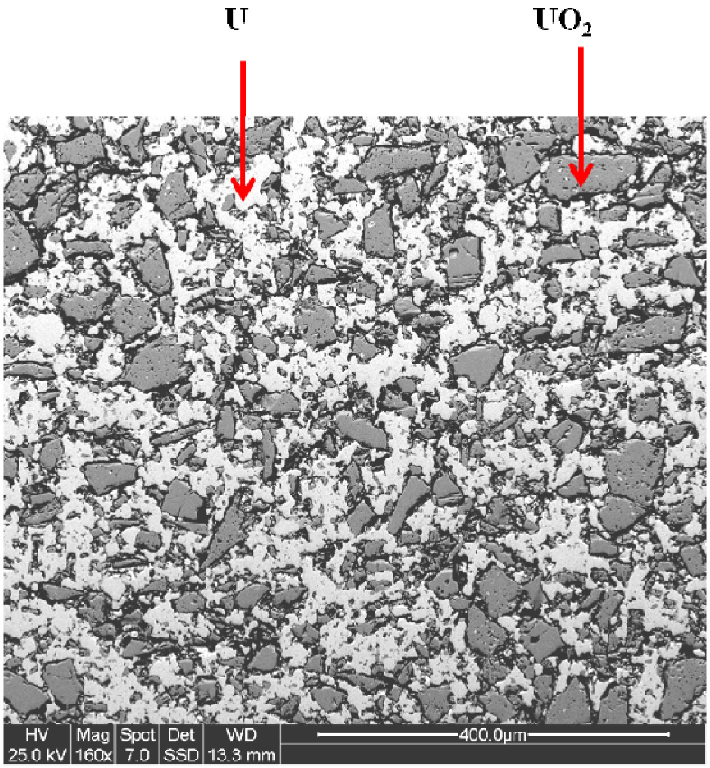

Fig. 4.15.SEM micrograph showing darker UO_2 particles in U metal matrix for U-30wt% UO_2 cermet

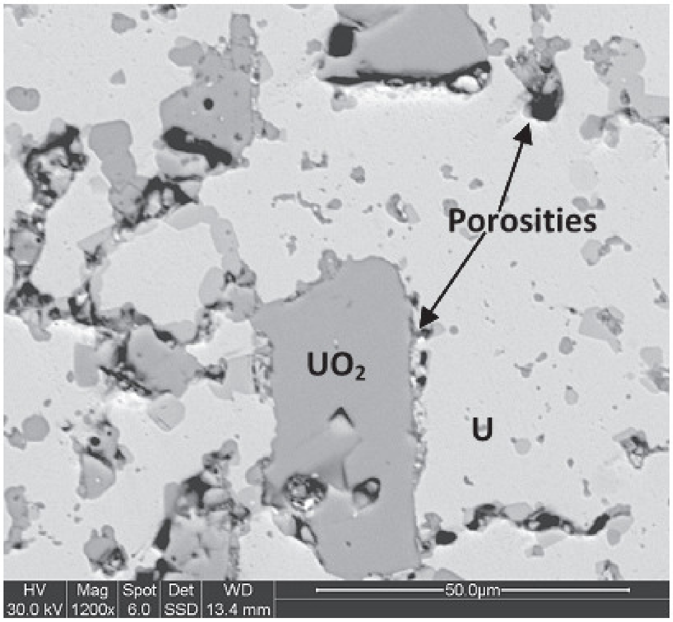

Fig. 4.16.SEM micrograph showing inter particle porosities between U and UO_2 phases

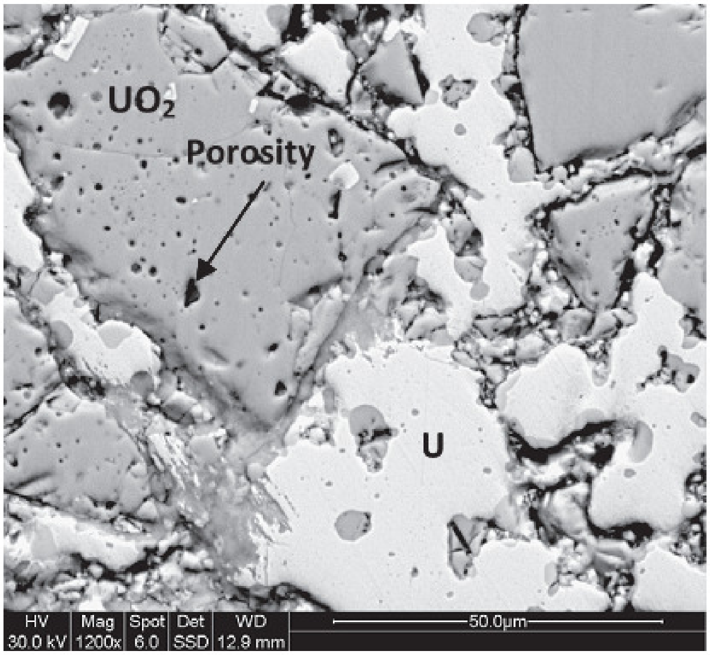

Fig. 4.17. SEM micrograph showing intra particle porosities in UO$_2$ phases

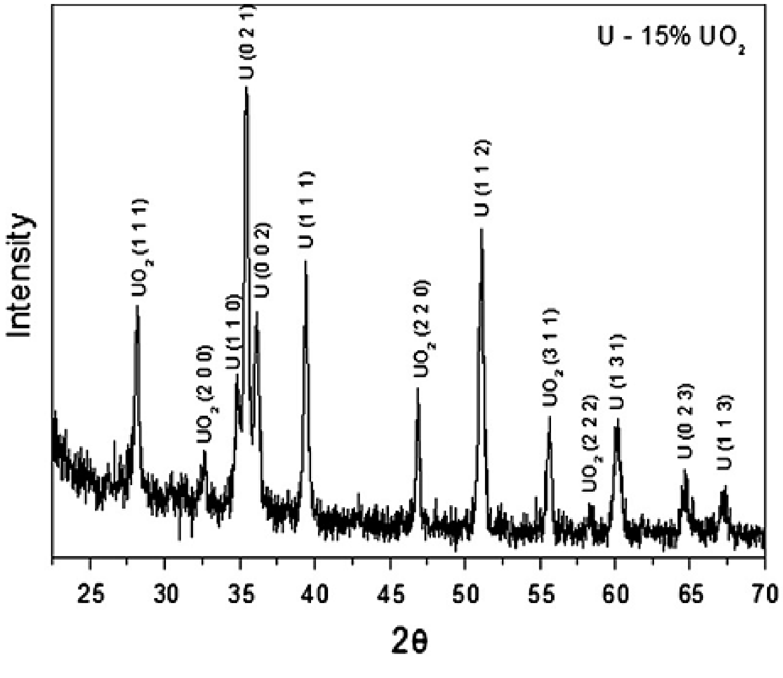

Fig. 4.18.XRD pattern of sintered U-15wt% UO$_2$ cermet compact

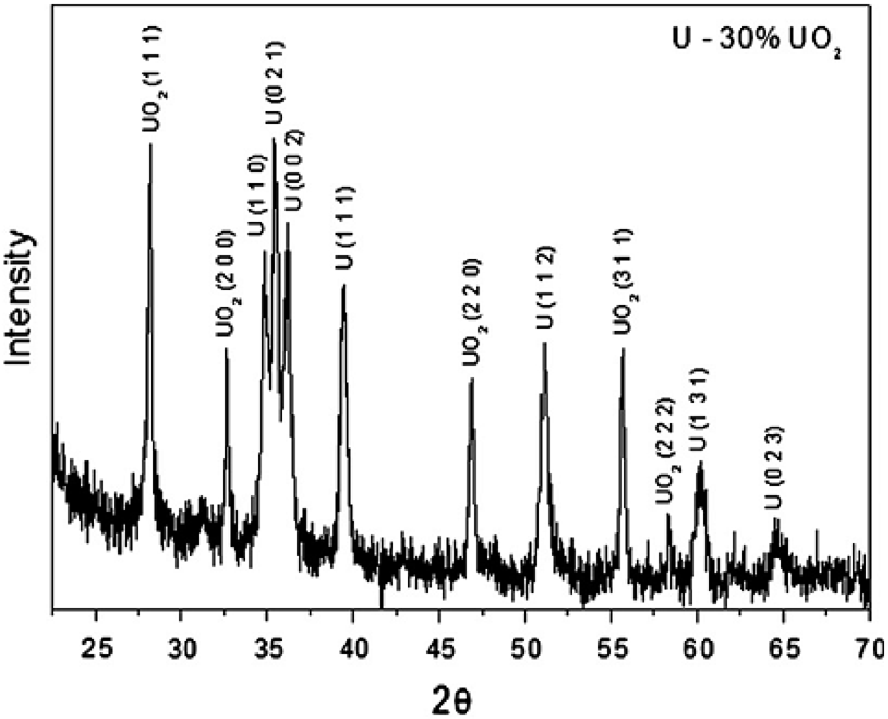

Fig. 4.19. XRD pattern of sintered U-30wt% UO_2 cermet

4.6 Thermal stability of fuel compact

The microstructures of the as-sintered and annealed U-30%UO_2 fuel pellets are shown in fig. 4.20. In both the microstructures UO_2 particles are observed to be homogeneously distributed throughout the U metal matrix. The magnified micrographs and elemental mapping of uranium for both the sintered and annealed samples are shown in fig. 4.21 (a-d). The elemental distribution of U is found to be similar in both the cases. The dark patches observed in the elemental mapping (fig. 4.21 (b & d)) could be because of the presence of the porosities.

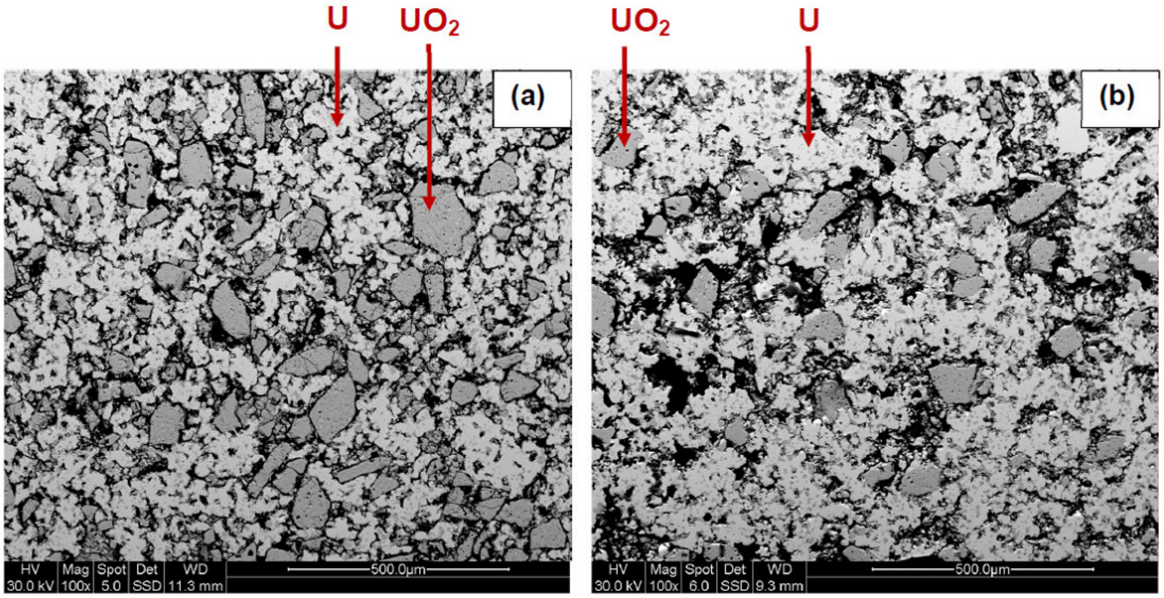

Fig. 4.20. Microstructures (back scattered electron image) of U-30%UO_2 fuel pellets (a) as-sintered and (b) after annealing at 1223 K for 1000 h

The results of thermal stability of U-15%UO_2 cermet were found to be similar to that of U-30%UO_2 cermet fuel. The elemental map of uranium was incorporated to highlight its distribution throughout the sample in correlation with microstructure. It also gives an idea about the presence of porosity in the matrix. Since, it is a U-UO_2 composite cermet, the expected elements are uranium and oxygen. The EDS analysis may not be accurate for low Z element like oxygen. Hence, the elemental mapping of oxygen has not been incorporated here.

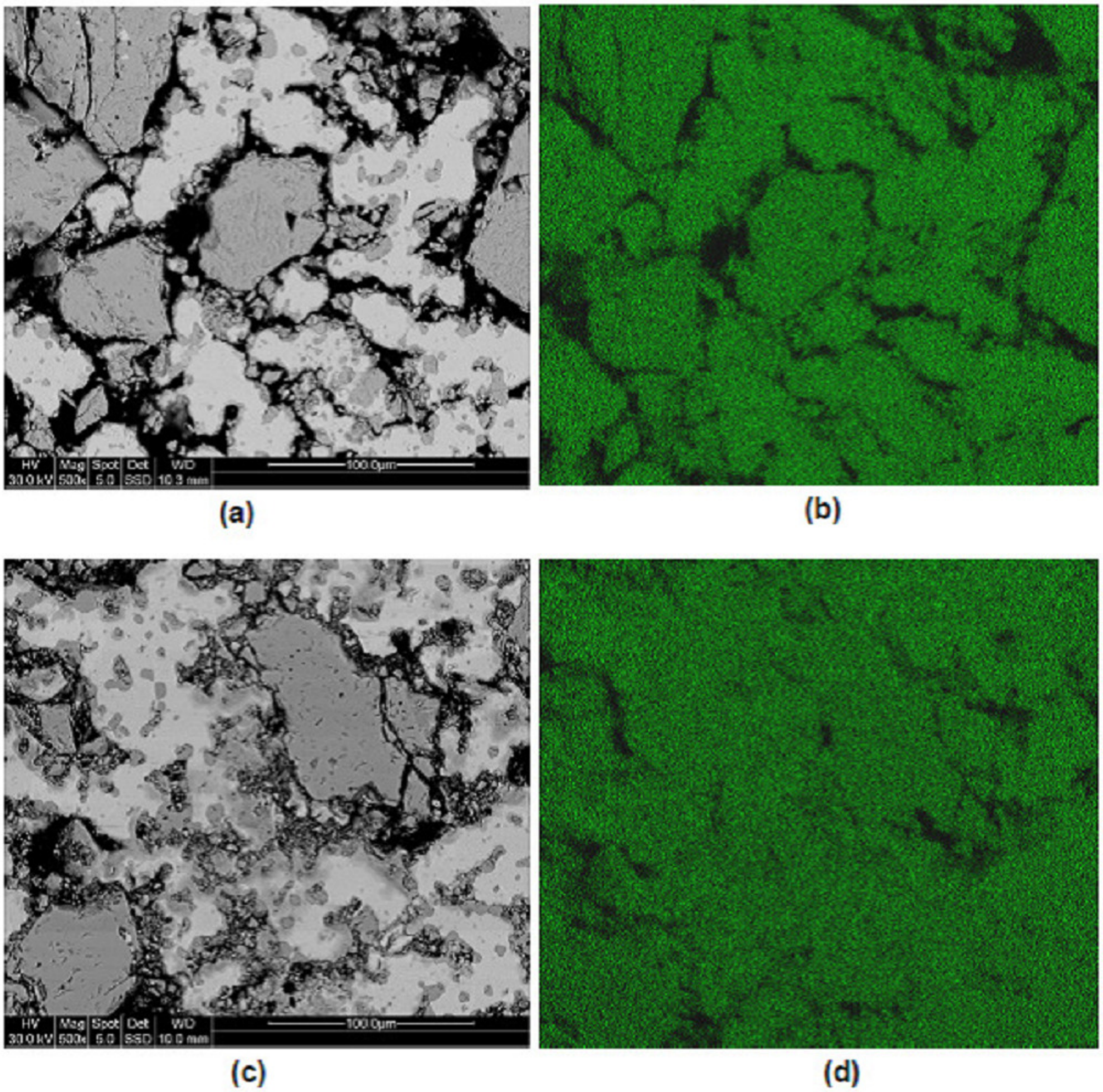

(a) (b)

(c) (d)

Fig. 4.21. (a) and (b) Microstructure (back scattered electron image) and elemental mapping of uranium for sintered U-30%UO_2 fuel pellet. (c) and (d) Microstructure and elemental mapping of uranium for annealed U-30%UO_2 fuel pellets after annealing at 1223 K for 1000hrs

4.7 Discussion

Uranium metal powders have poor compressibility and sinterability [148]. Higher inter-particle friction and work hardening of the metal powder during compaction raise the compaction pressure essential for the fabrication of green compacts. In order to reduce the inter-particle friction, oleic acid/ 10% glycerol in ethanol was used as die wall lubricants. The available particle size distribution of U metal powder for the present experiment was in the range of 1-15μm and this kind of narrow size distribution also enhances the compaction pressure necessary for pelletisation. In broad particle size distribution smaller particles contained in the powder mixture fit into the interstices between larger powder particles. This facilitates the filling and settling of the powder in the die and subsequently compaction is easier. For narrow size distribution, settling of the powder in the die is not very effective leading to application of comparatively higher pressure to obtain similar result.

The presence of admixed lubricant and binder has negative effect on the sintered density of compacts. It is observed that with presence of admixed binder and lubricant in the powder, the final density of the pellets reduces as compared to pellets without binder as seen in table 4.3.The sinterability of U is observed to be poor because of phase transformation with temperature. The presence of binder and lubricant between the particles in the powder leaves pores during heating and considering even smallest gap, since the sinterability of U is as such poor, sinterability gets further affected. From fig.4.4 it is observed that the compression ratio for both U-15wt% UO_2 and U-30wt%UO_2 cermet increases with increase of pressure and at 1050 MPa the maximum value of the ratio is 2.40 and 2.18 respectively. The compression ratio of the powder decreases with increase of UO_2 content in the cermet composition. This may be because of the presence of harder sintered UO_2 particles in the matrix. The reason for choosing sintered UO_2 particles was to have controlled O/U ratio and higher bulk density so as to have optimum volume of UO_2 in the fuel matrix. From fig.4.4 it is observed that density drops in case of sintering of compacts in vacuum atmosphere and this outcome is in contrast with the reported result of better sintering of Uranium in vacuum atmosphere [148].

This difference could be because of level of vacuum achievable during sintering. In the present investigation the maximum vacuum which could be reached in all metal furnace was

0.2 pascal. Probably this level of vacuum may not be sufficient for sintering of uranium based cermet. Hence it is possible that U oxidises to UO_{2-x} resulting in higher volume of pellet and consequently lower density. This effect is more pronounced at higher temperature because of faster kinetics resulting in larger volume changes and greater fall in density of compacts. Oxidation of Uranium was also noted in dilatometer experiment. It was observed that oxygen impurity in the carrier gas causes significant amount of oxidation of metallic uranium which leads to the formation of less dense UO_2-x type product. At high temperature the oxidation becomes more prominent because of reactive nature of Uranium metal.

The density vs. compaction pressure plot is shown in fig.4.5 &4.6. It is observed from the plot that the green as well as sintered density of the cermet for both the compositions increases with increase in the compaction pressure. The maximum shrinkage observed during sintering of cermets U-15wt%UO_2 and U-30wt%UO_2 is approximately 5% and 3% respectively.

From literature [148] it is learnt that hot compaction at 900K and 450 MPa yields density up to 90%TD. But use of hot compaction inside glove-box under negative pressure with radioactive material becomes a difficult job. So cold compaction is preferred over hot compaction provided required density is achieved. Nevertheless density up to 80%TD achieved in present case of cermet fuel is acceptable for fast reactor application

The shrinkage decreases with increase in content of ceramic particles in the matrix. This is because the ceramic particles are already sintered and the sintering temperature of the cermet is not enough to cause further shrinkage in these particles. The shrinkage of the composite compact is also influenced by dislocations present in the metal particles. The material transport effects by dislocation depend on the particle size of the powder and they contribute to material transport by means of diffusion [149].

It has been reported that the Uranium compact requires a temperature of about 85% of the melting temperature for densification to start. In comparison to the densification temperature of U, metals like Zr, Ni start shrinking at a temperature around 45% of their melting temperatures while Th begins to shrink at temperature 65% of its melting temperature [148]. In case of U metal powder two phase changes take place during heating. First at 937 K (α U having orthorhombic structure changes to β U which is tetragonal) and other at 1040 K when β U changes to γ Uranium which has cubic structure. The density of α U is 19.07gm/cc, β U is 18.11gm/cc and γ U is18.06gm/cc. It is observed that as the temperature increases density of the metal decreases. In other words volume increases. So increase in volume due to phase transformation dominates shrinkage due to sintering. This phenomenon continues up to 1125K at which shrinkage initiates. Hence it may infered that phase transformation hinders and delays sintering of the U metal powder.

Fig. 4.10 shows the shrinkage plot for U-15wt%UO_2 and U-30wt%UO_2 cermet. It is observed that the shrinkage initiates above 1125 K, which is about 82% of the solidus temperature of the cermet (fig.4.9). This is high sintering temperature when compared to melting temperature of the U metal.

Solidus temperature of the U-15wt%UO_2 cermet fuel is around 1370 K, as observed from the DTA plot in fig.4.9.This shows that the fuel has fairly high solidus temperature which is favourable for higher in- reactor operating temperature of the fuel. It is observed from the fig.4.9 that in DTA plot solidus temperature peak is smaller compared to phase transformation peaks. In general, the enthalpy of melting is higher than the solid state phase transformation for the materials.This is also true for U metal if it is heated to high temperature in very pure environment. It may be noted here that the uranium metal is highly reactive in nature.The melting peak of uranium was found to be significantly lower because of the high temperature oxidation of uranium metal. The oxidation is exothermic in nature which leads to decrease in height of melting endotherm.

Coefficient of thermal expansion is an important fuel design parameter. Larger coefficient of thermal expansion is good from safety consideration as it provides substantial negative reactivity feedback with the rise of fuel temperature in case of reactor transient [150]. When the fuel expands, the distances between the fissile nuclei increase. This slows the chain reaction because the neutrons necessary to drive the reaction strike fewer fissile nuclei, thus resulting in negative reactivity. Thermal expansion vs. temperature plot (fig.4.12) for sintered cermet shows that there are phase transformations in the temperature range from ambient to 1373 K. The first phase change is observed at 937 K and the second at 1040 K. The phase change occurs at the same temperature as that observed on heating U powder. The calculated average coefficient of linear thermal expansion is 17.08×10^{-6} K^{-1} for U-15wt%UO_2 and 12.8x 10^{-6} K^{-1} for U-30wt%UO_2 composition for temperature range $473 < T \leq 923$ K. The coefficient of thermal expansion is lower for U-30wt%UO_2 as compared to U-15wt% UO_2 because of presence of UO_2 which has lower thermal expansion than the U metal. The thermal expansion coefficient for U-15Pu-10Zr is reported to be 17.6×10^{-6} K^{-1} for $298 < T \leq 900$ K [151]. The thermal expansion value for the U-15wt% UO_2 cermet fuel is close to the reported value of U–15Pu–10Zr which is considered to be a worthy parameter for the safe operation of fuel during transient.

Thermal conductivity was measured by TPS method. By this method the thermal conductivity value is calculated directly, unlike the laser flash technique where thermal conductivity data is calculated by measured thermal diffusivity value, measured density and estimated specific heat value. However one negative side of this method of measurement is pre-requisite of bigger size sample to conduct the experiment. Thermal conductivity of U-30wt%UO_2 cermet is lower than U-15wt%UO_2 cermet as observed from the fig.4.13. This indicates that the addition of UO_2 results in lowering of thermal conductivity of cermet. It is observed that thermal conductivity increases with increase in temperature. This is certainly due to the higher contribution of U to the overall thermal conductivity at higher temperatures. The thermal conductivity of a material is mainly due to lattice/phonon and electronic contribution

It can be expressed as $\lambda = \lambda_l + \lambda_e$

where, λ_l and λ_e are the lattice and electronic thermal conductivities.

Thermal conductivity of ceramic UO_2 decreases with temperature. In a ceramic, phonons are important contributor for thermal conductivity. The decrease in conductivity with temperature is due to the phonon-phonon and phonon-defects scatterings.

The thermal conductivity of U increases with temperature contrary to other metal where it falls. In a metal, electrons are free to move and thus electronic contribution dominates thermal conductivity. In case of uranium the increase in thermal conductivity with temperature is mainly due to the electronic contribution.

Thermal conductivity of cermets U-15wt% UO_2 and U-30wt% UO_2 was found to be 15 W/m K and 8 W/m K respectively at 873 K compared to 4.68 W/m K for 100 % dense UO_2 [152] and 38 W/m K for pure U [153] at the same temperature. The thermal conductivity value for U-15wt% UO_2 cermet is near the average value reported for U-20Pu-10Zr metallic fuel [55]. Higher thermal conductivity is beneficial as it results in a low centreline operating temperature of the fuel at a higher linear power rating [151]. Calculation was carried out to find whether composite follows simple rule of mixture or logarithmic rule of mixture for thermal conductivity values obtained from experiment. It was concluded that data of thermal conductivity values were governed by logarithmic rule of mixture which is illustrated as follows.

U-15 w%UO_2

Volume of U in the cermet =85/ 19.1 (Considering density of U as 19.1 gm/cc) = 4.45 cc

Volume of UO_2 in cermet= 15/10.96 (Considering density of UO_2 as 10.96 gm/cc) =1.37 cc

Volume fraction of U=4.45/ (4.45+1.37) =0.77

Volume fraction of UO_2=1.37/ (4.45+1.37=0.23

Now applying logarithmic rule of mixture (K for UO_2 & U is 4.68 Wm/K & 38 Wm/K respectively at 873 K)

Log K=0.77*log 38+0.23*log4.68=1.21+0.154=1.36

Therefore K=22.90, Considering 80 % density of cermet K is nearly equal to 18 W/mK and this reading is close to the value obtained by experiment.

U-30 w%UO_2

Volume of U in the cermet =70/ 19.1 (Considering density of U as 19.1 gm/cc) = 3.66 cc

Volume of UO_2 in cermet= 30/10.96 (Considering density of UO_2 as 10.96 gm/cc) =2.73 cc

Volume fraction of U=3.66/ (3.66+2.73) =0.57

Volume fraction of UO_2=2.73/ (3.66+2.73) =0.43

Now applying logarithmic rule of mixture ((K for UO_2 & U is 4.68 Wm/K & 38 Wm/K respectively)

Log K=0.57*log 38+0.43*log4.68=0.90+0.28=1.18

Therefore K=15.13, Considering 80 % density of cermet K is nearly equal to 12W/mK and this reading is close to the value obtained by experiment.

The microstructure of the cermets show the presence of bright U and dark UO_2 phase in the fuel matrix as observed in figs.4.14 & 4.15. For U-15wt%UO_2 composition, the area fraction of bright U phase is observed to be more as compared to the other composition. XRD result revealed presence of α U and UO_2 phases in the fuel for both the compositions. Absence of any other peak is an evidence of the fact that there is no any other phase formed during the course of heat treatment. Sinha etal.[154] have worked with three compositions namely 20, 25 and 30 wt%UO_2 in U metal matrix also report similar results of XRD analysis. They have estimated phase percentages of U and UO_2 in the fuel matrix in terms of volume by image analysis technique. In the present work the percentages of phases in the fuel matrix were quantified using direct method [155]. The estimated value of UO_2 phase percentage in U-15wt%UO_2 and in U-30wt%UO_2 composition was 19wt % and 34wt % respectively. The difference between the actual and the estimated phase percentage of UO_2 may be due to non-homogeneity in the distribution of the UO_2 particles in the fuel matrix. An attempt was made for estimation of phase fraction by XRD method. It being an NDT technique, recycling of the radioactive fuel is possible.

The interaction between U and UO_2 interface is not revealed in SEM examination. This is probably due to the presence of sintered UO_2 particle having O/M ratio near 2.0 and heat treatment in an inert argon atmosphere which rules out the possibility of formation of UO_2 oxides with higher O/M ratios. Decrease in the O/M ratio below 2.0 and release of oxygen may happen at a higher temperature like 1900 K in vacuum but that condition does not exist in the present case [156].

Porosities are observed inside UO_2 phase as well as in the inter particle region between U and UO_2 phase, as seen in figs. 4.16 & 4.17. The geometrical density of sintered UO_2 compacts used for the cermet was around 95% TD. The sintered pellets had nearly 5% porosity. These pellets were crushed and powder obtained subsequently was used for cermet fuel fabrication. The impression of the pores in the UO_2 particles dispersed in cermet is from the pores which were present in the UO_2 pellets before crushing. The available porosities in the fuel matrix act as site for the entrapment of fission products, resulting in lower damage of the fuel by fission product accumulation and lower swelling as compared to metallic fuel [55].

The thermal stability of the fuel compact was found to be fairly good. Any fall out of the fuel particles from the matrix is not observed. O/M ratio of the sintered UO_2 particle dispersed in the fuel compact was near 2.0 and annealing was carried out in inert atmosphere. Hence, the formation of higher oxides of UO_2 and the oxidation of uranium metal matrix may not have taken place.

Fast reactor fuels generally contain Pu/PuO_2 in range of 15 to 25wt %. The composition of the fuel in present study was chosen as U-15% UO_2 and U-30% UO_2. Pu has higher fission crossection for fast neutron compared to U [6] . So in order to compensate for equivalent fission the wt% of UO_2 needs to be enhanced. This was the reason for choosing one of the compositions of cermet with higher wt% UO_2. The values of different thermo physical properties which have been determined in this investigation are comparable to that of U-15%Pu-10%Zr metallic fuel. However the density of the cermet fuel obtained during sintering is around 80% TD. It may appear to be a low density result nevertheless this value of density is acceptable for fast reactor application as the smear density of the fuel pin of fast reactor is maintained around 70-75% TD. This allows the fuel to accommodate swelling during irradiation resulting in lesser stress on the cladding. The presence of porosities in the cermet fuel is useful in reducing the extent of swelling.

5. CHAPTER 5. U-PuO_2, U-PuC, U-PuN Cermet Fuel

Cermet fuel combines beneficial properties of both ceramic and metal and attracts global interest for research as candidate fuel for nuclear reactors. Plutonium bearing U-PuO_2, U-PuC, U-PuN cermet fuels are the new concept as advance fuel for fast reactor. This chapter describes development of flow sheet for fabrication of Pu bearing cermet fuel by powder pellet route. This involves cold compaction of mixed powders followed by sintering. Thermo physical properties of the sintered compacts were investigated. Characterization of the fuel was carried out using Dilatometer, Differential Thermal analysis (DTA), X-ray diffractometer and Optical microscope.

5.1 Preparation of powders of different compounds of Pu

Sintered PuO_2 powder was prepared by heat treatment of raw PuO_2 powder. PuC and PuN powders were produced by carbothermic and carbonitridation reaction respectively. It may be noted that during preparation of PuC powder Pu_2C_3 phase was also formed which could be observed in the XRD pattern of the powder. However for simplicity powder has been mentioned as PuC throughout the manuscript. The details of the preparation of PuO_2, PuC and PuN are mentioned in subsequent sections.

5.1.1 Preparation of sintered PuO_2 powder

PuO_2 powder received from the reprocessing plant was used for sintering. The particle size of PuO_2 powder received from reprocessing plant was around 3-5 µm. PuO_2 powder was mixed with 0.6 % polyethylene glycol (PEG) binder and pressed in the form of tablets of 30 mm dia and 4 mm thickness at pressure of 105 MPa in a hydraulic press. The tablets were loaded in tungsten tray. The trays were stacked in all metal furnace and heated to 1823 K temperature for 4 h in Ar atmosphere. The heat treatment of the powder was done in all metal furnace which uses either Molybdenum or Tungsten tray as charge carrier and heater made up of

Tungsten. So to avoid oxidation of these accessories Ar as inert atmosphere was used .The total heating and cooling cycle was of 15 hrs. The sintered tablets thus obtained were crushed and milled in attritor at 250 rpm with tungsten carbide ball. The powder was then sieved and powders of sizes below 75 µm were used for investigation. Some of the important characteristics of the heat treated powder are given in table 5.1 XRD of the crushed powder was carried out to know different phases present (fig 5.1)

Table 5.1. Characteristics of different powders used for cermet fabrication

Material	Surface area(m^2/gm)	Apparent density(g/cm$^{3)}$	% of main Constituent (wt. %)	Moisture (wt. %)	Total impurities	O/M
PuO_2(after sintering)	0.5 to 1	2.0	Pu=87.6	<0.2	<1500	2
PuC powder	0.7-0.8	4.15	N_2=0.005, C=5.0	-	-	
PuN powder	0.65-0.75	4.5	C=0.011 N_2=5.50	-	-	

5.1.2 Preparation of sintered PuC powder

PuC powder was prepared by carbothermic reduction of PuO_2 by C under vacuum [106]. PuO_2 and nuclear grade graphite powders were taken as starting material. The proportion of two powders was calculated as per stoichiometry in Eq. (1) and a batch of 200 gms was prepared. The two different powders were mixed thoroughly in attritor at 100 rpm for 90 minutes. 0.4% oleic acid was added in the powder mixture.

$$PuO_2 + 3C \leftrightarrow PuC + 2CO\uparrow \qquad (1)$$

The blended powders were compacted at 105 MPa in hydraulic press to fabricate tablets of 30 mm dia and 4 mm thickness. The tablets were loaded in tungsten tray and heated in all metal furnace. The temperature of furnace was raised to 1773K under vacuum of the order 0.2 pascal and carbothermic reduction continued for 4 h at this temperature. The clinkers obtained from the furnace were crushed and milled in attritor. The milled powder was sieved to obtain particle size between 75 and 20 µm. The left over particles up to 25% (of the amount taken for dispersion) below 20 µm were also recycled [157] . It may be noted that the volume fraction of dispersed particles is fixed because of the fixed composition.The size range of the particles was chosen from the point of performance of fuel in the reactor. The size of the particles should be such that the fission recoil zone of the two particles should not overlap each other else the virgin matrix available for heat transfer will get reduced and overall heat transfer will get affected [36]. The powder was characterized for O_2, N_2 and C content (table 5.1). XRD of the powder was carried out to determine the phases present (fig.5.2)

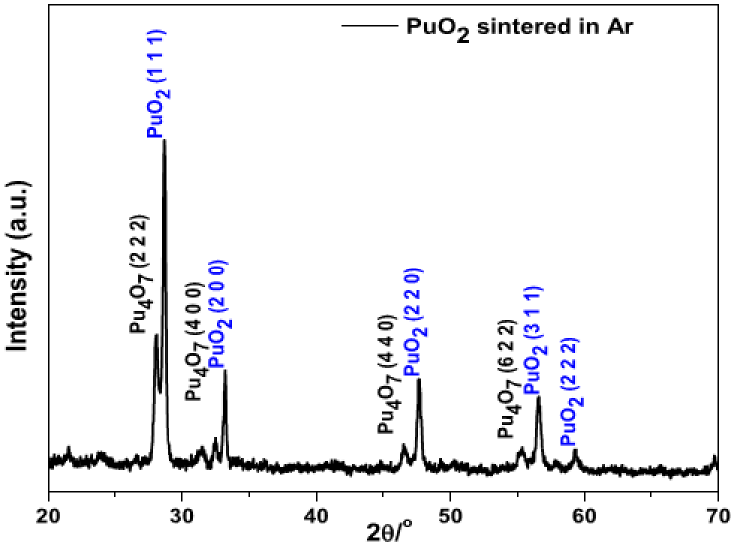

Fig. 5.1. XRD patterns of sintered PuO_2 powder

5.1.3 Preparation of sintered PuN powder

PuN was prepared by carbonitridation method [106]. The proportion of the PuO_2 and C was decided from the chemical Eq. (2) mentioned below

$PuO_2 + 2C + 0.5\ N_2 \leftrightarrow PuN + 2CO\uparrow$ (2)

PuO_2 and graphite powder were weighed in proportion as mentioned above and a batch of 200 gm was prepared. The powders were mixed together in a stirred ball mill for 90 minutes at 100 rpm. The mixed powder was compacted into tablets of 30 mm dia and 3mm height at 105 MPa. The tablets were loaded in charge carrier made of tungsten and heated in all metal furnace. The temperature was raised to 1773 K in 100 minutes in presence of N_2 atmosphere and maintained for 15 h, followed by 4 h soak in presence of N_2+H_2 atmosphere at same temperature. Nitrogen plays the dual role of a reactant and carrier gas for removal of CO. The furnace was cooled to 873 K in 90 minutes followed by natural cooling. The total cycle of the furnace is shown in the fig.5.3. The product from the furnace was crushed and milled for 120 minutes in attritor at 250 rpm with tungsten carbide ball to obtain fine powder. The powder was analysed for O_2, C and N_2 impurities. The different characteristics of powder are shown in table 5.1.The milled powder was sieved to obtain powder particle size below 75 μm. XRD on powder was carried out to estimate different phases present. Fig.5.4 shows the XRD pattern for PuN compound.

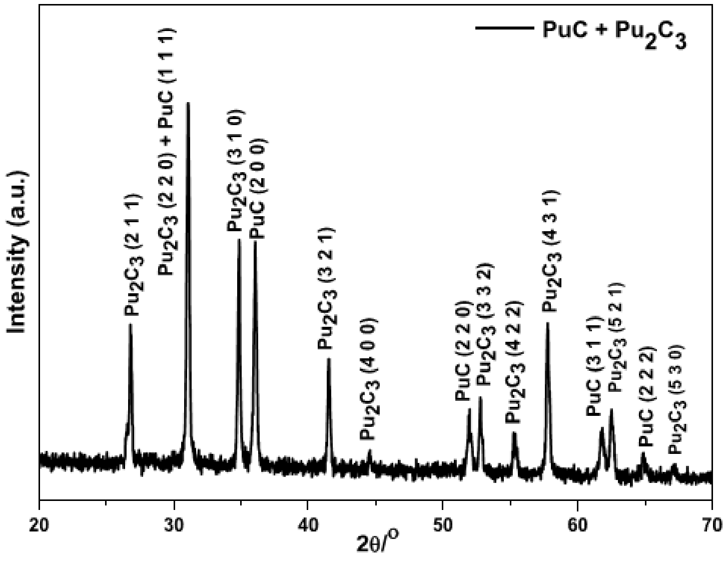

Fig. 5.2. XRD patterns of sintered PuC powder

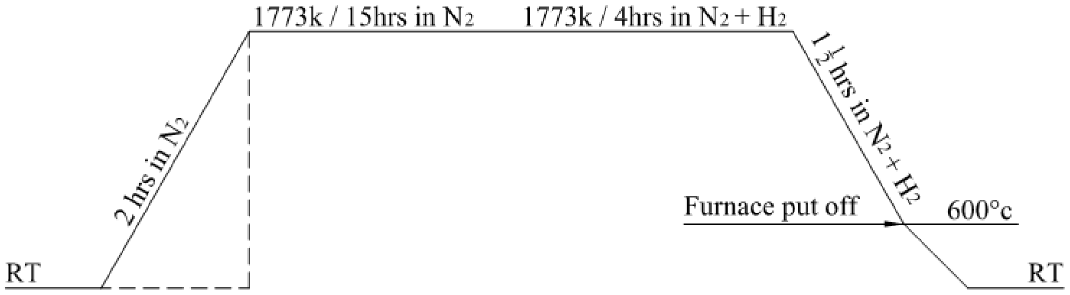

Fig. 5.3. Heating and cooling cycle for fabrication of PuN

5.2 Fuel pellet fabrication

For the preparation of fuel pellets, each of these powders was mixed with U powder. For each powder, three compositions were tried.

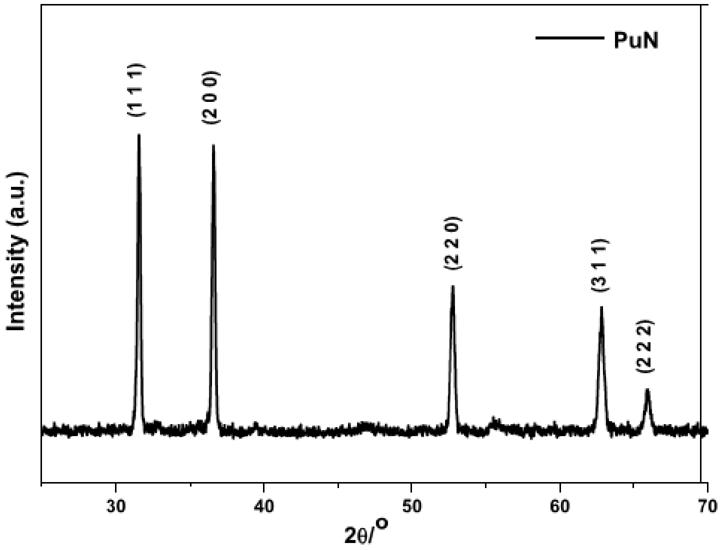

Fig. 5.4. XRD patterns of sintered PuN powder

For example for PuO_2 powder cermets of composition U-15 wt. % PuO_2, U-20wt% PuO_2 and U-25 wt. % PuO_2 were fabricated. Likewise U-PuC and U-PuN cermets were also prepared using identical proportion. Uniform mixing of the powders was ensured using a blender. Compaction was done at different pressure varying from 500 MPa to 1050 MPa using a double action hydraulic press. Fig. 5.5 shows the flow sheet developed for the fabrication of the cermet compacts. Sintering of the green pellets was carried out in argon atmosphere at 1223 K for 8 hrs. The variation in density of the green and sintered pellet with pressure is shown in fig.5.6 and fig.5.7 respectively.

U, PuC, PuN powders are very much prone to oxidation and pyrophoric in nature.The oxidation of all the three powders is likely to change the sintering behavior of the compact. Hence handling of the powders need dry boxes filled with protective atmosphere like argon or helium. Dynamic flow of the argon gas was maintained inside the glove-box during the entire process of fabrication. The O_2 and H_2O level in the glove box was maintained below 10 ppm. Figs. 5.8, 5.9 and 5.10 show photographs of sintered cermets U-PuO_2, U-PuC and U-PuN respectively.

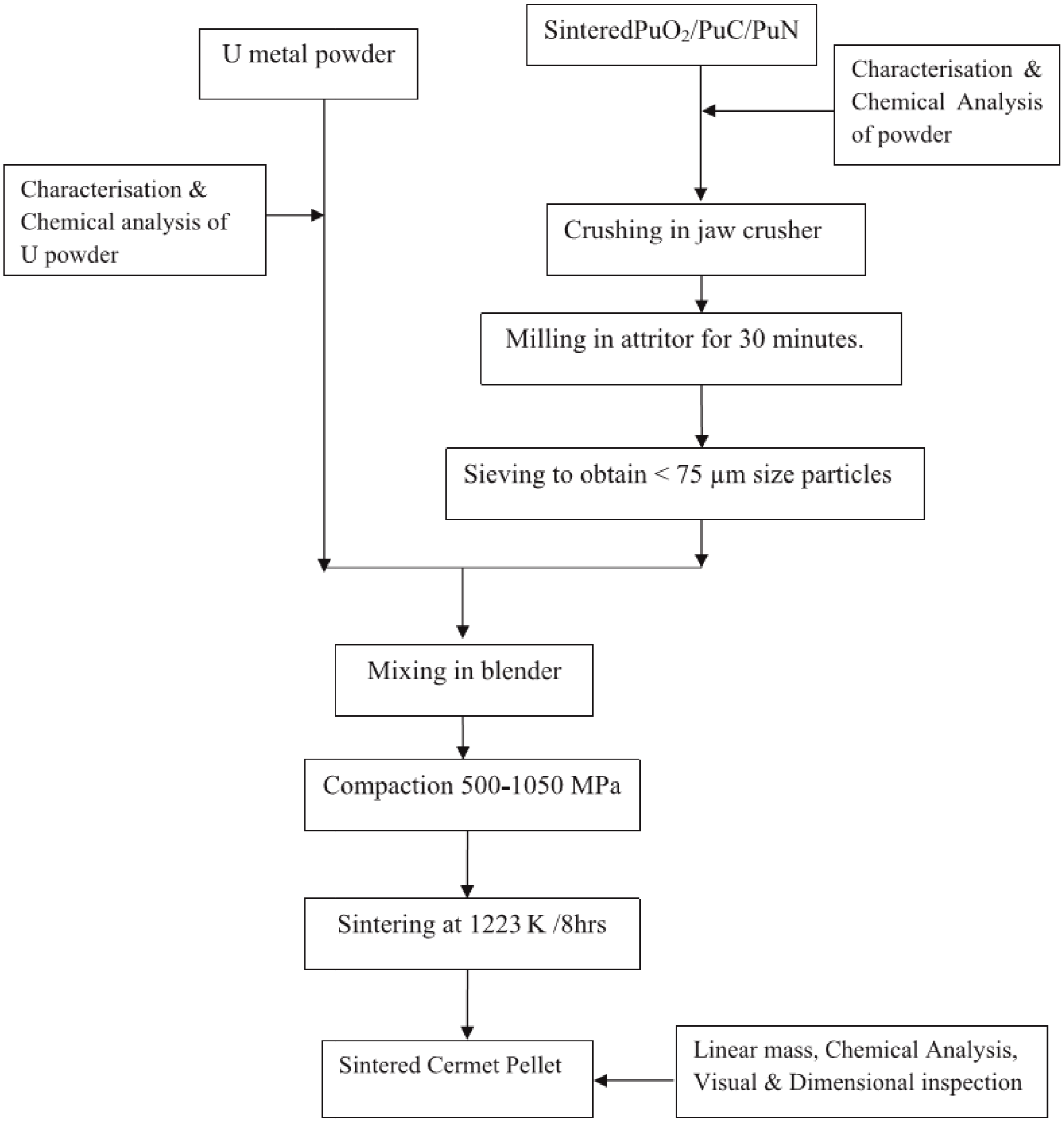

Fig. 5.5. Flow sheet for the fabrication of cermet fuel compact

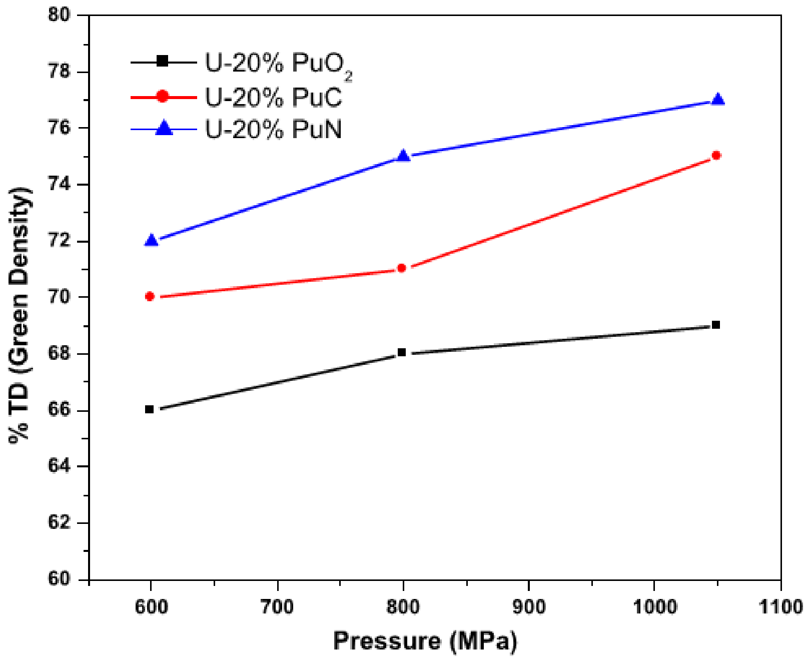

Fig. 5.6.Density vs. Compaction pressure plot of green pellets of U-20wt%PuO_2, U-20wt%PuC and U-20wt%PuN

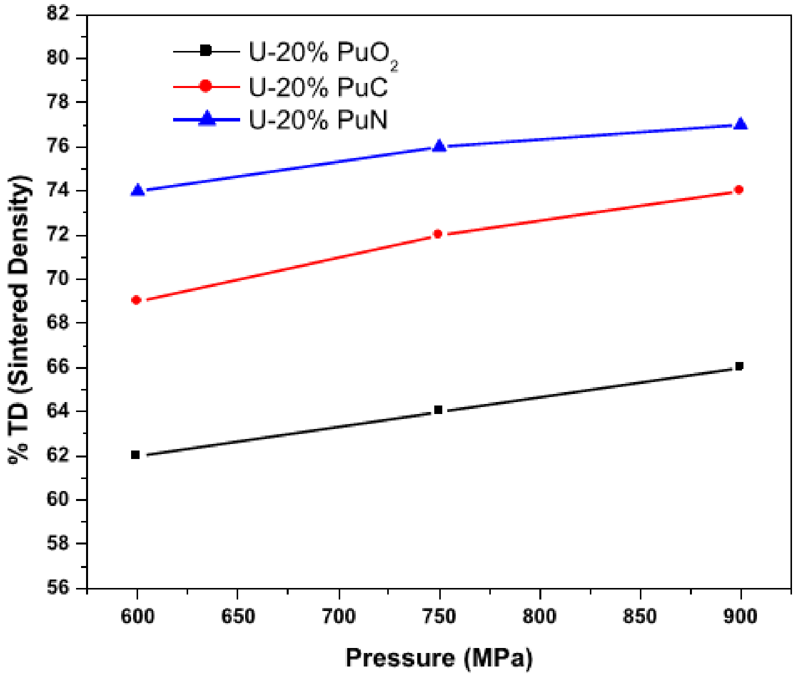

Fig. 5.7. Density vs. Compaction pressure plot of sintered pellets of U-20wt%PuO_2, U-20wt%PuC and U-20wt%PuN

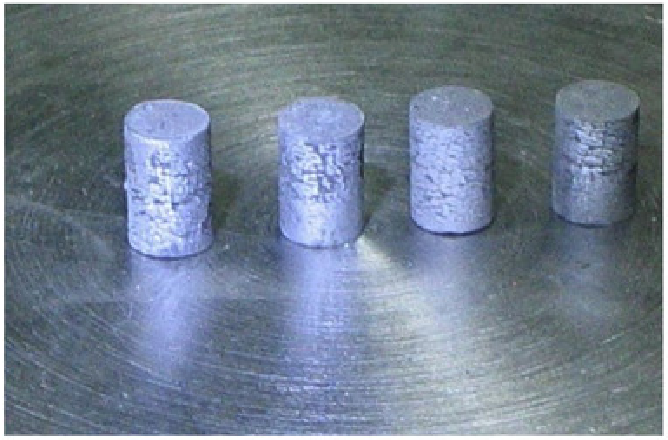

Fig. 5.8. Photograph of sintered U-20wt%PuO_2 cermet pellet

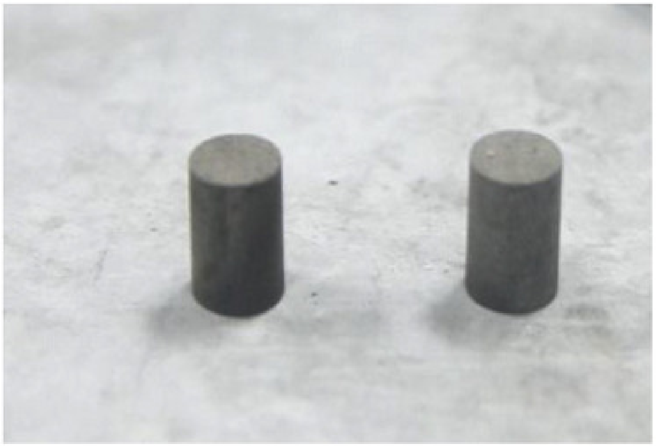

Fig. 5.9 Photograph of sintered U-20wt%PuC cermet pellet

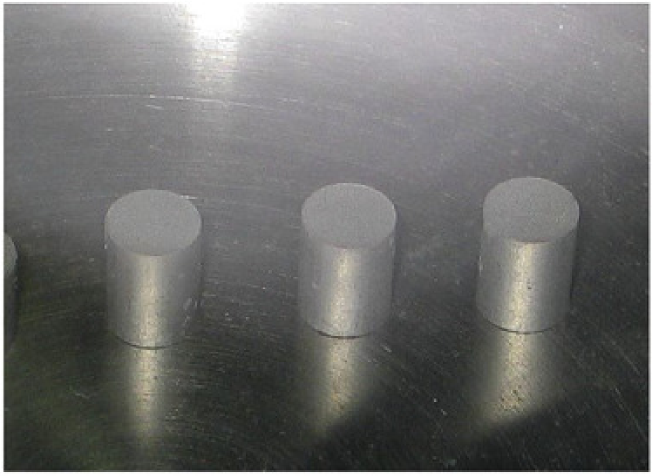

Fig. 5.10. Photograph of sintered U-20wt%PuN cermet pellet

5.3 Results

5.3.1 DTA

Fig. 5.11 shows the phase transformation plot for U, U-15%PuO_2 and U-20%PuO_2 obtained through DTA experiment. Fig. 5.12 shows variation of phase transformation temperature with respect to composition. It is observed from the plot that as PuO_2 content in cermet increases; various phase transformation temperatures (e.g. $\alpha \rightarrow \beta$, $\beta \rightarrow \gamma$ and solidus) of cermet shift to lower value as compared to that of U metal. Similar results were observed in case of U-PuC and U-PuN cermet as shown in fig. 5.14 and fig. 5.16 respectively. In fig. 5.17, comparison of phase transformation temperatures for three different cermets having similar weight fraction i.e. U-20%PuO_2, U-20%PuC and U-20%PuN is depicted.

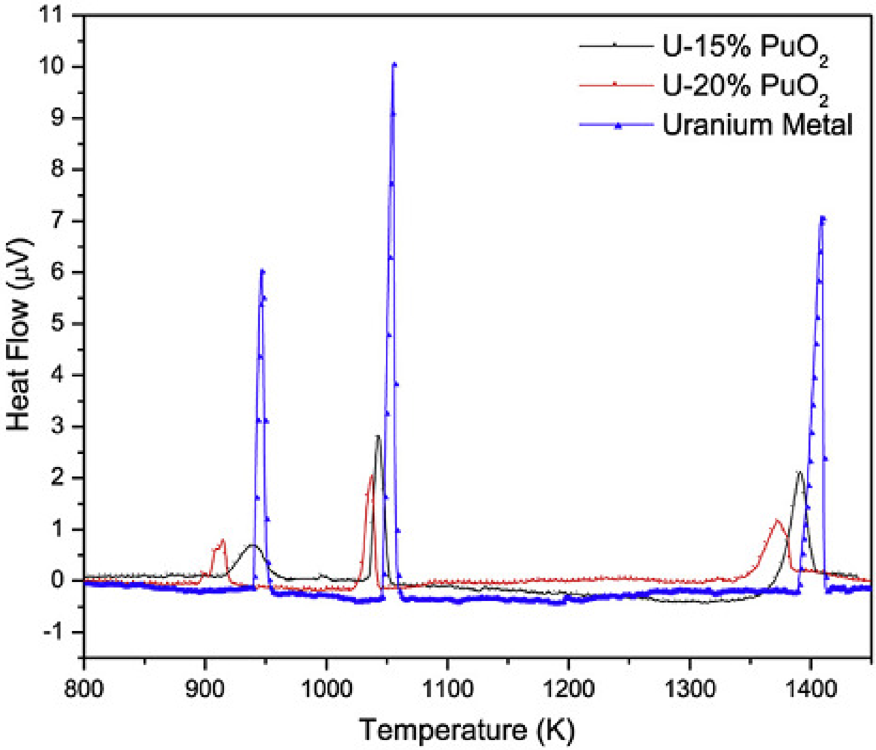

Fig. 5.11. Phase transformation plot of U-15wt%PuO_2, U-20wt%PuO_2 and U with temperature

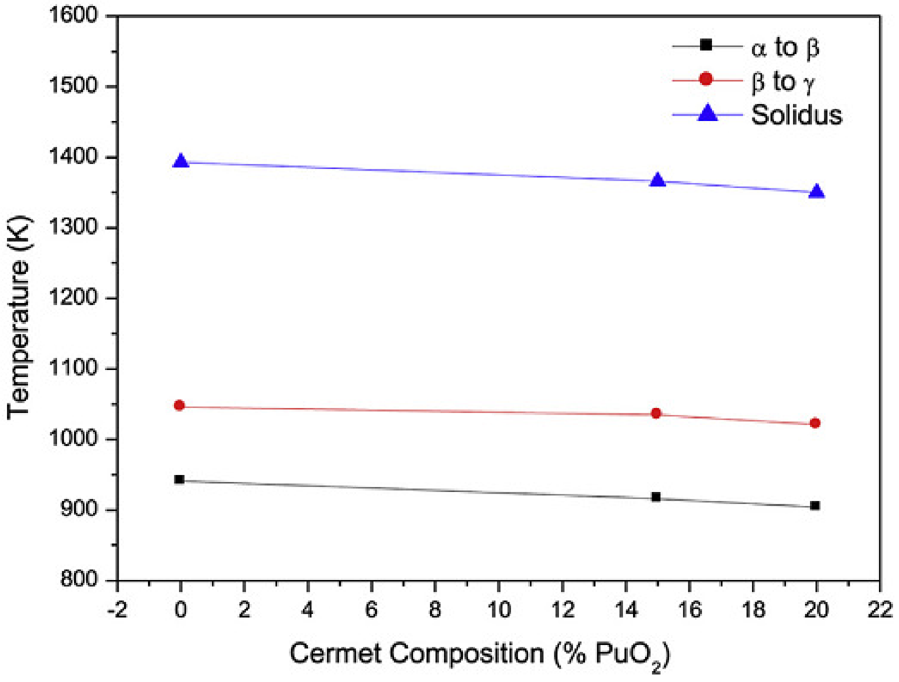

Fig. 5.12. Variation in phase transformation temperature with respect to composition

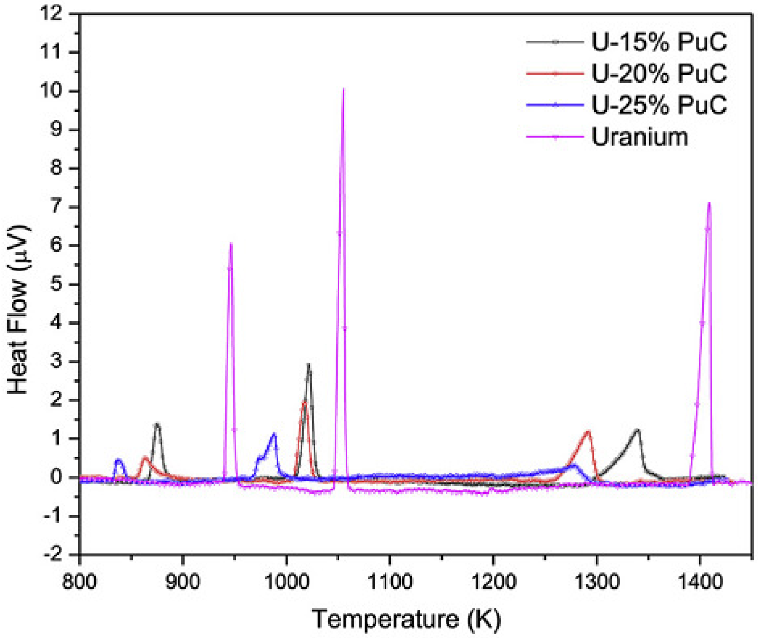

Fig. 5.13. Phase transformation temperature of (a) U-15wt%PuC, U-20wt%PuC and U-25wt%PuC cermet with temperature

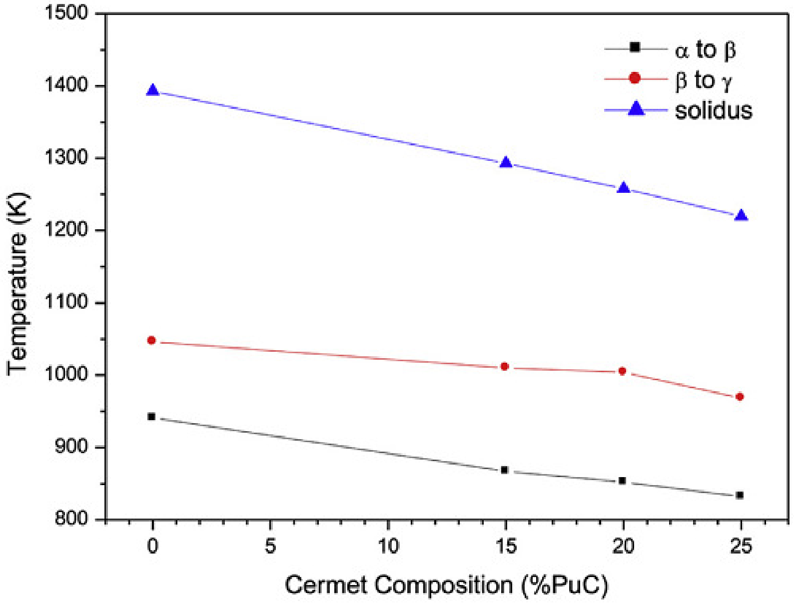

Fig.5.14. Variation in phase transformation temperature with respect to composition.

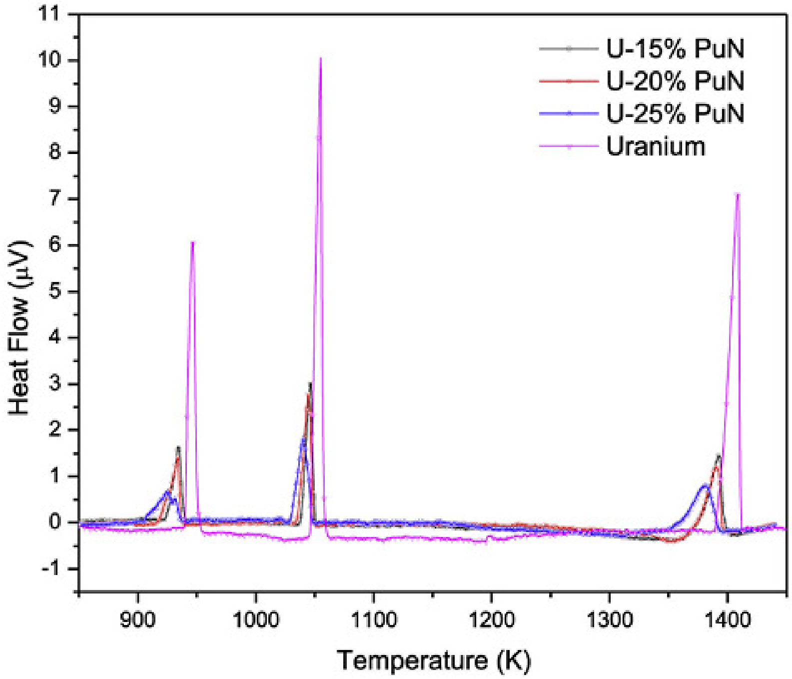

Fig. 5.15. Shows phase transformation for different U matrix PuO_2/PuC/PuN cermet, with respect to change in temperature

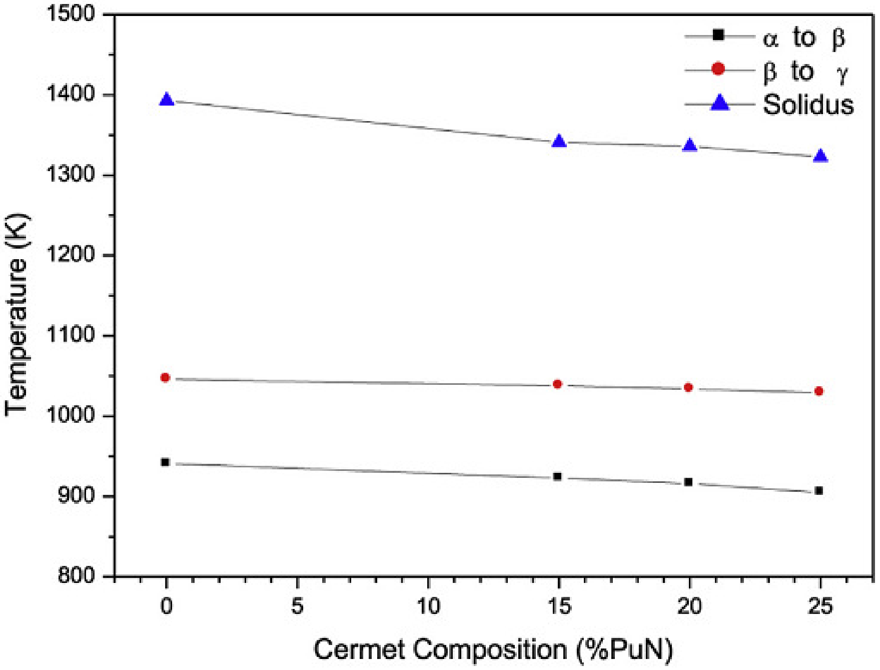

Fig. 5.16. Variation in phase transformation temperature with respect to composition

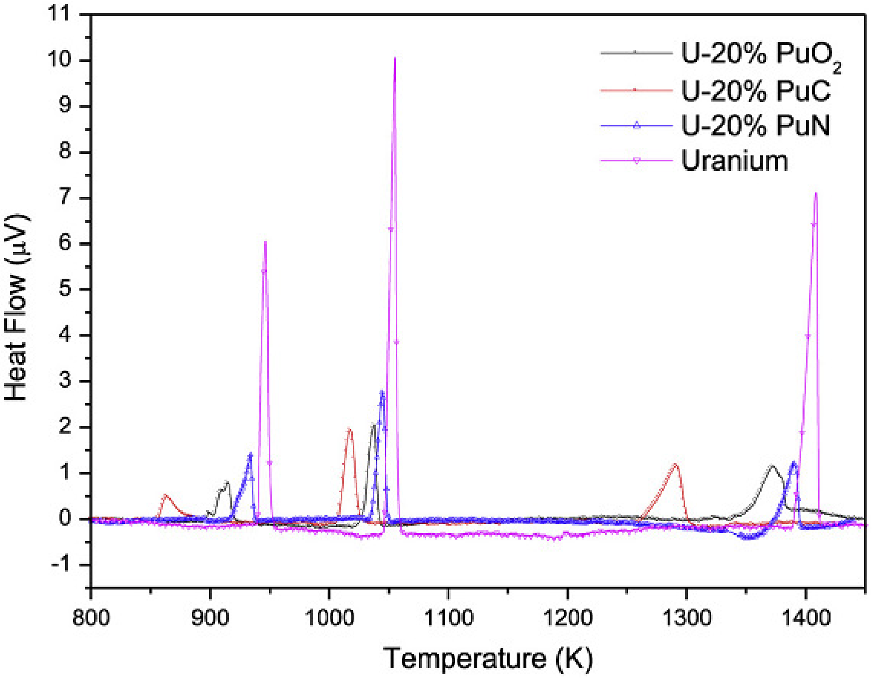

Fig. 5.17. Shows phase transformation for different U matrix PuO_2/PuC/PuN cermet, with respect to change in temperature

5.3.2 Thermal Expansion

Fig. 5.18 represents the plot of thermal expansion data as a function of temperature for all the three U matrix cermet fuels containing 20wt% ceramic particles. Two distinct phase transformations are observed for the cermets in the temperature range from 400 K to 1350 K. Coefficient of linear thermal expansion was determined from the experimental thermal expansion data. The third degree polynomial equations (validity: 373K to 823 K) of percentage thermal expansion data with respect to temperature for above three compositions are given below (Eq. (4)-(6)).

U-20%PuO_2:

$$(\Delta L/L_0)\times 100 = 0.039 - 3.908\times10^{-4}\times T + 3.162\times10^{-7}\times T^2 + 2.739\times10^{-9}\times T^3 \qquad (4)$$

U-20%PuC:

$$(\Delta L/L_0) \times 100 = -0.788 + 0.004\times T - 7.634\times 10^{-6} \times T^2 + 6.659\times 10^{-9}\times T^3 \qquad (5)$$

U-20%PuN:

$$(\Delta L/L_0) \times 100 = -0.750 + 0.004\times T - 6.804\times 10^{-6}\times T2 + 5.859\times 10^{-9} \times T^3 \qquad (6)$$

where, L_0 is the initial length (at 298 K) and ΔL is the difference between the instantaneous length at any temperature T and L_0.

The average coefficient of linear thermal expansion, for the temperature range 373-823 K, has been determined and was found to be 30.81×10^{-6} /K, 27.34×10^{-6} /K and 23.74×10^{-6} /K for U-20%PuO2 , U-20%PuC and U-20%PuN cermet respectively.

5.3.3 Thermal conductivity

Thermal conductivity of the fuel could be measured directly by TPS method as described in chapter 3 for UO_2 bearing cermet. However this method was not used for Pu bearing cermet because sample size required in TPS method is large as compared to that needed in laser flash technique.

For Pu bearing cermet laser flash technique was used for measurement of thermal conductivity. To begin with the thermal diffusivity was calculated using $t_{1/2}$ value obtained from the experiment using relation:

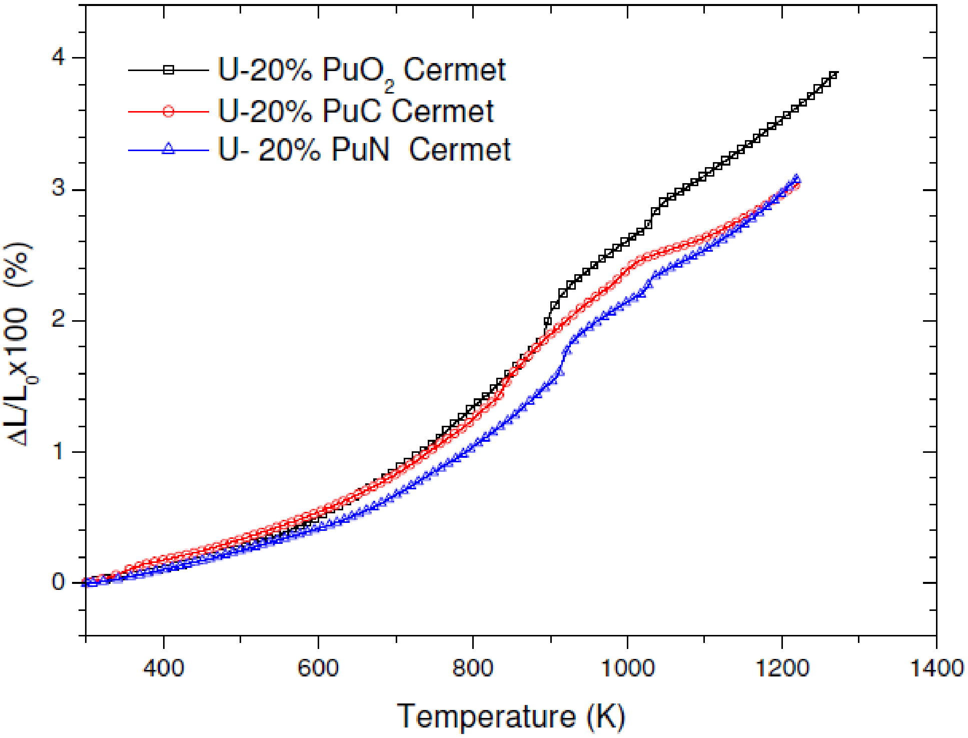

Fig. 5.18. Thermal expansion behaviour of sintered U-20wt%PuO2, U-20wt%PuC and U-20wt%PuN cermet as observed in dilatometer experiment.

$$\alpha = \frac{W \times L^2}{t_{1/2}} \quad (7)$$

where, α is thermal diffusivity, L is the thickness of the pellet and *W* is correction factor which depends upon the degree of heat losses. The value of the correction factor *W* was taken as 0.139 in the absence of heat loss [158]. Thermal conductivity values were calculated as a product of the measured thermal diffusivity and density and specific heat data from literature as mentioned in Eq. (1). Since the experimental heat capacity data were not available, the values were computed using the measured heat capacity of U, PuC & PuN, taken from the literature [159]. Thermal conductivity was calculated for these cermets by multiplying the measured diffusivity value, calculated heat capacity value above room temperature and the room temperature density value of cermet pellet [160].The thermal conductivity plots for U-20%PuC, U-20%PuN and U-20% PuO_2 cermets are shown in fig.5.19

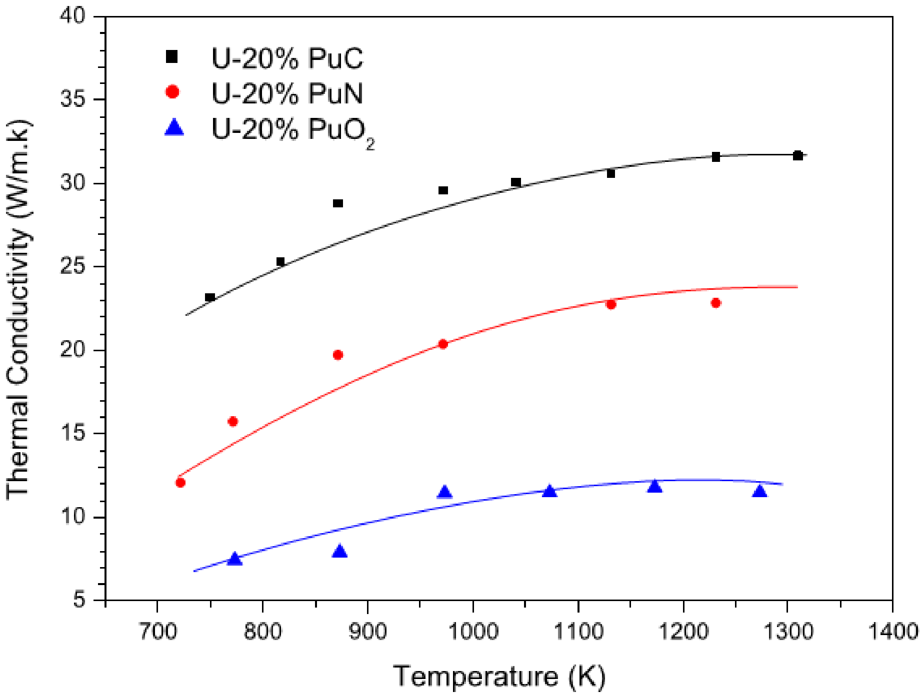

Fig. 5.19. Thermal conductivity plot of U-20 wt % PuC, U-20wt% PuN and U-20wt%PuO2 cermet

5.3.4 Microstructure and phase analysis

Optical micrographic examination of the sintered pellets was carried out to study the distribution of Pu compounds in the uranium matrix. Uniform distribution of ceramic particles in the U matrix was observed as shown in fig. 5.20 and fig.5.21. Small ceramic particles interspersed in U matrix were observed. Optical micrographic examination for U-PuO_2 samples could not be performed because of poor strength and disintegration of the sample during preparation. The XRD analyses of all these cermets for 20 wt. % compositions of Pu compounds are presented in figs.5.22-5.24. The peaks in the XRD pattern correspond to presence of αU and PuO_2/PuC/PuN phases.

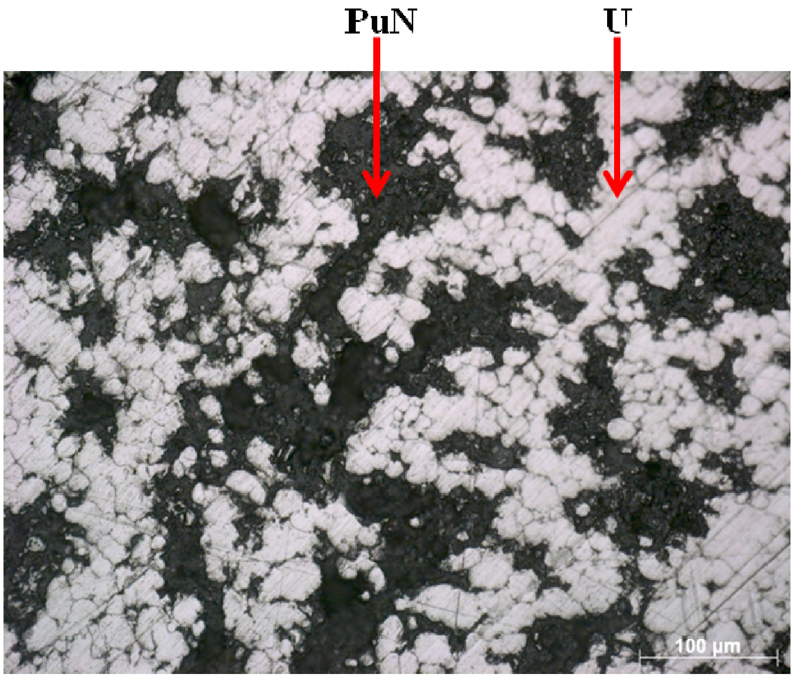

Fig. 5.20. Optical micrograph showing distribution of PuN ceramic particles in U matrix

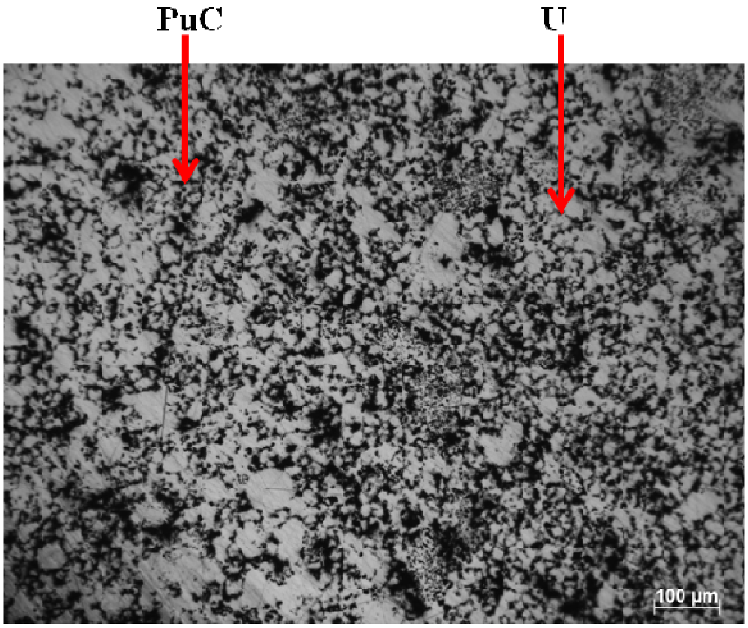

Fig. 5.21. showing distribution of PuC ceramic particles in U matrix Optical micrograph

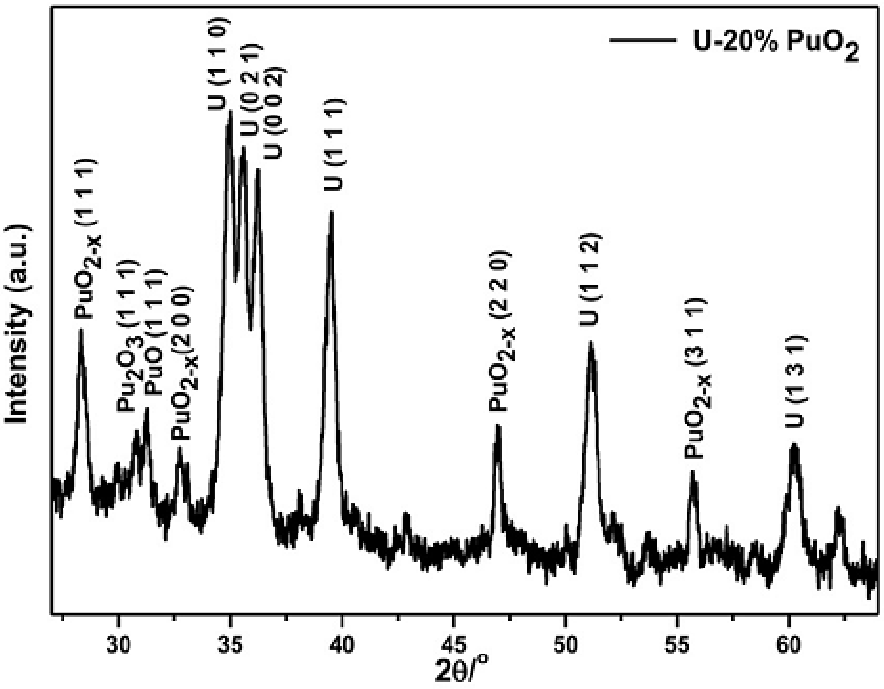

Fig. 5.22. XRD patterns of U-20wt%PuO_2 cermet showing different phases

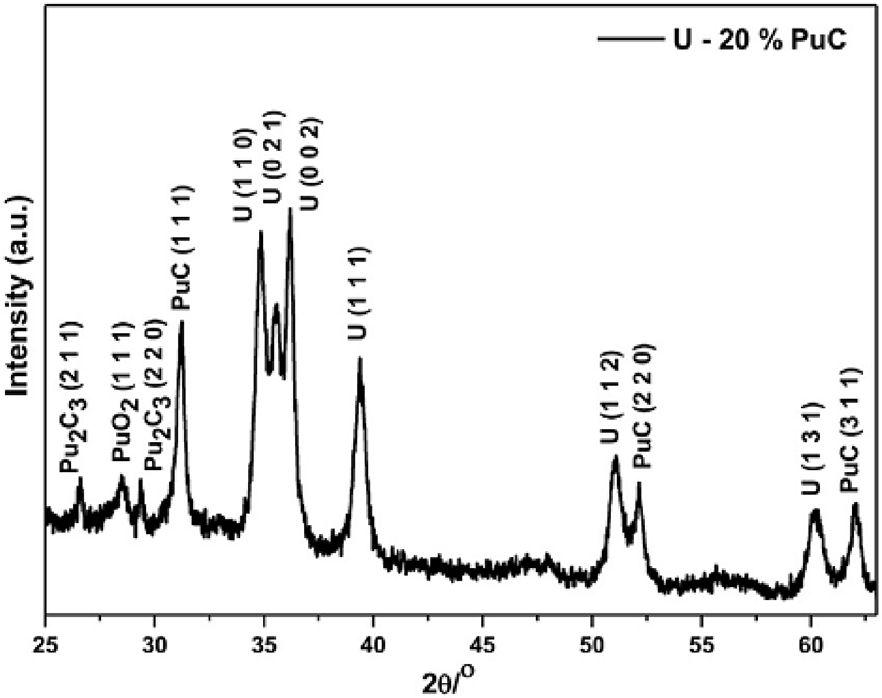

Fig. 5.23. XRD patterns of U-20wt%PuC cermet showing different phases

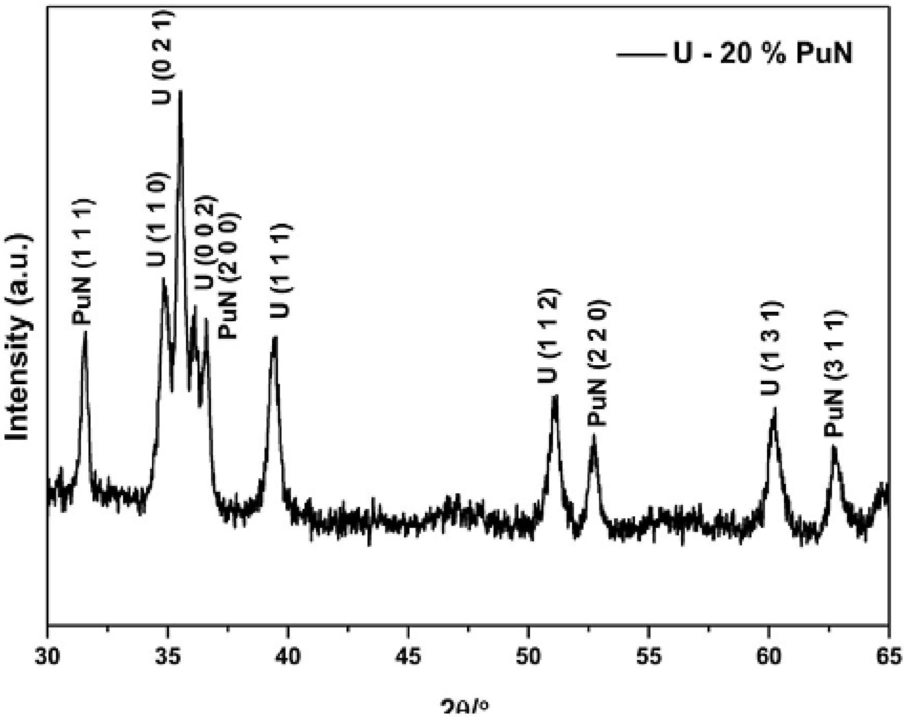

Fig. 5.24. XRD patterns of U-20wt%PuN cermet showing different phases

5.4 Alpha autoradiography

Alpha autoradiography was carried out to examine microhomogenity of plutonium particles dispersed across the cross section of the fuel sample. The autoradiographs are shown in fig.5.25 and fig 5.26. Tracks of Pu are seen distributed uniformly across the cross-section. The tracks of Pu are noticed as discontinuous dark spots uniformly spread in the matrix where as U is observed as comparatively bright region sandwiched between the dots. For both U-15% PuC and U-15% PuN the observation is similar. The alpha autoradiograph sample for U-20%PuO_2 could not be prepared because of poor integrity of the sample.

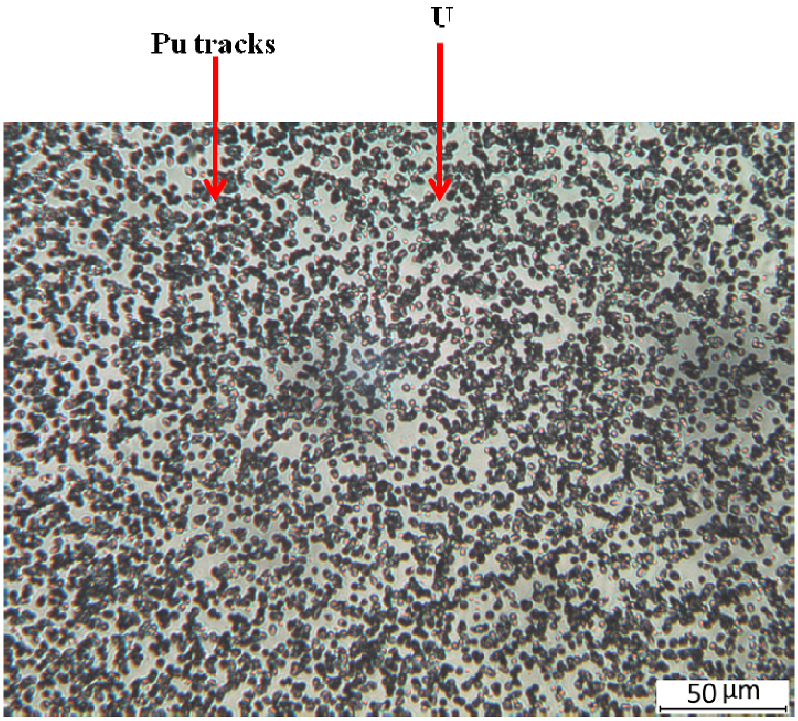

Fig. 5.25. Alpha autoradiograph of U-15%PuC cermet showing Pu tracks

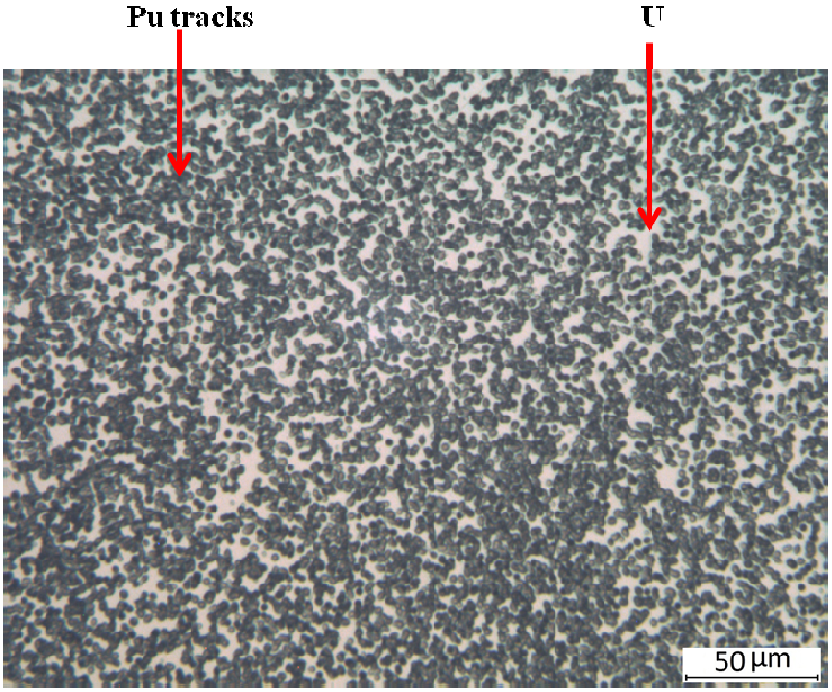

Fig. 5.26. Alpha autoradiograph of U-15%PuN cermet showing Pu tracks.

5.5 Discussion

Uranium metal powders require high pressure during compaction. Oleic acid was used as die wall lubricant to reduce friction between particles and die wall. The compaction pressure was varied from 500 MPa to 1050 MPa. For all the three cases the green density was observed to increase with increase of compaction pressure as shown in fig.5.6.

PuO_2 powder used for the investigation was obtained through PUREX process and Oxalate route [161]. The specific surface area of the powder measured by BET method [162] was 15 m^2/gm. Since PuO_2 is hygroscopic in nature, it has a tendency to absorb moisture. Higher specific surface area of this powder facilitates moisture absorption. The cermet pellets fabricated using as received powder had poor integrity and tendency to expand due to increase in the volume. Therefore, the as received powder was first stabilized by heating it at 1550ºC in presence of Ar. This powder was subsequently used for fabrication of U-PuO_2 cermet pellet. Pu-C system contains four carbides according to the phase diagram [163] shown in Fig. 2.4. In contrast to UC, the monocarbide PuC is always hypostichiometric [106]. Reaction of PuO_2 with C yields four different types of phases namely $PuC_{1-X,}$ PuC_2, Pu_2C_3 and Pu_3C_2 out of which Pu_3C_2 is a high temperature phase. Pu generally forms a hypostiochiometric compound with C.

In the present study preparation of metal carbide resulted in formation of two phases namely PuC_{1-X} and Pu_2C_3. The percentage of these two phases was assessed to be approximately 50% [155]. PuN forms a line compound according to the Pu-N phase diagram [107] shown in Fig. 2.6. Only one compound namely plutonium nitride exists in the Plutonium nitrogen system. The crystal structure of PuN is isomorphous with UN and is thus NaCl type. PuN is considered to be nearly stoichiometric compound below 2127K [164]. The green density of the cermets fabricated by dispersing different compounds of Pu is shown in fig. 5.6.

It is observed that for the same compaction pressure, density is maximum for U-PuN and minimum for U-PuO_2 cermet. This is because density of PuN is higher compared to other Pu compounds (table 5.1). For a given wt%, volume of PuN in U matrix will be less compared to PuO_2 because density of PuN is higher compared to PuO_2. So compaction ratio of cermet containing PuN will be higher compared to PuO_2 resulting in increase in green density.The sintered density of cermet is shown in fig. 5.7. The sintered density of U matrix PuO_2 cermet is low compared to PuC and PuN dispersed cermet. On comparison of figures 5.6 and 5.7 one can see that the both green and sintered density of U-PuO_2 cermet was less for all compaction pressures covered in the study. On investigation it was observed that during heat treatment of PuO_2 powder, Pu_4O_7 phase has formed (fig.5.1). The sintering of U-20wt%PuO_2 cermet, results in formation of α Pu_2O_3 and PuO_{2-X} phases as observed from the XRD pattern (fig. 5.22). From the fig. 2.2 which shows phase diagram of Pu-O system [100] it is observed that for O/M ratio between 1.5 and 2, phases like α Pu_2O_3 and PuO_{2-X} co-exist. α Pu_2O_3 compound has lower density than PuO_2 and its (αPu_2O_3) presence along with the latter results in higher overall volume of the pellet [100].

Table 5.2 ΔG_f^o, melting point and theoretical density values of different compounds of U and Pu [106, 159]

Name of compound	Melting Point (K)	Theoretical Density(gm/cm^3)	ΔG_f^o (Standard heat of formation) at 1223K calories/mole	Relative difference of ΔG_f^o between the compounds at 1223K calories/mole
UO_2	3138	10.96	-208948	11813
PuO_2	2663	11.46	-197135	
UC	2780	11.68	-25968	11888
PuC	1875	13.60	-14080	
UN	3035	14.33	-45876	1934
PuN	2843	14.24	-43942	

Further during sintering reduction of PuO_2 by U may take place resulting in formation of UO_2 as evident from ΔG° vs. T diagram [165] shown in fig.5.27. The UO_2 line lies below PuO_2 line as observed in fig.5.27 which means UO_2 is more stable compared to PuO_2. Thus formation of more stable UO_2 further results in volume increase. Since UO_2 is less dense compared to PuO_2 it will subsequently decrease the density of U-PuO_2 cermet. This could be the reason for lower density observed for U-PuO_2 cermet compared to the other two cermets.

Compounds of Uranium namely UO_2, UC, UN are more stable than compounds of Plutonium like PuO_2, PuC, PuN respectively [106, 159]. Hence, from the thermodynamics point of view, it is possible that Pu compounds get reduced by U to form metallic Pu at high temperature. Subsequently, combination of free Pu, thus formed, with surrounding U may result in formation of (U,Pu) alloy at locations where ceramic particles are present .Thus formation of metal phase will result in the drop of phase transformation temperatures as well as a reduction in solidus temperature of the fuel. As more and more Pu is formed it will lower the phase transformation temperatures and the solidus temperature of the fuel. This is evident from U-Pu phase diagram [166] shown in fig. 5.28. It can be clearly seen from phase diagram that as % of Pu increases the solidus temperature of the alloy reduces. Further when we compare for solidus and other phase transformation temperatures of U-PuO_2, U-PuC and U-PuN of similar composition it is observed that maximum decrease is in case of PuC dispersed cermet and is least for PuN dispersed cermet. A comparison of standard Gibb's free energy of formation for different compounds of Pu is shown in the table 5.2. The table also shows the relative difference of ΔG_f^{o} for different compounds of Pu. From the table it is observed that for UC-PuC and UO_2-PuO_2 cases relative difference of ΔG_f^{o} at 1223 K is 11888 calories/mole and 11813 calories/mole respectively.

The relative difference in Gibb's free energy of formation of UN and PuN compounds is 1934 calories/mole. It is lowest in case of UN-PuN compounds. This may be the reason for comparatively lesser reduction of PuN by U than other two cases, resulting in less release of Pu at localised region in the matrix to alloy with U. Hence fall in solidus temperature is lowest in case of U-PuN cermet. Further it is observed that relative free energy differences for UC/PuC and UO_2/PuO_2 cases are almost similar. However out of U-PuC and U-PuO_2 cermets, the more dip in the solidus temperature is observed in case of U-PuC cermet system. The reason for this deviation may be because of kinetics effect at reaction temperature. The melting point of PuC is less compared to PuO_2; hence mobility of atoms due to diffusion at the reaction temperature for U-PuC system will be higher compared to U-PuO_2 cermet system. Therefore the kinetics of reduction reaction may be more favourable for U-PuC cermet than U-PuO_2 cermet. It is interesting to note that formation of UN is not highly favoured in comparision to formation of UO_2 by reduction of PuO_2 as indicated by Gibb's free energy difference. Even then change in solidus is nearly identical for U-PuN, U-PuO_2 compositions. Though reduction of PuO_2 by U will be more because of high free energy difference but fall in solidus will depend upon kinetics of diffusion of atoms which may not be favourable because of presence of UO_2 layer over Pu particle. Hence, it is expected that the rate of inter diffusion between metal and oxide is slower than that between metal and nitride. Hence the change in solidus appears to be identical.

Solidus temperature of the U-20wt%PuN is highest amongst the three type of cermet studied. It is around 1350K, as observed from the DTA plot in fig.5.17. The designers prefer a fuel that has the higher solidus temperature and therefore U-20%PuN is attractive. Thermal expansion vs. temperature plot (fig.5.18) for sintered cermet shows phase transformations that are matching with DTA results. The coefficient of thermal expansion is lowest for U-20%PuN and highest for U-20%PuO_2 cermet. The coefficient of thermal expansion of U-20%PuO_2 cermet is highest obtained in this study.

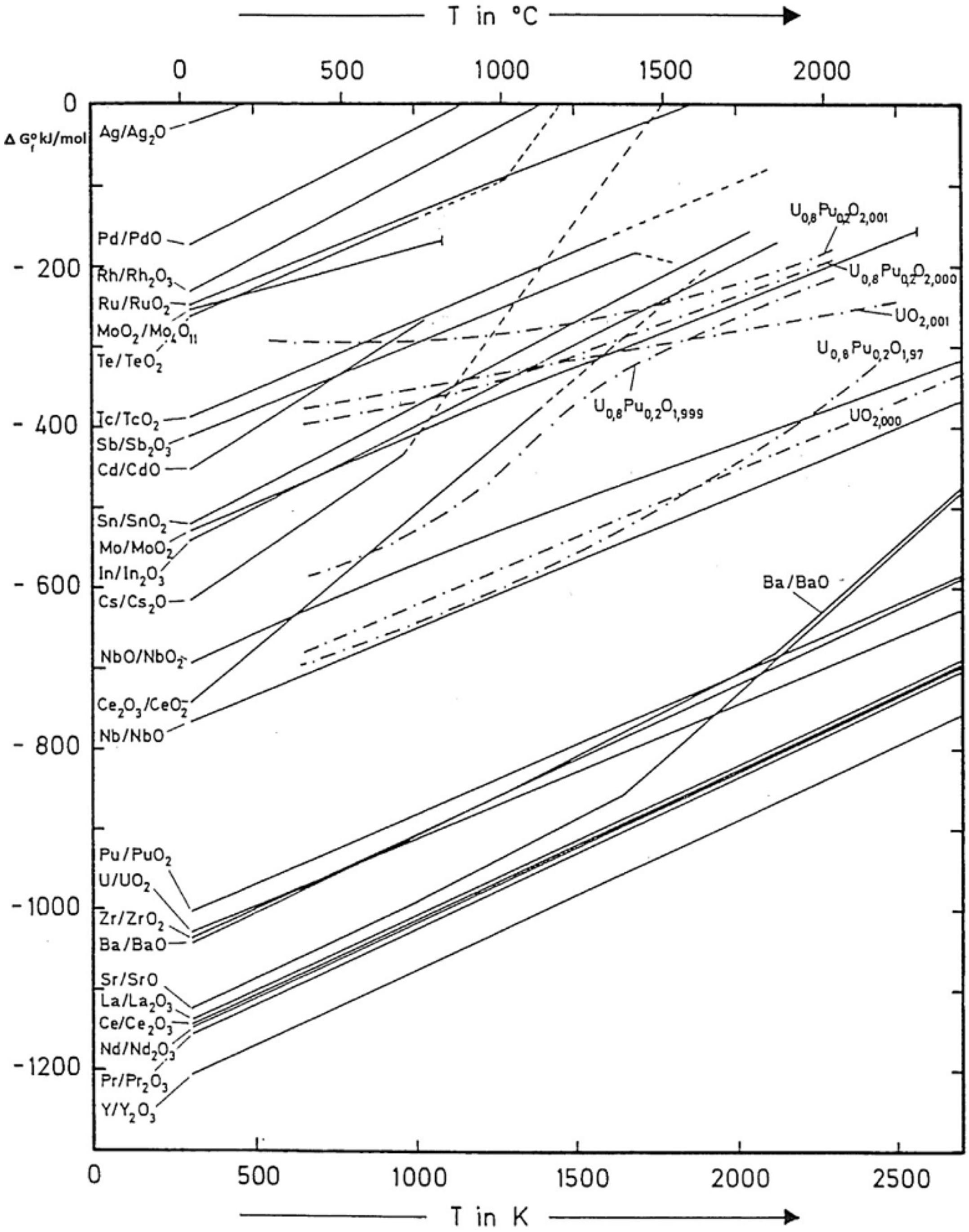

Fig. 5.27.Standard Gibb's Free Energy ΔG^0 vs. Temperature diagram showing position of UO_2, PuO_2 line

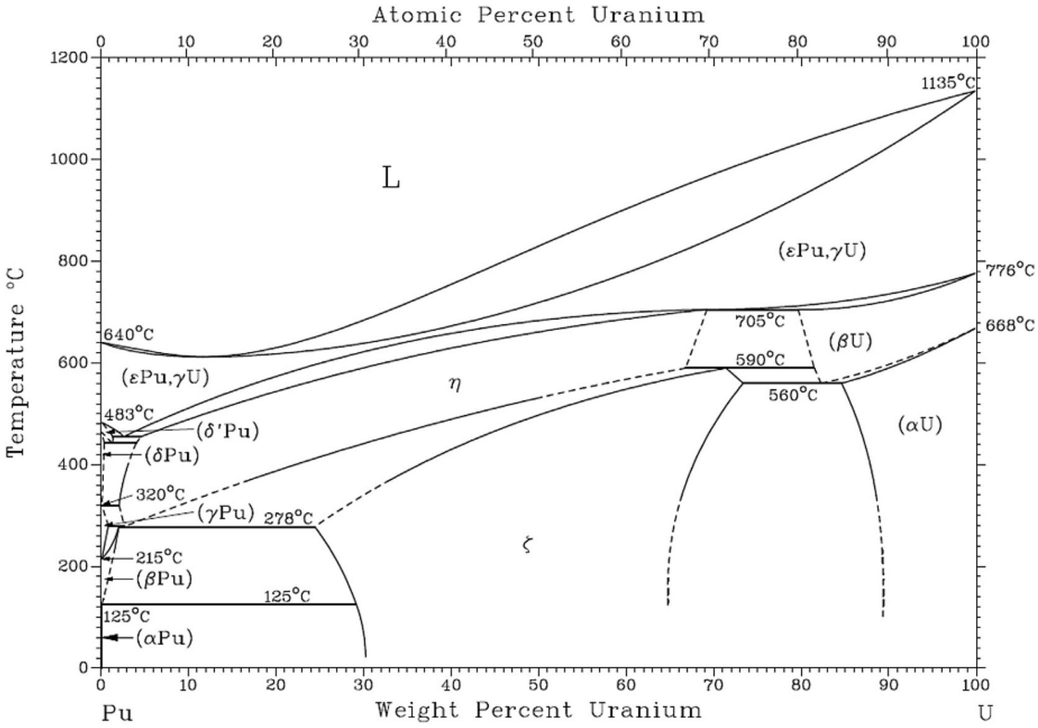

Fig. 5.28. Pu-U phase diagram showing formation of different phases with respect to wt.% U and temperature

As mentioned earlier PuO_2 transforms to Pu_2O_3 at higher temperature. Since Pu^{+3} present in Pu_2O_3 has a larger ionic radius, the fuel pellet containing this compound show higher expansion. The thermal expansion coefficient for U-15Pu-10Zr is reported to be 17.6 $\times10^{-6}$ K^{-1} for $298 < T \leq 900$ K [151] . The thermal expansion value for the all above cermets is of the same order as reported for U–15Pu–10Zr. Larger coefficient of thermal expansion of fuel is good from safety consideration of a nuclear reactor as it provides substantial negative reactivity feedback with the rise of fuel temperature in case of reactor transient [167]. When the fuel expands, the distances between the fissile nuclei increase. This reduces probability of neutron striking a fissile nucleus and resulting fission reaction. Therefore reduction in reactivity of the reactor takes place. Thermal conductivity of U-20%PuC and U-20% PuO_2 are the highest and lowest respectively among the samples covered in this study (fig.5.19).

One of the important factors for higher contribution towards thermal conductivity of U-20%PuC cermet is the presence of almost 50 % Pu_2C_3 in the ceramic phase. The specific heat of Pu_2C_3 [159] is more than double that of PuC which effectively increases overall thermal conductivity of U-20%PuC cermet. Specific heat is less sensitive to defects unlike diffusivity which is very much sensitive. However overall thermal conductivity is decided by product of three components i.e. specific heat, diffusivity and density, so increase in value of any of these components will increase the thermal conductivity. Thus presence of Pu_2C_3 is desirable in the fuel matrix as it enhances the thermal conductivity of the fuel. Its presence is also favourable from irradiation point of view as many fission products generated during irradiation are C seekers which may react with PuC to reduce it to Pu leading to lowering of solidus temperature. Therefore presence of higher carbides of Pu as Pu_2C_3 is sought as it may be helpful in restricting the solidus temperature of the fuel to lower down. PuO_2 has poor thermal conductivity compared to PuC and PuN for any particular temperature and also it decreases with increase in temperature[106, 107, 168] .Therefore U matrix PuO_2 cermet shows the lowest thermal conductivity. Thermal conductivity values of U-PuO_2, U-PuC, U-PuN as determined in this study are 9 W/m K, 25 W/m K and 18 W/m K respectively at 873 K. Thermal conductivity of PuC and PuN is almost same at 873 K being 13 W/m K [106]. The thermal conductivity of PuO_2 is 2.47 W/mK [100] K at the same temperature, which is very low compared to PuC and PuN. On the other hand thermal conductivity of pure U is 38 W/m K [153] at 873 K. The addition of PuO_2 in U matrix results in lowering of thermal conductivity of cermet. However it is observed that thermal conductivity of U-20 wt. % PuO_2 increases with increase in temperature. This is certainly due to the higher contribution of U to the overall thermal conductivity at higher temperatures. Higher thermal conductivity is beneficial as it results in a low centreline operating temperature of the fuel at a higher linear power rating [151].

The optical microstructure for U-20%PuC and U-20% PuN cermet shows the presence of bright U and dark ceramic phase in the fuel matrix as shown in figs 5.20 and 5.21. XRD result revealed presence of αU and Pu bearing phases in the fuel for different cermet. Absence of any other peak is an evidence of the fact that there is no other phase formed during the course of heat treatment.

Alpha autoradiographs (figs 5.25 & 5.26) illustrate the homogeneous distribution of Pu particles in the fuel matrix. This is desirable feature for a fuel as uniformity in distribution of fissile material results in consistent heat generation in the matrix avoiding any hot spot creation. In optical micrograph we see microstructure along with other features like phases etc. but in auto radiograph we see only distribution of plutonium across the cross-section. In Pu active sample it is difficult to prepare optical sample inside glove-box where as sample preparation for autoradiograph is comparatively easier. The auto radiographs show distribution of plutonium across the cross-section of the fuel. It gives an idea about homogeneity of Pu in the matrix of the fuel. The autoradiograph may show Pu dissolved or dispersed in the matrix .

In all the three cermets it is observed that reduction of Pu compounds namely PuO_2, PuC, PuN takes place in the matrix of U because of more stability of new compounds UO_2, UC, UN formed due to interaction of Pu compounds with U. Also the phase transformation temperature of the cermets gets affected . The phase transformation temperature is reduced as compared to that of pure U metal. The formation of new compounds in the matrix of the fuel is not a welcome feature as it creats negative affect on the thermo-physical property such as thermal conductivity.

In short it may be mentioned that flow sheet for fabrication of Pu bearing cermet has been established. However U-PuO_2 cermet produced by this route is not acceptable as it has un-satisfactory physical appearance and poor integrity. U-PuN cermet is most stable and has adequate strength. These pellets could be stored in glove-box without any damage for longer period. The solidus temperature of the PuN bearing cermet is also high which is desirable for in reactor use of a fuel. U-PuC cermet has higher thermal conductivity. The other properties are also satisfactory.

6. CHAPTER 6. COMPATIBILITY STUDY BETWEEN U-UO_2 CERMET FUEL AND T91 CLADDING

Fuel clad chemical interaction (FCCI) is considered as a potential problem area in the application of the fuel in liquid-metal cooled fast reactors. The problem can be eliminated in two ways i.e. either by alloying of uranium or by using a barrier layer between fuel and clad. Zr is known to increase the solidus temperature and to improve the chemical compatibility between fuel and steel cladding material by suppressing the interdiffusion between the fuel and cladding components [44]. Hence, Zr is chosen as an alloying element as well as a barrier layer.

The clad provides a barrier to the release of radionuclides hence its integrity is a very important issue. For reliable operation of a fast breeder reactor, the fuel elements must be resistant to breaching even in case of overpower transients [81]. The eutectic liquefaction at the interface may lead to accelerated rate of cladding attack during accident transients. So to design a fuel element the eutectic reaction temperature between clad and fuel is a critical parameter [90].

One of the important cladding material for fast reactor is T91 grade steel suitable for high burn-up operation because of low-swelling behavior. T91 is ferretic martensitic steel comprising primarily of 9% Cr, 1% Mo and rest Fe. T91 grade steel used in this study was in the standard normalized and tempered condition. Its hardness, measured using Vicker's hardness tester at a test load of 200g was 220 kg/mm^2. The heat treatment of T91 involves austenization at 1323 K and air quenching, followed by tempering at 1023 K for 1 h. This steel is being proposed to be the cladding material for future fast reactors in India. Therefore, FCCI study is important between the fuel and T91 steel. The main objectives of the present study are

- To understand chemical compatibility behaviour between U-UO_2 fuel and T91 cladding by diffusion couple experiments
- To evaluate performance of Zr as FCCI barrier layer between U-UO_2 cermet and T91 by diffusion couple experiments

6.1 Diffusion Couples

Two types of diffusion couple as described in chapter 3 were prepared. The chemical composition of T91 steel is given in table 6.1. It may be noted that before deciding the annealing temperture of the diffusion couples it was nnecessary to know the phase transformation tempertaure of U-T91 composite and also U-15%UO_2 + T91 composite. DTA run for these composites were carried out taking small samples and result obtained is discussed in subsequent section. Table 6.2 shows details of temperature and duation of annealing for the two different types of couples.

Table 6.1. Chemical composition of T91 (wt.%)

Cr	Mo	V	Nb	Al	Ti	Ni	Cu	Mn	Si	C	N
9.16	0.882	0.207	0.079	0.008	0.003	0.197	0.068	0.368	0.209	0.099	0.0457
P	S	Fe									
0.015	0.0013	Balance									

Table 6.2. Details of annealing temperature and time of diffusion couples

Type of Diffusion couple	Temperature of annealing	Duration of annealing (hrs.)
U-15%UO_2/T91	923K, 973K, 993K, 1023K , 1073K	1000
U-15%UO_2/T91	1223 K	50
U-15%UO_2/Zr/T91	1023	1000
U-30%UO_2/Zr/T91	1023	1000

6.2 Results

6.2.1 DTA

The DTA curves obtained for U-T91 and U-15%UO_2-T91 composites on heating and cooling are shown in figs. 6.1-6.2 and figs. 6.3-6.4, respectively. The phase transition temperatures were determined from this DTA curve. The interaction between U and U based cermet fuel with T91 cladding can be best explained by U-Fe binary phase system. Since T91 is mainly Fe based steel, U-T91 system may be considered as pseudo binary. Table 6.3 shows the peak temperatures of various reactions between U/T91 and U-15%UO_2/T91 observed during DTA experiment. For comparison, information regarding different phase transformations in U, U-15%UO_2 and T91 has also been provided in table 6.3. In fig 6.1 the peak observed at 941 K corresponds to $\alpha \leftrightarrow \beta$ transition of U. The peak noticed at 1006 K is the result of a magnetic transition of T91 from a ferromagnetic to a paramagnetic state. $\beta \leftrightarrow \gamma$ phase transformation of U takes place at 1043 K and ferrite to austenite transition of T91 is observed at 1108 K. The exothermic reaction between T91 and U metal initiates at 1372 K and melting of unreacted Uranium occurs at 1395 K. Fig 6.2 represents the cooling curve for the U-T91 composite. The peak at 1400 K corresponds to melting point of unreacted U metal powder, and the one at 1291 K corresponds to the solidus temperature of U-T91 alloy. $\beta \leftrightarrow \gamma$ phase transformation of U takes place at 1016 K. The eutectic temperature peak is observed at 994 K and $\alpha \leftrightarrow \beta$ phase transformation of U occurs at 905 K. In fig. 6.3 which represents phase transition for U-15%UO_2/T91 composite, all the peaks similar to the ones in fig. 6.1 are observed except the peak at 1372 where reaction between U and T91 initiates. In fig.6.4 three prominent peaks corresponding to temperature at 905 K ($\alpha \leftrightarrow \beta$ transformation of U), 1035 K ($\beta \leftrightarrow \gamma$ transformation of U) and 1398 K (melting temperature of U) are observed.

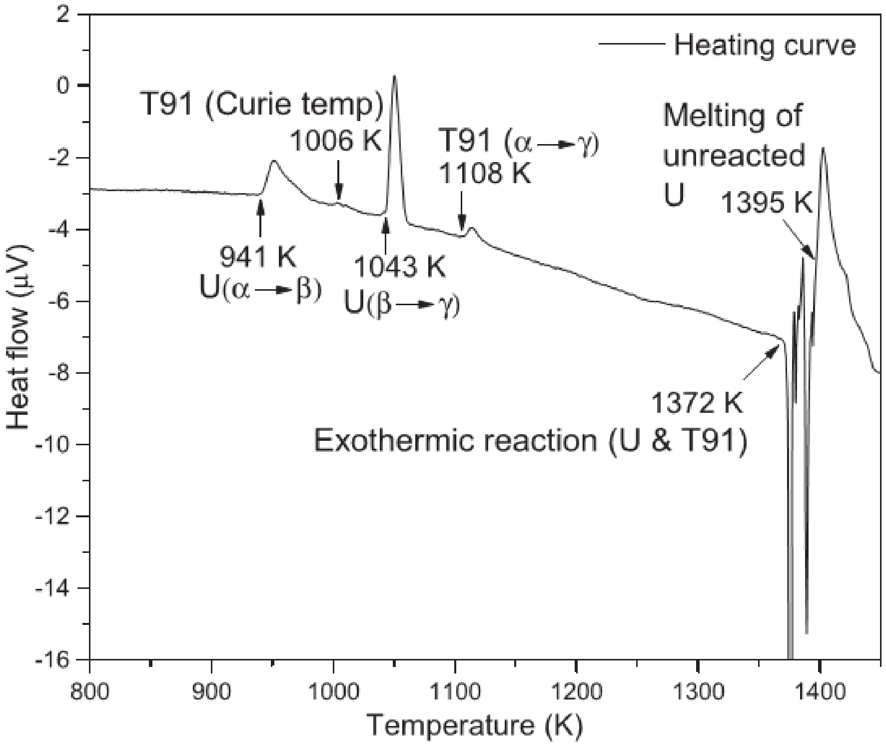

Fig. 6.1. DTA curve for U-T91 composite during heating

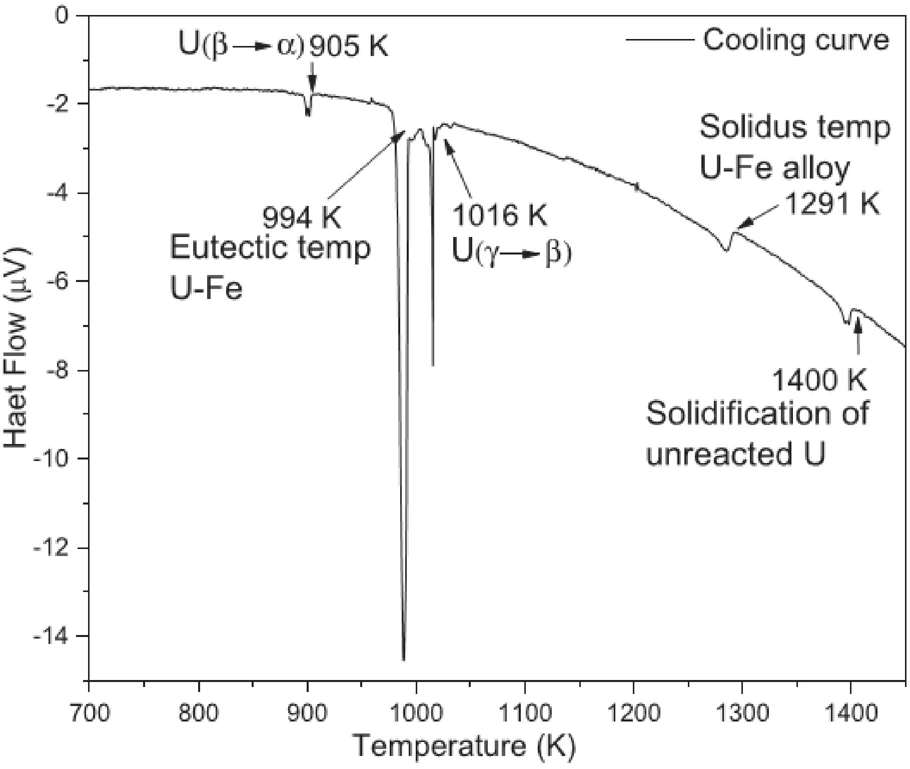

Fig. 6.2. DTA curve for U-T91 composite during cooling

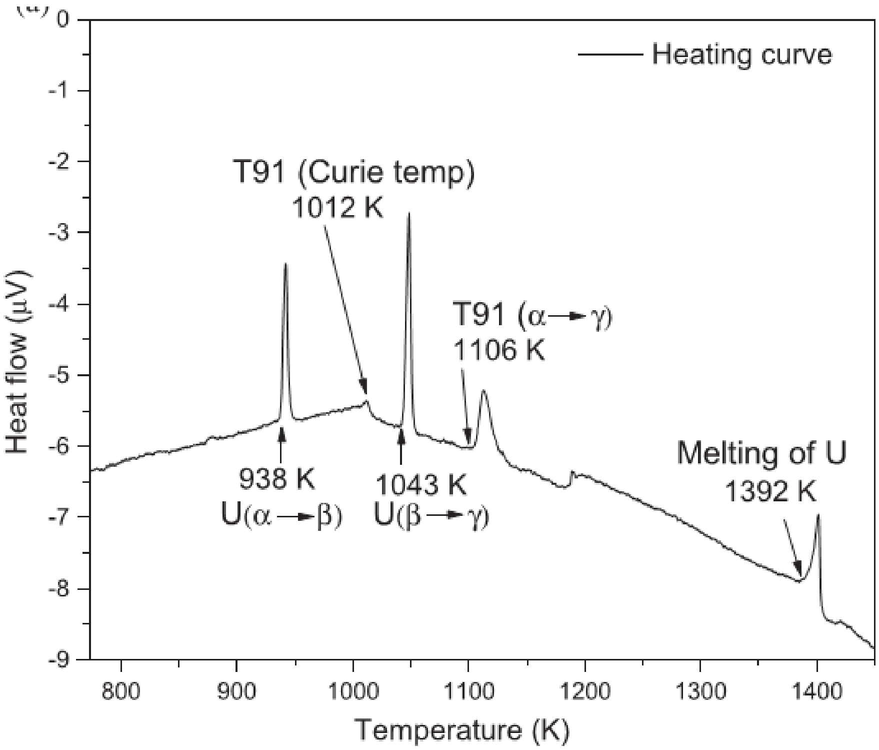

Fig. 6.3. DTA curve for U-15% UO_2/T91 composite during heating

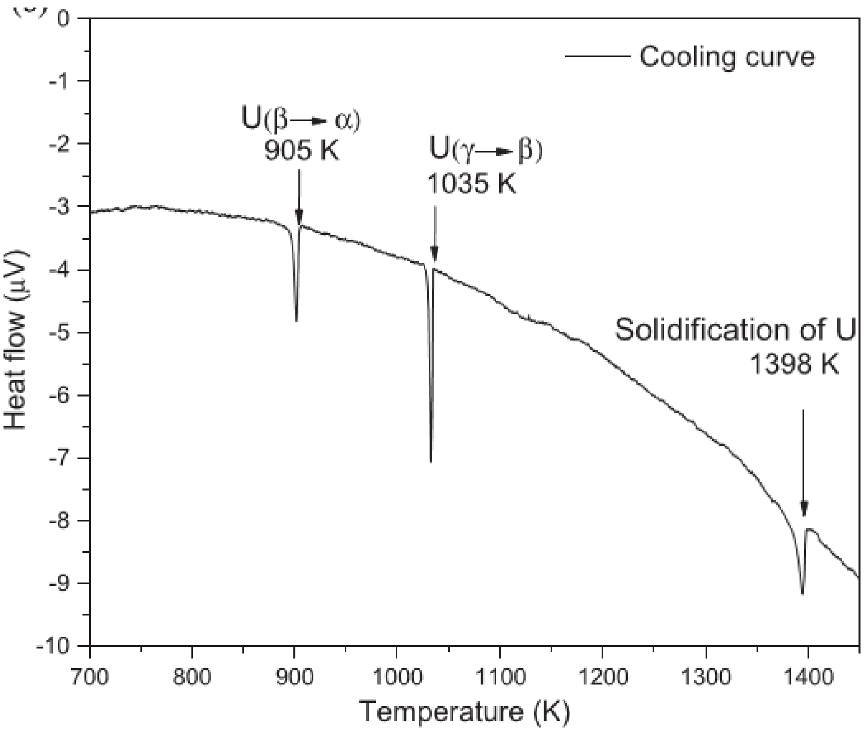

Fig. 6.4. DTA curve for U-15% UO_2/T91 composite during cooling

Table 6.3. Peak temperatures of various reactions between U/ T91 and U-15%UO$_2$/T91 observed during DTA experiment

	Reaction	U	T91	U-T91	U-15%UO$_2$	U-15%UO$_2$/T91
During Heating	$\alpha \leftrightarrow \beta$ phase transformation of U	937 K	------	941 K	940 K	938 K
	Ferro to Para magnetic transformation of T91		740 K	1006 K	------	1012 K
	$\beta \leftrightarrow \gamma$ phase transformation of U	1040 K		1043 K	1063 K	1043 K
	$\alpha \leftrightarrow \gamma$ phase transformation of T91		1110 K	1108 K	------	1106 K
	Exothermic reaction between T91 and U metal			1372 K	------	Not detected
	Melting point of unreacted Uranium/ T91	1393 K	1520 K	1395 K	1370 K	1392 K
During Cooling	Solidification temperature of unreacted Uranium			1400 K		1398 K
	Solidus temperature of U-T91 alloy			1291 K		Not detected
	Para to Ferro magnetic transformation of T91					
	$\gamma \leftrightarrow \alpha$ phase transformation of T91					
	$\beta \leftrightarrow \gamma$ phase transformation of U			1016 K		1035 K
	Eutectic temperature of T91 and U metal			994 K		Not detected
	$\alpha \leftrightarrow \beta$ phase transformation of U			905 K		905 K

6.2.2 Interfacial reactions without Zr layer

6.2.2.1 U-UO_2/T91 couples at 923 K

Fig. 6.5(a) shows secondary electron micrograph of U-15%UO_2/T91 diffusion couple annealed at 923 K for 1000 h. The microstructural analysis of U-15%UO_2/T91diffusion couple revealed an excellent bond formation at interface after annealing. The microstructure, as seen in Fig.6.5 (a), reveals development of discrete U(Fe,Cr)$_2$ intermetallic phase (31 at.%U, 62 at.% Fe,7 at.% Cr) at the interface. The magnified micrograph of interface is shown in fig. 6.5 (b). The intensity profiles of U-Mα, Fe-Kα, Cr-Kα and O-Kα X-rays (fig. 6.5(d)) were recorded along line AB shown in fig 6.5(c). The thickness of interdiffusion layer across the interface is around 3.5 µm (table 6.4). EDS was employed to determine composition at point X as shown in fig. 6.5 (c). The estimated composition at point X was 95 at.%U, 5 at.% Fe which does not correspond to any intermetallic phase.

6.2.2.2 U-UO_2/ T91 couples at 973K

The micrograph of U-15%UO_2/T91 diffusion couple annealed at 973 K for 1000 h is shown in Fig.6.6(a). The microstructural analysis of diffusion couples revealed an excellent bond formation at the interfaces after annealing. Fig. 6.6(b) shows magnified micrograph of the diffusion couple. Development of U(Fe,Cr)$_2$ intermetallic phase (32 at.%U, 60 at.% Fe,8 at.% Cr) is observed at the interface as seen in fig. 6.6(b). The intensity profiles (fig. 6.6(c)) of U-Mα, Fe-Kα, Cr-Kα and O-Kα X rays were recorded along CD (Fig. 6.6(b)). The thicknes of interdiffusion layer obtained from intensity profile is around 5µm (table 6.4). EDS was employed to determine the composition of the elements at point Y (fig.6.6(b)). The estimated composition at Y(96 at.%U,4 at.%Fe) is in agreement with the fact that no intermetallic phase exists at this point.

Table 6.4. Width of reaction layer at U-UO_2 and T91 interface under different heat treatment conditions

Temperature (K)	Time (h)	Reaction layer width (w) (μm)
923	1000	3.6
973	1000	5
993	1000	9
1023	1000	25-30
1073	1000	∽ 300
1223	50	∽ 250

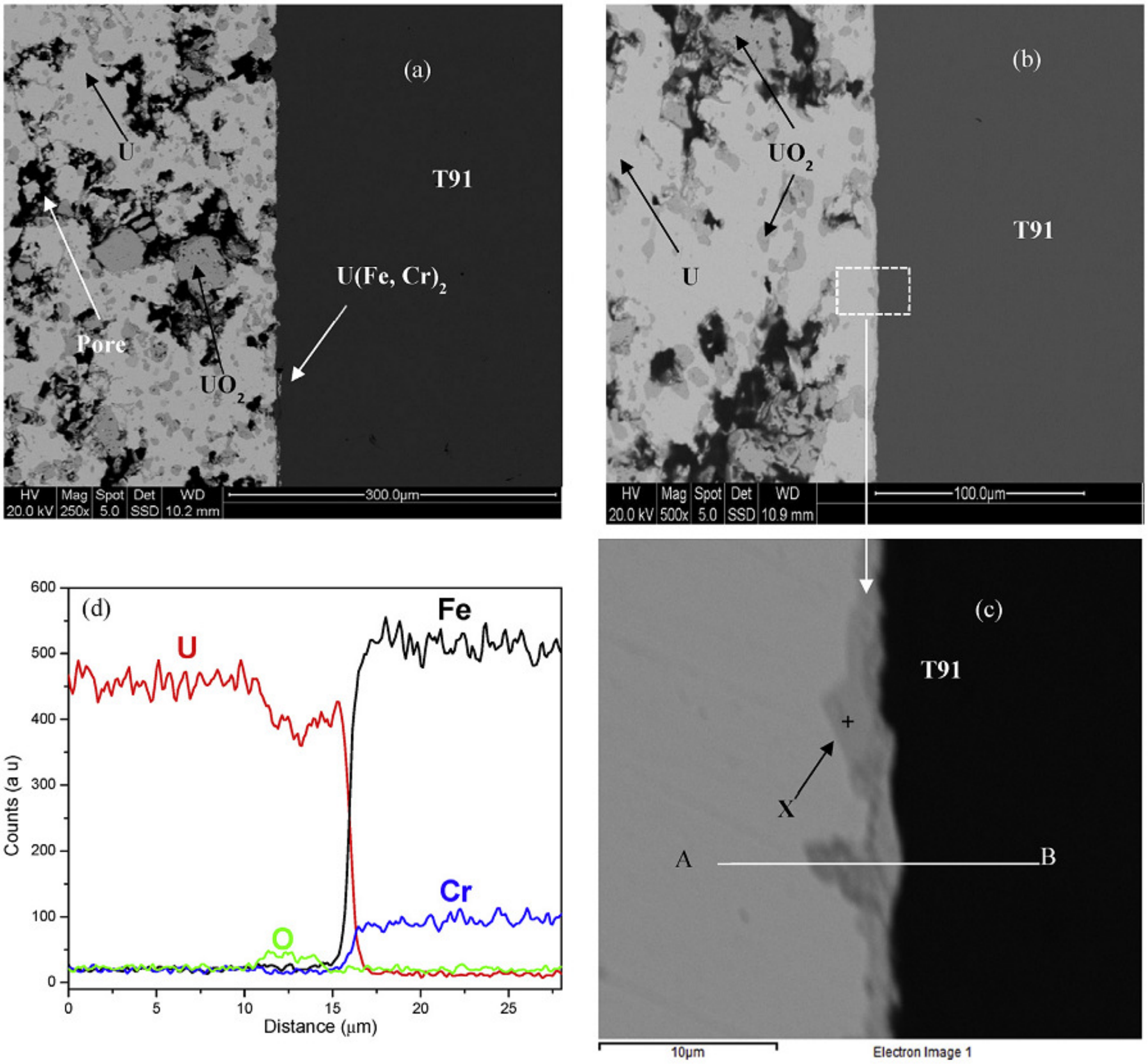

Fig. 6.5. (a) Secondary electron micrograph of diffusion couple U-15%UO2/T91 annealed at 923 K for 1000 h (b) Enlarged micrograph of diffusion couple (c) Enlarged micrograph of box region shown in Fig (b) & (d) Intensity profiles of U-Mα, Fe-Kα, Cr-Kα and O- Kα X-rays line along AB shown in fig. (c)

.

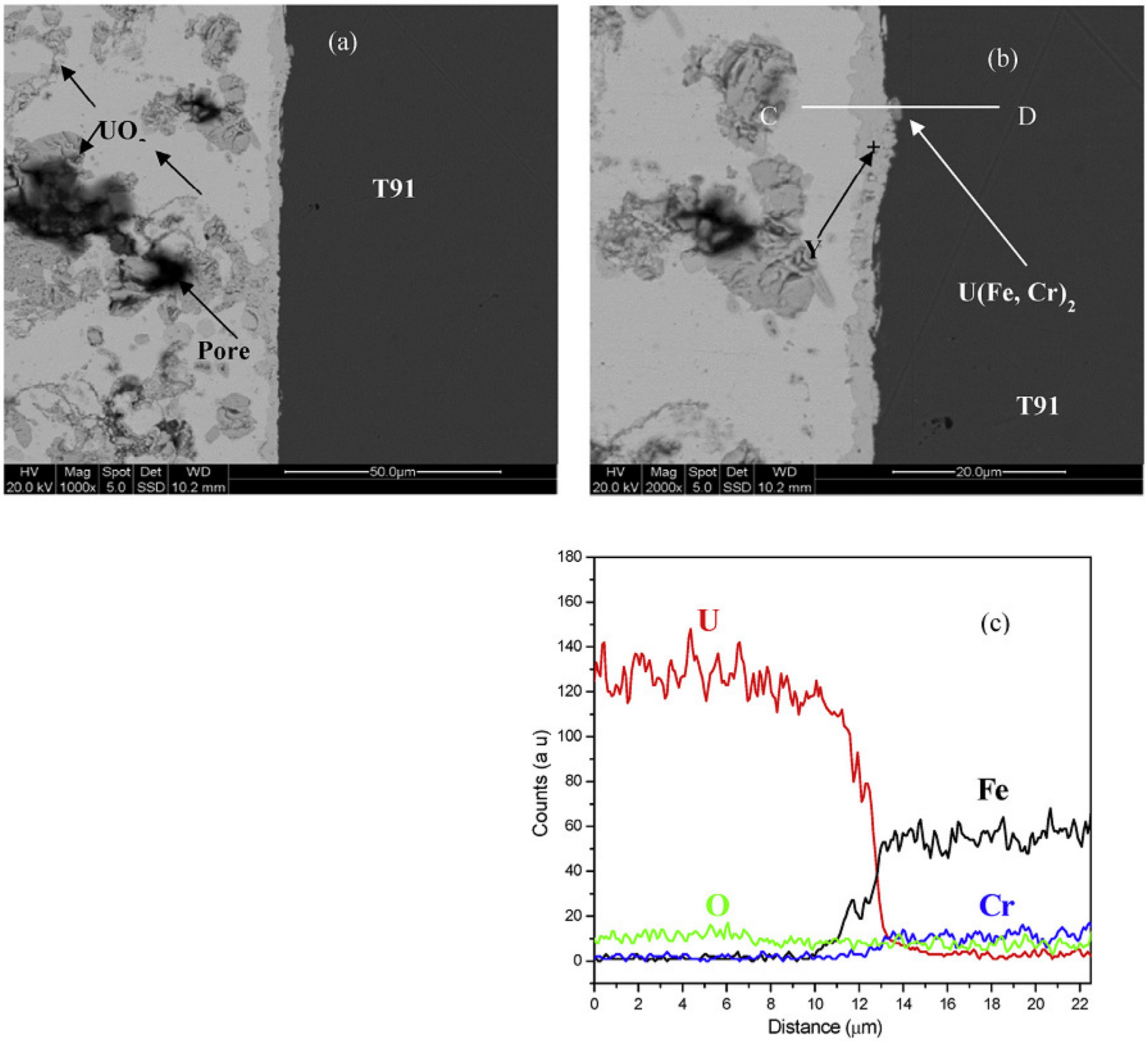

Fig. 6.6. (a) Secondary electron micrograph of diffusion couple U-15%UO_2/T91 annealed at 973 K for 1000 h (b) Enlarged micrograph of diffusion couple (c) Intensity profiles of U-Mα, Fe-Kα, Cr-Kα and O-Kα X-rays line along CD shown in Fig. (b)

6.2.2.3 U-UO_2/T91 couples at 993 K

Fig.6.7(a) shows secondary electron micrograph of U-15%UO_2/T91 diffusion couple which reveals an excellent bond formation at the interface after annealing. Intensity profile of U-Mα, Fe-Kα, Cr-Kα and O-Kα X rays were recorded along EF (Fig. 6.7a). The diffusion layer thickness was found to be around 9 μm (table 6.4). EDS, performed at point Z, (86 at.%U, 13at. %Fe, 1at.% Cr) shows existence of intermetallic phase U_6 (Fe, Cr).

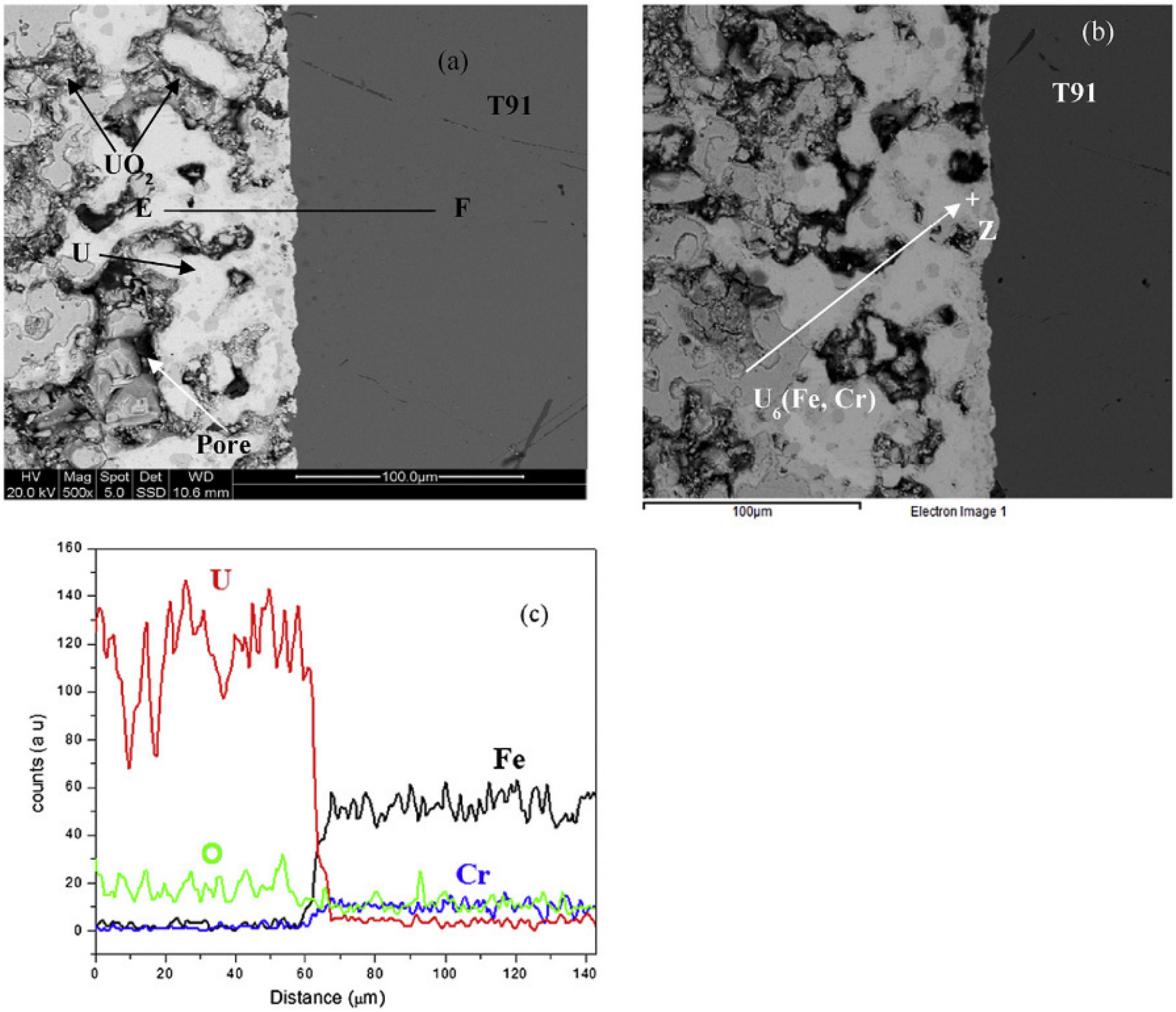

Fig. 6.7.(a) Secondary electron micrograph of diffusion couple U-15%UO_2/T91 annealed at 993 K for 1000 h (b) Micrograph of a different location of diffusion couple (c) Intensity profiles of U-Mα, Fe-Kα, Cr-Kα and O-Kα X-rays line along EF shown in Fig. (a)

6.2.2.4 U-UO_2/T91 couple at 1023 K

The micrograph of U-UO_2/T91 diffusion couple annealed at 1023 K for 1000 h is shown in Fig 6.8(a). It is observed that, at this temperature U reacts with constituents of T91 and a reaction zone of around 25-30 μm thickness is developed at the interface. The existence of reaction zone is not continuous along the interface.

Fig. 6.8(b) shows the magnified view of the reaction zone. The microstructure of reaction zone as seen in fig. 6.8(b) reveals formation of two different phases due to interdiffusion of U, Fe and Cr across the interface. EDS was employed to determine the composition of phases at point 1 & 2 shown in Fig. 6.8(b). EDS spectra for these locations is shown in Fig. 6.8(c-d). The composition of point 1 is 87 at.% U,11 at.% Fe and 2 at.% Cr which represents intermetallic phase $U_6(Fe,Cr)$. The composition at point 2 is 33 at.% U, 60 at. % Fe and 7 at.% Cr which corresponds to development of intermetallic phase $U(Fe,Cr)_2$.

EPMA was performed across the thickness of the reaction layer to understand the diffusion behaviour of the different elements. Intensity profile of U,Cr,Fe was recorded along line marked GH in Fig. 6.9(a). It is observed from the intensity profile that there is increase in Cr concentration at the front end of the interface (3 to 4 μm) whereas Fe concentration falls. A sudden rise in U concentration is observed at the interface.

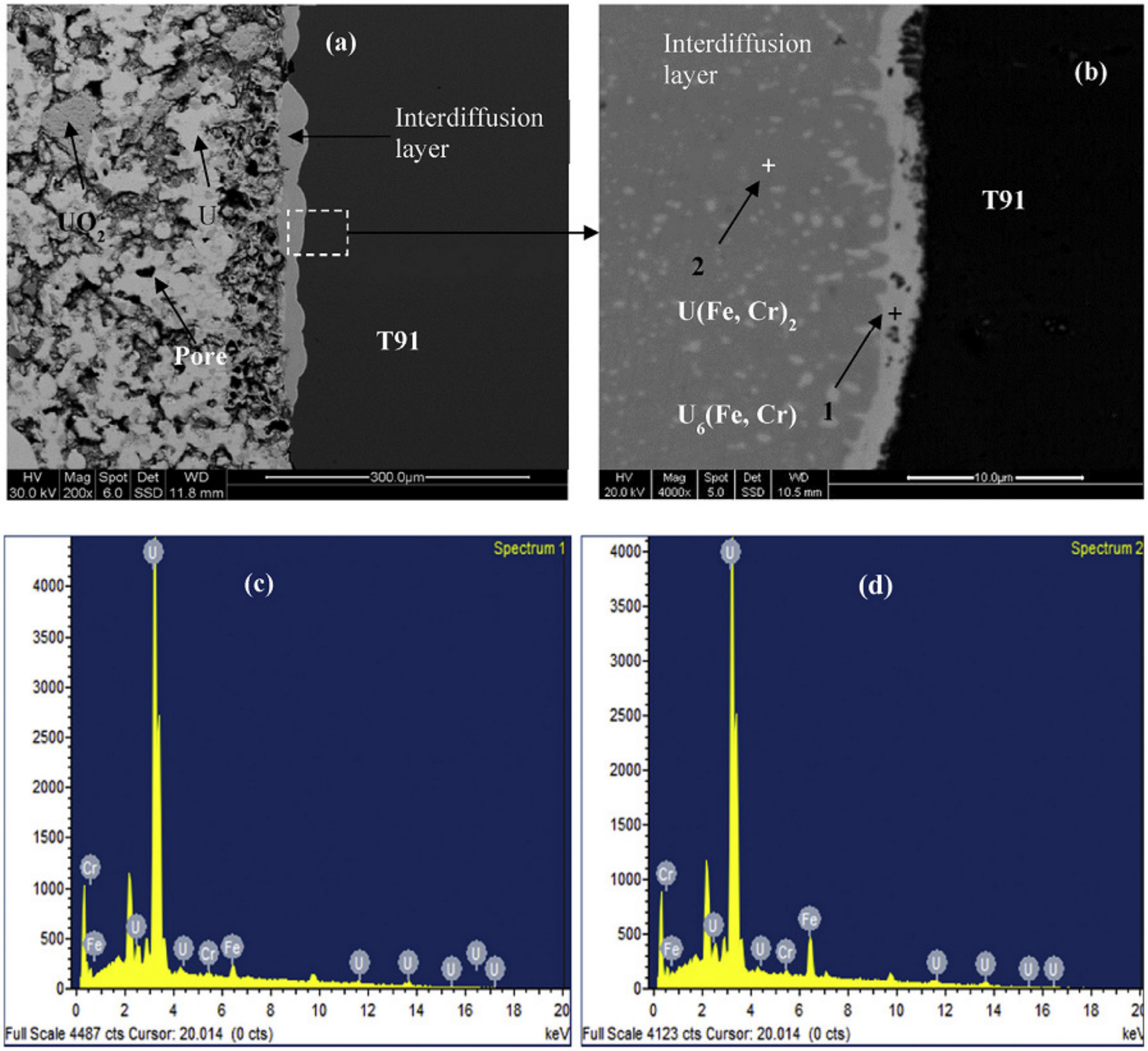

Fig. 6.8. (a) Secondary electron micrograph of diffusion couple U-15%UO2/T91 annealed at 1023 K for 1000 h (b) Magnified micrograph of reaction zone showing different phases marked 1&2, (c) and (d) represent EDS spectrum at point 1 and 2

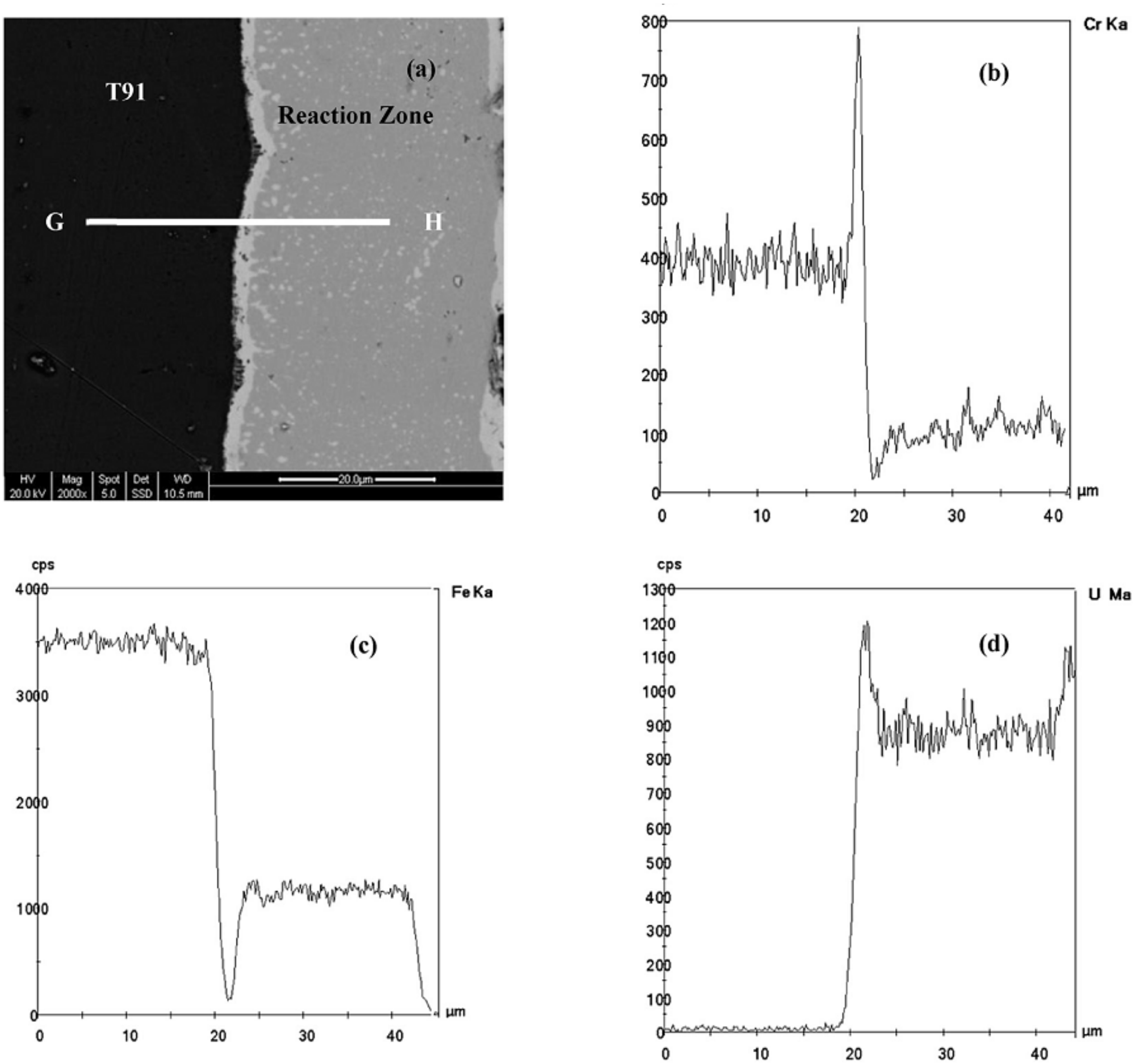

Fig. 6.9. (a) Secondary Electron micrograph of reaction zone of U-15%UO2/T9 couple annealed at 1023K for 1000h (b) Intensity profile of Cr-Kα X-ray line (c) Intensity profile of Fe-Kα X-ray line (d) Intensity profile of U-Mα X-ray line

6.2.2.5 U-15%UO_2/T91 couple at 1073 K

Micrograph of U-15%UO_2/T91 diffusion couple annealed at 1073 K for 1000 h is shown in fig. 6.10 (a). It is observed from the figure that there is extensive interaction at the interface.

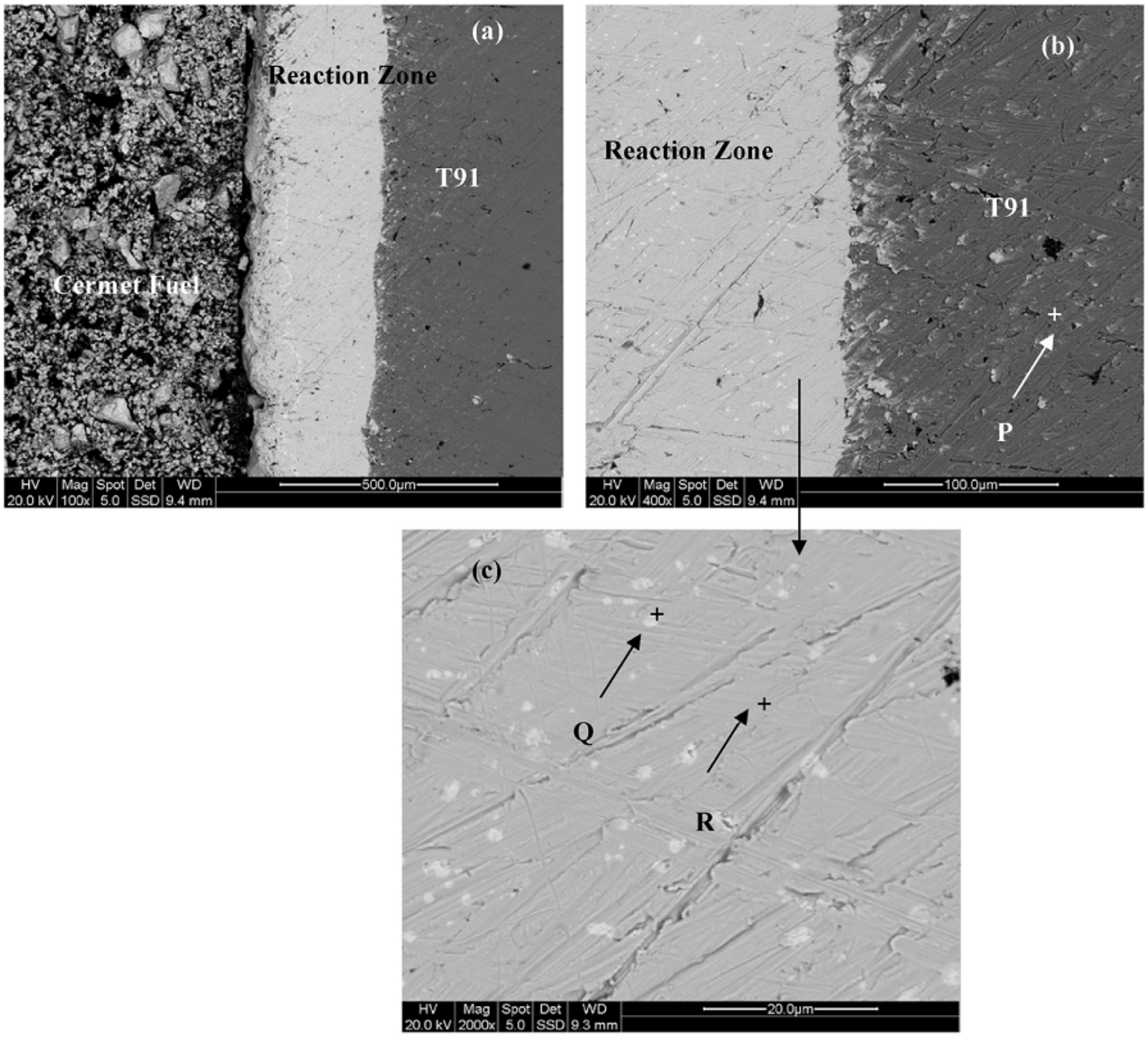

Fig. 6.10. (a) Secondary Electron micrograph of U-15%UO_2/ T9 diffusion couple annealed at 1073K for 1000 h (b) Enlarged view of the reaction zone and T91 clad and (c) Enlarged view of reaction zone .

A reaction zone of thickness 300 μ is formed at the interface. Figs. 6.10 (b) and (c) show the enlarged view of the interface and reaction zone, respectively. It is evident from the microstructure that there has been significant diffusion of U atoms from the fuel towards the interface resulting in the development of thicker reaction zone. Two types of phases are observed in the reaction zone. EDS was employed at point P, Q and R as shown in figs. 6.10

(b) and (c) to determine composition of phases. The composition at point P (89 at.% Fe,11 at. %Cr) is same as that of T91 cladding. The composition for the phase at point Q is 86 at.% U, 12 at. % Fe and 2 at.% Cr which corresponds to formation of intermetallic $U_6(Fe,Cr)$. The composition at R (35 at.% U,60 at. %Fe and 5 at.%Cr) is in agreement with formation of intermetallic $U(Fe,Cr)_2$.

6.2.2.6 U-15%UO_2/T91 diffusion couple at 1223 K

Fig. 6.11 (a) shows SEM micrograph of U-15%UO_2/T91 diffusion coupled annealed at 1223 K for 50 h. A reaction zone of thickness 250 μm is formed at the interface. Enlarged view of the interface and reaction zone is shown in fig. 6.11 (b). Two type of phases have developed at the interface as seen in the figure. Applying EDS at point S and T it was confirmed that the bright phase at S corresponds to $U_6(Fe,Cr)$ phase and composition at T reperesents $U(Fe,Cr)_2$ phase. Fig. 6.14(c) shows enlarged view of eutectic region. In fig. 6.11(d), microstructure corresponding to eutectic reaction is observed. Plate like crystals of $U_6(Fe,Cr)$ and $U(Fe,Cr)_2$ arranged in parallel fashion, characteristics of eutectic microsructure are observed.

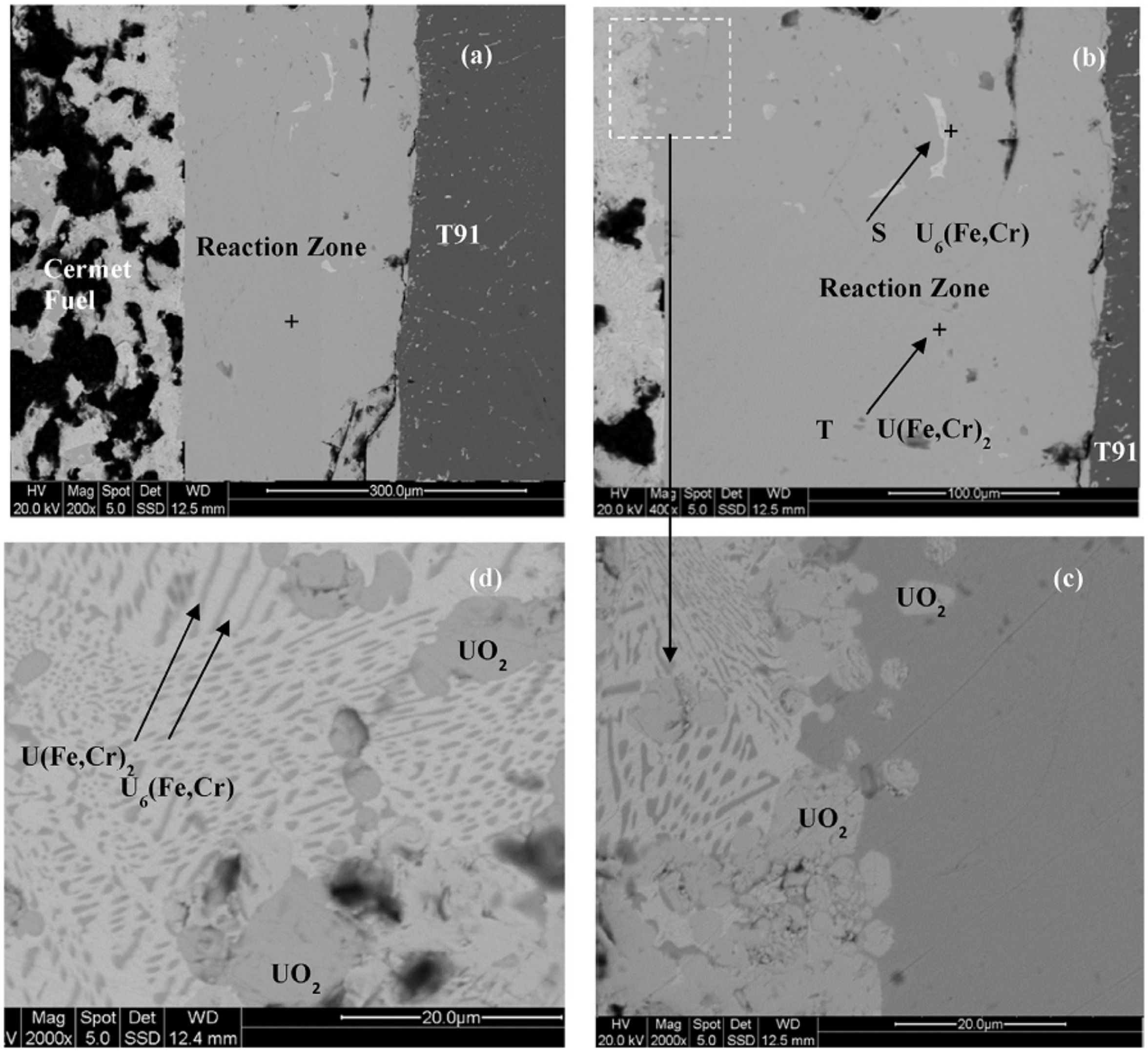

Fig.6.11. (a) Secondary Electron micrograph of U-15%UO_2/ T91diffusion couple annealed at 1223K for 50h (b) Enlarged view of the reaction zone and T91 clad (c) Enlarged view of interface showing eutectic reaction region and (d) Eutectic microstructure

6.2.3 Interfacial reaction in diffusion couple with Zr layer

The microstructure of the U-15%UO_2/Zr/T91 diffusion couple annealed at 1023 K for 1000 h is shown in fig. 6.12. The microstructure and the elemental mapping across the interface of U-15%UO_2/Zr/T91 couple annealed at 1023 K for 1000 h are shown in Fig. 6.13(a-e). The microstructural analysis of U-15%UO_2/Zr/T91diffusion couples revealed an excellent bond formation at both the U-15%UO_2/Zr and Zr/T91 interfaces after annealing. The microstructure of U-15%UO_2/Zr/T91 diffusion couple shows that there is no sign of eutectic melting between U-15%UO_2/Zr and Zr/T91 interface. Also the formation of any intermetallic compound was not observed at the Zr/T91 interface, even at 1023 K. It is also evident from U, Zr, Fe and Cr X-ray mapping that, there is no penetration of U in Zr metal as well as that of Zr in T91.

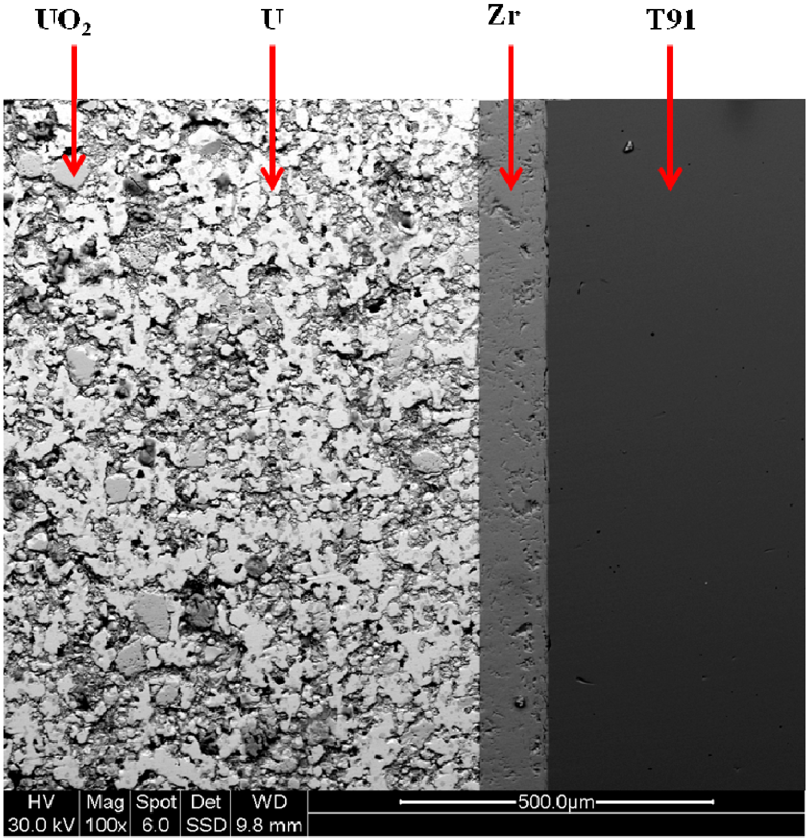

Fig. 6.12.SEM micrograph of diffusion couple U-15%UO_2/Zr/T91 annealed at 1023 K for 1000hrs.

.

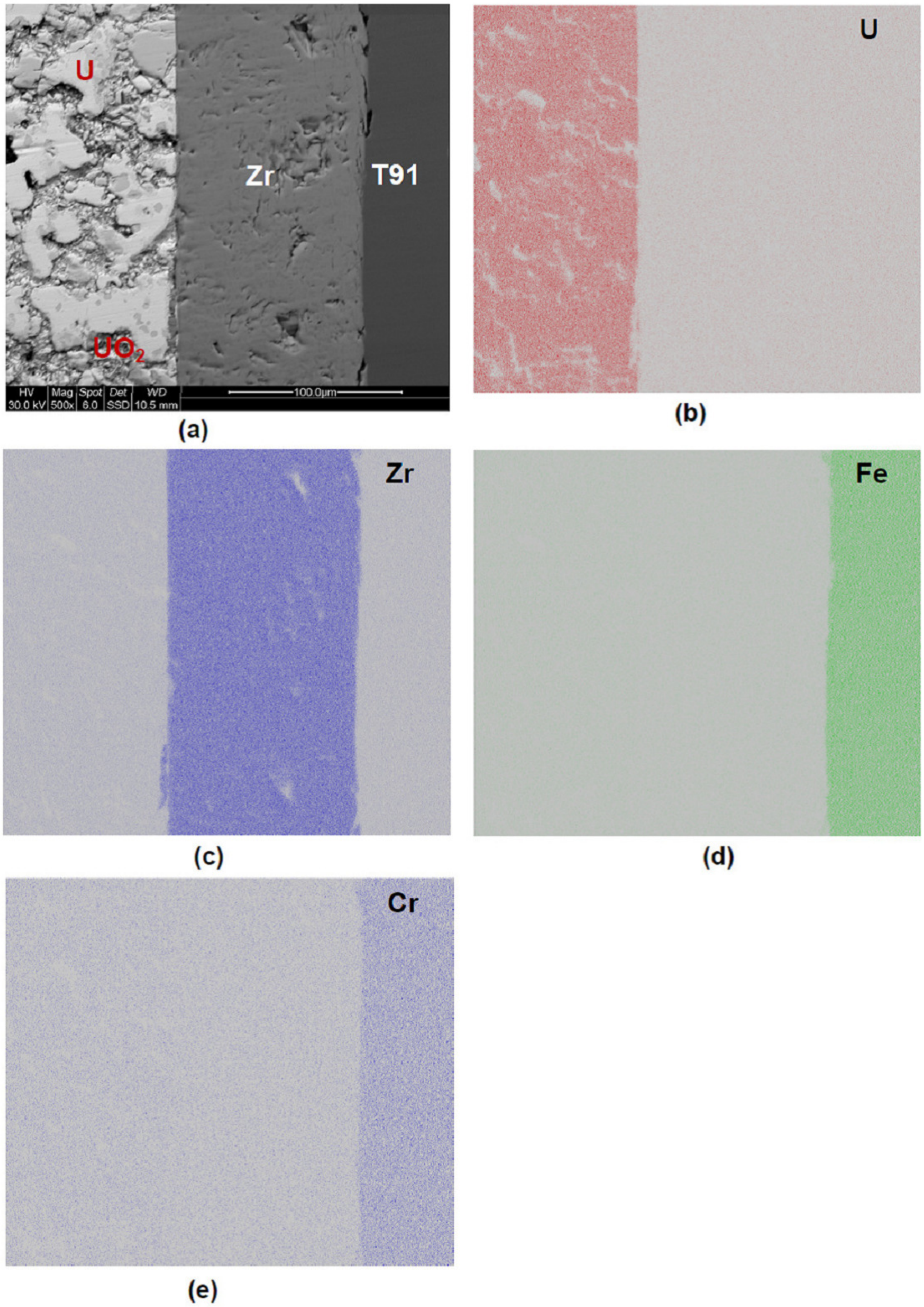

(a) (b) (c) (d) (e)

Fig. 6.13.SEM image and EDS results showing the distribution of different elements at the interfaces of U–15%UO_2/Zr/T91diffusion couple after heat treatment at 1023 K for 1000 h: (a) SEM image and mapping results of (b) U, (c) Zr, (d) Fe, and (e) Cr.

The microstructure of the U-30%UO_2/Zr/T91 diffusion couple annealed at 1023 K for 1000 h is shown in fig. 6.14. The diffusion couples revealed an excellent bond formation at both the U-30%UO_2/Zr and Zr/T91 interfaces after annealing. The results of the U-30%UO_2/Zr/T91 diffusion couple was found to be similar to that of U-15%UO_2/Zr/T91 diffusion couple. The results of the U-UO_2/Zr/T91 diffusion couples indicate that the Zr liner was effective in preventing fuel-clad chemical interaction.

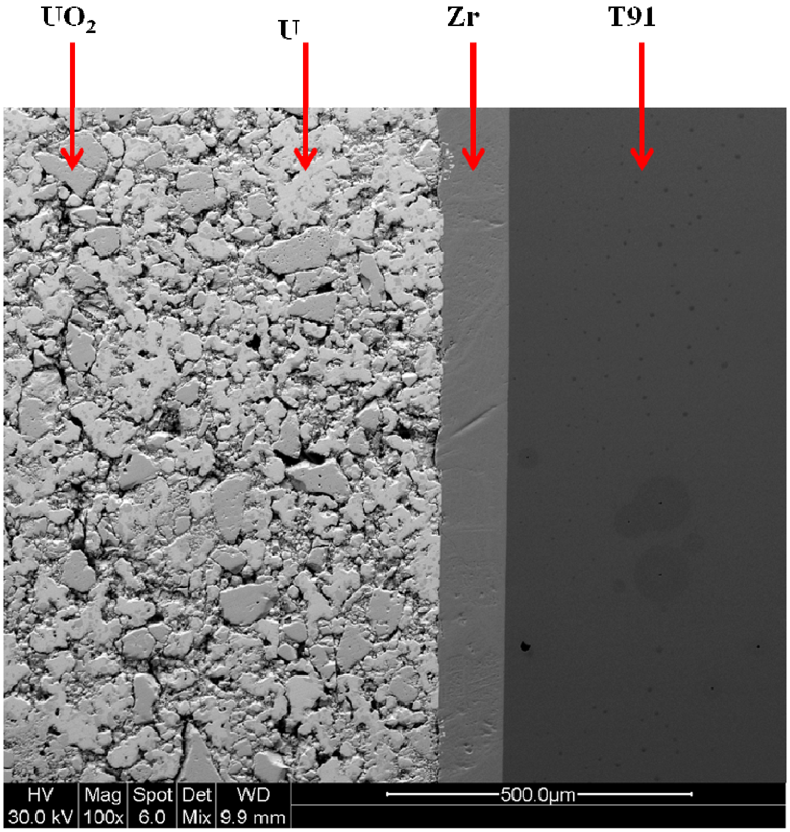

Fig. 6.14. Microstructure of U-30%UO_2/Zr/T91 diffusion couple annealed at 1023 K for 1000 hrs

6.3 Discussion

6.3.1 Interfacial reaction in U-15%UO_2/T91 diffusion couples

The integrity of the cladding is of great importance to the designers as it provides primary barrier to release of radionuclides [81-83]. The aim of the present study was to investigate the reaction between fuel and cladding at different temperatures. Fuel clad chemical interaction (FCCI) between U based cermet fuel and T91 clad is crucial because of formation of low melting eutectic between U and Fe. The U-Fe system (fig.6.15) forms two eutectic reactions at 998 K (89 wt% U) and 1353 K (47 wt% U). From reactor safety point of view eutectic formation at 998 K is of more importance. At this temperature eutectic reaction results in formation of two intermetallic namely U_6Fe and UFe_2 . The chemical interaction between the fuel and clad is a complex problem because a number of elements are involved in the reaction. With steel cladding T91 and the fuel U-UO_2, major constituents which participate in the diffusion process are Fe, U, Cr and O.

The liquefaction temperature between U and T91 due to eutectic reaction between U and Fe based T91 is 995 K as reported by Kaity et al [90]. However in the diffusion couple study even with good contact between fuel and T91 as observed in fig. 6.7 no such liquefaction reaction is observed between U-15%UO_2 fuel and cladding components up to 993 K , which

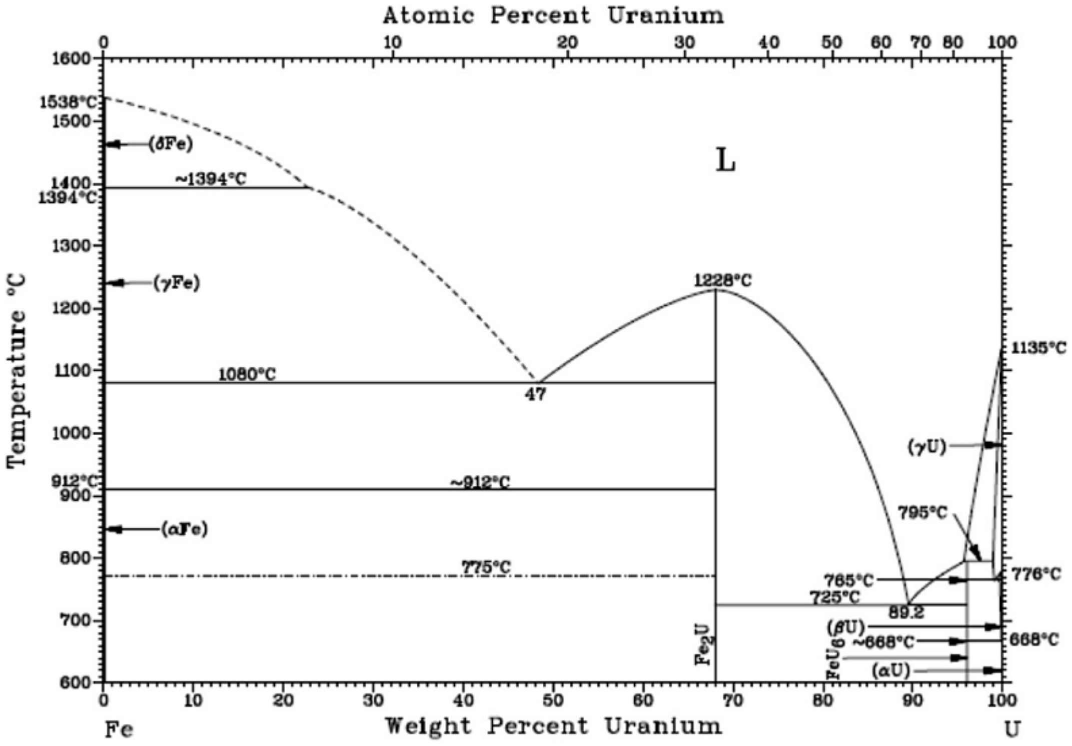

Fig. 6.15. Binary U-Fe equilibrium phase diagram [169]

is very close to liquefaction tempertaure. This may be because of the presence of UO_2 particles in the fuel matrix which creats hinderance in the diffusion path of the elements like U, Fe, Cr etc. Consequently at this temperature the proportion of Fe and U required for eutectic reaction at the interface may not have been achieved because of relatively slow diffusion process of elements in presence of UO_2 particles resulting in no liquefaction at the interface. Before performing the actual isothermal runs of the diffusion couples at different temperatures, DTA was carried out both for U/T91 and U–15% UO_2/ T91 couples to understand the different phase transformation reactions with respect to temperature. The most important observation of this study was the presence of an exothermic peak at 1372 K while heating and peak due to liquefaction reaction at 994 K while cooling in case of U-T91 couple (figs.6.1 & 6.2) . Similar observation could not be detected in case of U–15% UO_2/ T91 couple (figs.6.3 & 6.4). The absence of eutectic reaction peak during DTA experiment in case of U-15%UO_2/T91 couple may be because of lack of good contact between cermet fuel powder and metal pieces in presence of UO_2 particles which occupy large volume because of comparatively lower density.

The results of U-15%UO_2/T91 diffusion couple annealed at 923 K and 973 K indicate that there is discrete development of $U(Fe,Cr)_2$ intermetallic phase along the interface after 1000 h of annealing. A maximum of 3 μm width of diffusion layer is observed at 923 K. However the thickness of the dffusion layer increased up to 5 and 9 μm with increase in annealing tempertaure to 973 K and 993 K respectively. No distinct reaction zone was observed for the couples annealed up to 993 K . Thickness of diffusion layer for U vs Fe-15 wt% Cr alloy have been determined by K.Huang et al. [85] for similar temperature. In this diffusion couple two distinct layers of U_6Fe and UFe_2 phases were developed. The thickness of each layer was in the range of 40 to 50 μm.

For the diffusion couple annealed at 1023 K, development of a distinct reaction zone is observed at the interface as evident from the microstructure (fig.6.8(a)). Further it is also observed that there is removal of U from the region close to the fuel leading to a U lean areas along the interface. However, U metal away from the interface has not taken part in the diffusion reaction. This may be due to the reduced area of contact between U and Fe in the U-UO_2/T91 diffusion couple and sluggish diffusion reaction between U and Fe in presence of UO_2. The thickness of reaction zone is around 30 μm. From microstructural analysis by SEM and elemental analysis by EDS it was estimated that two different type of phases are present in the reaction zone. The continuous bright region close to T91 is $U_6(Fe,Cr)$ phase. The composition of gray region next to continous bright region corresponds to $U(Fe,Cr)_2$ phase. This result is in agreement with existence of phase acoording to U-Fe phase diagram (fig.6.15). The interaction of Fe with U leads to formation of two types of intermetallics namely U_6Fe and UFe_2. Both of them are line compounds. UFe_2 melts congruently at 1508 K and U_6Fe shows a peritectic transformation at 1083 K [170, 171]. U_6Fe has a body centred tetragonal crystal structure which is similar to β U where as UFe_2 has complex laves phase structure.

As said earlier, U atoms closer to the interface only appear to have taken part in the development of reaction zone, therefore atoms of U, which have moved out of the fuel diffuse towards cladding resulting in higher concentation of U at the front end of reaction zone. Hence, at the front end of the reaction zone, fuel and cladding constituents form $U_6(Fe,Cr)$ intermetallic phases. The rise in Cr concentration at the front end of the reaction zone infers that there is less diffusivity of this elemet in $U_6(Fe,Cr)$ intermetallic phase which is in consistent with results reported by other reaserchers [172]. In fact, it may be noted from the U-Cr phase diagram [173] solubility of Cr is poor in U and therefore, its diffusivity is less in the U_6Fe phase.

It is reported that in case of austenetic stainless steel, UFe_2 type phase forms “finger” like diffusion front [174]. This structure is observed when two of the diffusing species (U and Ni) diffuse by rapid exchange mechanism. The U_6Fe phase forms behind finger. In case of Ni free steel, like HT-9, the U_6Fe and UFe_2 type phases form a single zone without the formation of finger like structure. T91 is also a Ni free steel. In the present investigation, $U_6(Fe,Cr)$ and $U(Fe,Cr)_2$ phases are found to confine in a single zone.

The thickness of the reaction layer at fuel/T91 interface increased significantly when the annealing temperature was increased from 1023 K to 1073 K for the same annealing time. It infers that rate of interdiffusion is very much dependent on temperature and increases effectively with the rise in temperature. The higher rate of diffusion at the interface at 1073 K may also be attributed to formation of solid solution between U and Fe over a wide range of composition. The microstrucure of the diffusion couple shows development of a distinct bright reaction zone of 300 µm. U apparently diffuses out from the fuel and reacts with the constituents of T91. In general, the diffusion layers formed in the couples correspond to those dictated mainly by the interaction of U with Fe.

When the annealing temperature was increased to 1223 K eutectic microstructure was observed as shown in the fig.6.16 and it was different from the microstructure formed at lower temperature. At higher temperature, the kinetics of interdiffusion of both U and Fe becomes higher, leading to eutectic melting in lesser time.

6.3.2 Interfacial reaction in U-UO_2/Zr/T91 couples

It is evident from the experiment and characterization of diffusion couple with Zr barrier that, because of presence of Zr the inter diffusion of various elements across the interface has not taken place to the extent that formation of intermetallic or eutectic phase prevails upon. So Zr helps in forbidding chemical interaction between fuel and cladding.

6.3.3 Kinetics of the interfacial raection at fuel cladding interface

Based on the width of the interdiffusion layer developed at three different temperatures (923, 973 and 993 K), kinetics of the reaction was studied. At higher temperature a reaction zone is formed at the interface because of melting. So, it is difficult to get the exact width of reaction layers and the rate equation used in the solid state diffusion reaction may not be valid. Because of this reason higher temperatures and longer times have not been considered. The growth kinetics of a reaction layer formed at the interface can be reperesented by the folowing relation

$$w=kt^{1/n} \qquad (1)$$

where w is width of reaction layer, t is time of reaction, k is reaction constant, n is reaction index.

The value of the index, n depends on the mechanism of the growth of reaction layer. In case of solid reactions the growth is diffusion controlled and the value of n is taken as 2 [175].

The reaction constant k is temperature dependent parameter and increases exponentially with temperature as follows,

$$k=k_0 \exp(-Q/RT) \qquad (2)$$

where, Q is the activation energy required for the growth of the layer.

Combining equations (1) and (2),

$$w= k_0t^{1/n} \exp(-Q/RT) \qquad (3)$$

As mentioned earlier, for solid state reaction,the value of n is 2. Sustituting the value of n, the above equation becomes,

$$w = k_0t^{1/2} \exp(-Q/RT) \qquad (4)$$

$$w/ t^{½} = k_0 \exp(-Q/RT) \qquad (5)$$

The value of activation energy Q can be evaluated from log $(w/ t^{½})$ versus 1/T plot.

Width of the reaction layer at three different temperatures 923 K, 973 K and 993 K, is given in table 6.4.

The plot of log (w/ $t^{½}$) versus 1/T is as shown in fig. 6.2. The value of pre-exponential factor k_0 was calculated from the intercept of the plot. The value of the constant was 2.139×10^{-04} m $s^{-1/2.}$. The value of activation energy, Q was determined and found to be 89.75 kJ/mole. Hence, the growth of the interdiffusional layer at the fuel metal interface can be written as,

$$k= 2.139\times10^{-04}\ \exp(-89.75kJmol^{-1}/RT) \quad (923<T/K<993) \tag{6}$$

Equation (3) can also be expressed as :

$$w=2.139\times10^{-04}\ t^{1/2} \exp(-89.75kJmol^{-1}/RT) \quad (923<T/K<993) \tag{7}$$

The growth rate constant and activation energy for U-Fe 15% Cr diffusion couple have been reported by K Huang et al [85, 176]. They have used following equations

$$w = (2k_pt)^{1/2} \text{ where } k_p \text{ is growth rate constant} \tag{8}$$

$$\text{and } k_p = k_0 \exp(-Q_{kp}/RT) \text{ where } Q_{kp} \text{ is activation energy} \tag{9}$$

From equations (1), (2), (8) and (9), it is evident that value of k is comparable with $(2k_p)^{1/2}$ and value of Q is comparble with $0.5Q_{kp}$.

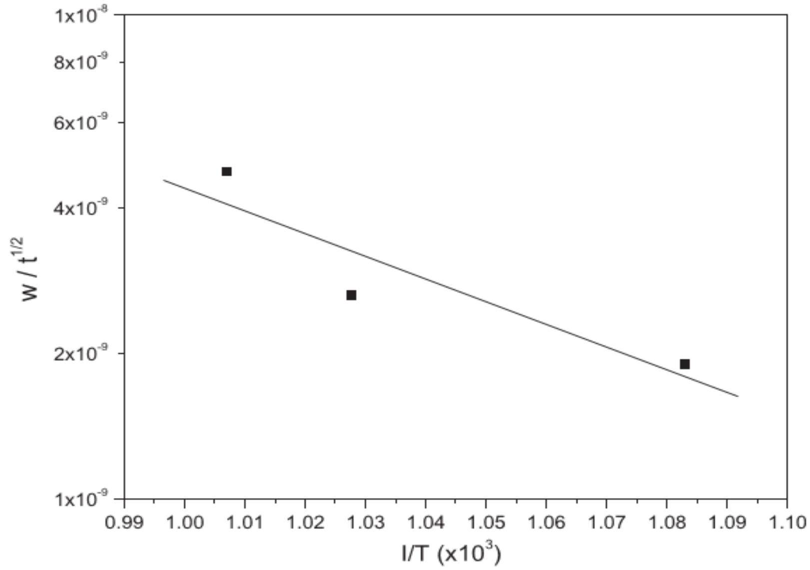

Fig.6.16. Plot of $w/t^{1/2}$ versus 1/T ($\times10^3$)

The total activation energy for the growth of intermetallic phases calculated by them for U vs Fe ,U vs Fe-15% Cr, U vs Fe-15%Cr-15%Ni are 137 kJ/mole (Q_{kp}), 230 kJ/mole (Q_{kp}) ,135 kJ/mole (Q_{kp}) respectively whereas, the activation energy in the present study has been determined to be 89.75 kJ/mole (Q). K Huang et al [85] have reported that interdiffusion and reactions in the U vs. Fe and U vs. Fe–Cr–Ni show similar temperature dependence, while the U vs. Fe–Cr diffusion couples exhibited a larger magnitude of activation energy for growth constants. U vs. Fe–Cr diffusion couples, without the presence of Ni, yielded greater activation energy for the growth of intermetallic phases. However the activation energy value obtained for cermet could not be expected to be similar to that reported by K Huang et al because the present cermet system under investigation is different from the alloy system studied by them.

From the compatibility study it is concluded that diffusion of the components of fuel and T91 cladding take place at all temperature beginning from 923 K. The interdiffusion zone has thickness of about 3 μm at this temperature. Formation of intermetallic phase is also observed. The thickness of interdiffusion zone increases with temperature and also the intermetallic phases are observed at random locations at the interface. However a distinct layer continuous along the interface is not observed up to 993 K. The eutectic temperature for fuel and steel component is around 993K but no eutectic reaction is observed at the interface. The reaction becomes significant at temperature 1023 K when a diffusion layer of thickness 25 micron is observed but this layer of reaction zone is again discrete in nature. So it is apparent that presence of ceramic particle at the fuel matrix retards the reaction between fuel and steel components. However at 1073 K and above continuous reaction zone is observed at the interface and at 1223 K eutectic reaction with formation of eutectic microstructure is monitored. The formation of reaction zone is not a welcome feature for fuel element as it reduces the mechanical strength of the cladding material. If the fuel centreline temperature does not cross 973 K during reactor operation the interaction between fuel and cladding may not be very significant as we observe from the present study. At this temperature maximum intediffusion layer formed is 5μm in 1000 h.The thickness of the cadding material is supposed to be around 370 μm. However as the fast reactor fuel element are meant for high burn up, a long residence time in the reactor at 973 K may result in formation of thicker interdiffusion layer. The formation of thicker interdiffusion layer may be detrimental from strength reduction point of view. Nevertheless this rate of interaction will be slower in case of cermet fuel compared to binary metallic fuel (e.g.U-Pu alloy mechanically bonded with cladding) because of presence of ceramic particles which make the reaction sluggish. Still if the reaction has to be totally cordoned between fuel and cladding, a Zr layer of 100 μm thick in between fuel and cladding could be the solution.

The thickness of the interaction layer formed during the reaction at any temperature in the range of 923-973 K between fuel and cladding without Zr layer can be calculated from the equation 7. Assuming the fuel central line temperature to be 973 K the time required for development of interaction layer of thickness of about 25 μm from equation 7 comes out to be nearly 2 yrs. So the expression obtained after compatibility study is useful in calculation of thickness of interaction layer. This may provide idea about duration of holding the fuel element in the reactor without any substantial damage.

Similar study could not be conducted with Pu bearing cermet. However it may be extrapolated that since U and Pu combine to form alloy reducing solidus temperature in all the Pu bearing cermet studied, the interdiffusion reaction may be faster in Pu bearing cermets which would certainly have higher adverse effect on the cladding compared to UO_2 bearing cermet. This can be probably be taken care of by using zirconium layer in between fuel and T91 cladding.

7. CHAPTER 7. CONCLUSION AND RECOMMENDATION FOR FURTHER RESEARCH WORK

The per capita power demand of India is growing fast. This requires mobilisation of different resources to meet the target. The contribution of Nuclear energy is one amongst others. The contribution from nuclear energy in this endeavour is possible in a significant mode only when our fast reactors start operating in large scale in the next half of this century. India is planning to install and operate fast reactors in large number in future. One of the important aspects of fast reactor technology is to use Plutonium bearing fuel which gives high breeding ratio and lower doubling time. The reprocessing of irradiated fuel to recover plutonium and to recycle for fuel fabrication is a challenging job. It demands high technological support to simplify the whole process system for easy handling of irradiated plutonium and make the process economical. Fuels like mixed oxide $(U, Pu)O_2$ have been used in most of fast reactors all over the world because of their ease in fabrication and well established reprocessing cycle. The use of mixed carbide and metallic fuel is limited. Though the (U,Pu,Zr) metallic alloy fuel has high breeding ratio and low doubling time but the fabrication and reprocessing aspects of the fuel is not comparable to oxide fuel.

The cermet fuel which contains dispersoids of ceramic particles in the metal matrix is a new concept for fast reactor fuel and is easier to fabricate by conventional powder pellet route. The pin design may be chosen as pellet-pin type where pellet pin bonding involves either He bonding or mechanical bonding of low density pellets (70% smear density). Of different fuel fabrication methods developed all over the world on laboratory scale, the powder pellet route involving cold compaction and sintering technique is easy to follow for production of pellets. However limited information is available in open literature regarding fabrication of cermet fuel by powder pellet route involving cold compaction and sintering process.

7.1 Feasibility of fabrication of cermet by powder pellet route

7.1.1 Starting powder and preparatory steps

One of the most important findings of this study is evaluation and eventual establishment of flow sheet of cermet pellet by powder pellet route. This work confirmed that the characteristics of starting powders U, UO_2, PuO_2, graphite play important role in controlling the reproducibility of the end product and achieving fast reaction rate during sintering. The particle size of U metal powder is an important process parameter. Finer the size of powder particles difficult is the process of fuel fabrication. Such powders oxidise very rapidly and also are potential hazard to fire. Further our experience with compaction of Uranium powder of ~15μ size conclude that die manufactured from OHNS steel material (2 % Carbon,12% Cr) is not suitable for high pressure compaction (600 MPa). Instead tungsten carbide die facilitates ejection of the pellet from the die after compaction which was not possible with OHNS steel die.

This study reaffirmed the fact that the O/M ratio of UO_2 powder plays an important role. The initial O/M ratio of the powder remains between 2.05 to 2.10 which need to be heat treated to bring it close to 2 so that interaction of UO_2 with U metal powder is avoided. Also heat treated powder yields higher bulk density which occupies lesser space in fuel matrix for same volume fraction.

7.1.2 Preparation of PuC/PuN powders

Low temperature is desirable for producing PuC and PuN powders to reduce volatilisation losses and also to produce powder with high sinerability.In this work PuO_2 powder derived from oxalate route was used for investigation. This powder has high specific surface area. This nature of the powder makes it hygroscopic and demands suitable heat treatment before use. Graphite powder possessing small particle size and very high surface area has not been found suitable for carbide production. Such powders resist mixing with other powder and coalesce to make their separate identity.

7.1.3 Treatment of powder before sintering

All the powders used in this study require pre-treatment prior to sintering. As produced powders of UO_2, PuO_2, PuC, PuN were crushed and milled before mixing with U metal powder. The milling process results in increase in specific surface area of the particles which is required for better sinterability of the powder. PuC, PuN powders are found to be resistant to comminution as compared to UO_2 and PuO_2 powder. A milling time of 90 minutes in attritor using tungsten carbide balls resulted in specific surface area of ~1 m^2/gm. for heat treated UO_2, PuO_2 powders in comparison to 0.5 to 0.6 m^2/gm for PuC and PuN powders. The surface area of the powder in the range mentioned above are considered good for sinterability [177]. Therefore milling time was optimised to 90 minutes. On the other hand, increasing the milling time probability of impurity pick up like tungsten, O_2 increases. The formation of oxide layer over the powder naturally acts as a barrier for interdiffusion of the metallic and non-metallic species.

The mixing of U metal powder with ceramic particles was done at a low speed in attritor with addition of 0.2% oleic acid. It has been found advantageous because it increases the intimacy between metal and ceramic powder facilitating homogeneity during mixing.

In order to avoid inter particle friction between die wall and particles during compaction 10% glycerol in methanol/oleic acid was used. A solid binder like zinc-behenate was also tried during compaction. The result in zinc-behenate case was not satisfactory. Disintegration of pellets was observed after sintering.

7.1.4 Sintering of the compacts/sintering parameters

U metal powder requires temperature more than $0.85T_m$ for effective consolidation owing to its poor sinterability.The sintering parameters were determined from dilatometer experiments.

In case of U-UO_2 cermet this temperature was higher as compared to U-PuO_2, U-PuC, and U-PuN cermet. The sinterability of U being poor and it requiring a temperature close to its melting temperature for shrinkage, the sintered density could be achieved up to 78-80% TD. Amongst the different cermet studied during the experiment it is observed that sintering at maximum temperature could be carried out in case of U-UO_2 cermet. In U-PuO_2, U-PuC and U-PuN cermet the sintering temperature was limited to 1223 K. This is because at temperature more than 1250 K the reaction between Pu bearing ceramic particles and metal particles becomes dominant resulting in reduction of ceramic particles with U. This in consequence alloys Pu with U metal and lowers solidus temperature of cermet. So sintering temperature could not be raised more than 1223K. However density achieved up to 78-80% is acceptable because the smear density required for fast reactor fuel pin for high metal content fuel is in range of 70 to 75% TD.

7.2 Stability of dispersoid in U metal matrix

Compound of U i.e. UO_2 and that of Pu namely PuO_2, PuC, PuN were used as dispersoid in the U metal matrix for the fabrication of cermet. The stability of UO_2 in U was found to be satisfactory. The UO_2 bearing cermet could be sintered to a temperature up to 1328 K. However in case of Pu bearing cermet the stability of PuO_2 in U matrix was observed to be very poor. The PuO_2 converts to higher volume Pu_2O_3 at higher temperature and also oxidises U metal to more voluminous UO_2 resulting ultimately in lowering of density of cermet. The physical appearance of U-PuO_2 cermt pellet was observed to be unsatisfactory. The stability of PuC bearing cermet is better compared to U-PuO_2 cermet. However the lowest solidus temperature was monitored for U-25%PuC cermet. The solidus temperature of all the cermets falls with increasing Pu content. The PuN bearing cermet was observed to be best from physical appearance and longer storage inside the container without damage. With similar wt.% in U matrix the U-20wt%PuN is monitored to have highest solidus temperature.

7.3 Study of thermo-physical properties of different cermets

The U-UO_2 Cermet fuel has high thermal expansion similar to U-15%Pu-10%Zr metallic fuel which ensures safe operation of the fuel. The high solidus temperature of the U-UO_2 fuel will provide larger margin between operating and melting temperature. The thermal conductivity of the U-UO_2 fuel increases with temperature which is favourable for low centerline operating temperature at higher linear power rating. The presences of porosities in the fuel matrix are beneficial as these may result in lowering the irradiation swelling in the fuel.

Amongst the Pu bearing cermet U-PuC cermet having combination of PuC and Pu_2C_3 in the ceramic matrix has highest thermal conductivity. U-PuN cermet has maximum stability and highest solidus temperature for similar fraction of ceramic particles. The thermal conductivity of all the fuels increases with temperature which is suitable for low centerline operation. The thermal expansion of the Pu bearing cermets are comparable to U-15%Pu-10%Zr fuel which is good for safe operation of the fuel.

7.4 Compatibility Study between fuel and cladding

In the diffusion couple experiment for U-15%UO_2/T91 couple for temperatures between 923 K to 993K, interdiffusion layers formed had a maximum thickness of 9µ. No liquid phase was observed at the interface. Presence of UO_2 particles in the fuel matrix impeded the growth of interdiffusion layer. The UO_2 particles acted as a barrier layer which reduced the reaction between Fe and U. Even holding near the eutectic temperature (993 K) for more than 40 days evidence of melting between fuel and cladding was not observed at the interface. Hence, it can be concluded that the fuel-clad chemical compatibility between U-UO_2 and T91 is satisfactory for fuel operating temperature as 993K.The growth kinetics of reaction layer formed at the interface was studied and activation energy for growth was found to be 89.75 kJ/mole. From growth kinetics study the equation for calculation of width of interaction layer could be deduced. From this equation the time required for growth of 25μm thick interaction layer at 973 K was estimated to be nearly 2 years. When the annealing temperature was increased to 1223 K eutectic microstructure was observed and it was different from the microstructure formed at lower temperature. However from U-15%UO_2/Zr/T91diffusion couple study it was concluded that 100 μm thick Zr barrier layer could be sufficient to inhibit fuel cladd interaction between 993 -1073 K .

7.5 Recommendation for future Work

1. To avoid interaction between between U and PuO_2 ceramic particle a study incorporating effect of coating of stable oxides over PuO_2 for fuel stability is required.
2. It would be of interest to evaluate performance of PuN/PuC cermet with T91 cladding by diffusion couple experiments.
3. Irradiation aspects of the cermet fuel in fast bredder test reactor can be studied
4. Dissolution behaviour of cermet is an important aspect of fuel cycle which needs to be established for reprocessing of the fuel.

8. REFERENCES:

[1] E. Fermi, The development of the first chain reacting pile, JSTOR 90(1) (1946) 20-24.

[2] E. Fermi, Elementary theory of the chain-reacting pile, JSTOR 105(2715) (1947) 27-32.

[3] J. Emsley, Uranium, Nature's Building Blocks, Oxford University Press Oxford, 2001.

[4] R.L. Murray, Nuclear reactors built, being built, or planned in the united states as of June 30, 1972: TID-8200 (26th Rev.), National Technical Information Service, US Department cf Commerce, Springfield Va. 22151. $3.00, Pergamon, 1973.

[5] History of Emergency Preparedness, US Nuclear Regulatory Commission (NRC), April, 2007.

[6] S. Glasstone, A. Sesonske, Nuclear reactor engineering: reactor systems engineering, Springer Science & Business Media.

[7] A.V. Bychkov, O.V. Skiba, A.A. Mayorshin, M.V. Kormilitsyn, O.V. Shishalov, I.Y. Zhemkov, V.A. Kisly, L.G. Babikov, Burning of Minor-Actinides in Fuel Cycle of the Fast Reactor. DOVITA Programme"Results of the 10-Year Activities", Proceedings 7th Information Exchange Meeting on Actinide and Fission Product Partitioning and Transmutation, Jeju, Republic of Korea, Citeseer, 2002.

[8] A.B. Reynolds, A.E. Walter, Fast Breeder Reactors, Pergamon Press, UK, 1980.

[9] www.world-nuclear.org/information-library/current-and.../fast-neutron-reactors.aspx, Fast Neutron Reactors | FBR - World Nuclear Association17 October 2017

[10] H.J. Bhabha, N.B. Prasad, A study of the contribution of atomic energy to a power programme in India, Atomic Energy Commission, India; Atomic Energy Establishment, Trombay, India, 1959.

[11] S.S. Bajaj, A.R. Gore, The Indian PHWR, Nucl. Eng. Design 236(7-8) (2006) 701-722.

[12] P.K. Dey, N.K. Bansal, Spent fuel reprocessing: a vital link in Indian nuclear power program, Nucl. Eng. Design 236(7-8) (2006) 723-729.

[13] A. Kakodkar, Salient features of design of thorium fuelled Advanced Heavy Water Reactor, Indo-Russian seminar on thorium utilisation, 1998, pp. 17-20.

[14] S.R. Paranjpe, An update on Indian fast breeder programme, International conference on fast reactors and related fuel cycles, IAEA INIS, 1991.

[15] S.C. Chetal, V. Balasubramaniyan, P. Chellapandi, P. Mohanakrishnan, P. Puthiyavinayagam, C.P. Pillai, S. Raghupathy, T.K. Shanmugham, C.S. Pillai, The design of the prototype fast breeder reactor, Nucl. Eng. Design 236(7-8) (2006) 852-860.

[16] P. Puthiyavinayagam, P. Selvaraj, V. Balasubramaniyan, S. Raghupathy, K. Velusamy, K. Devan, B.K. Nashine, G.P. Kumar, S. Varatharajan, P. Mohanakrishnan, Development of fast breeder reactor technology in India, Progr. in Nucl. Energy 101 (2017) 19-42.

[17] S.C. Chetal, P. Chellapandi, P. Puthiyavinayagam, S. Raghupathy, V. Balasubramaniyan, P. Selvaraj, P. Mohanakrishnan, B. Raj, Current status of fast reactors and future plans in India, Energy Procedia 7 (2011) 64-73.

[18] D.C. Crawford, D.L. Porter, S.L. Hayes, Fuels for sodium-cooled fast reactors: US perspective, J. Nucl. Mater. 371(1) (2007) 202-231.

[19] D.E. Burkes, R.S. Fielding, D.L. Porter, M.K. Meyer, B.J. Makenas, A US perspective on fast reactor fuel fabrication technology and experience. Part II: Ceramic fuels, J. Nucl. Mater. 393(1) (2009) 1-11.

[20] J.H. Kittel, B.R.T. Frost, J.P. Mustelier, K.Q. Bagley, G.C. Crittenden, J. Van Dievoet, History of fast reactor fuel development, J. Nucl. Mater. 204 (1993) 1-13.

[21] R.B. Baker, F.E. Bard, R.D. Leggett, A.L. Pitner, Status of fuel, blanket, and absorber testing in the fast flux test facility, Journal of Nuclear Materials 204 (1993) 109-118.

[22] A.K. Sengupta, K.B. Khan, J. Panakkal, H.S. Kamath, S. Banerjee, Evaluation of high plutonia (44% PuO2) MOX as a fuel for fast breeder test reactor, J. Nucl. Mater. 385(1) (2009) 173-177.

[23] B. Raj, H.S. Kamath, R. Natarajan, P.R.V. Rao, A perspective on fast reactor fuel cycle in India, Progr. in Nucl. Energy 47(1-4) (2005) 369-379.

[24] C. Ganguly, P.V. Hegde, G.C. Jain, U. Basak, R.S. Mehrotra, S. Majumdar, P.R. Roy, Development and Fabrication of 70% PuC -30% UC Fuel for the Fast Breeder Test Reactor in India, Nuclear Technology 72(1) (1986) 59-69.

[25] C. Ganguly, P.V. Hegde, A.K. Sengupta, Preparation, characterisation and out-of-pile property evaluation of (U, Pu) N fuel pellets, J. Nucl. Mater. 178(2-3) (1991) 234-241.

[26] Y. Arai, S. Fukushima, K. Shiozawa, M. Handa, Fabrication of (U, Pu) N fuel pellets, J. Nucl. Mater. 168(3) (1989) 280-289.

[27] A.A. Bauer, P.Cybulskis, J.L. Green, Proceedings of the Conference on Advanced LMFBR Fuels, ERDA-4455, 1977, p. 299.

[28] K.Q. Bagley, W.Batey, R.Paris, W.M.Sloss, C.P. snape, Proceddings of Conference on Advanced LMFBR Fuels ERDA-4455, 1977, p. 313.

[29] P. Combette, French irradiation test experience for carbide fuels, Advanced LMFBR fuels,1977.

[30] V.A. Tsykanov, V.M. Gryazev, E.F. Davydov, V.I. Kuz'min, A.A. Maershin, V.N. Syuzev, I.S. Golovnin, T.S. Men'skikova, Y.K. Bibilashvili, R.B. Kotel'nikov, Results of testing carbide fuel elements in the BOR-60 reactor, Soviet Atomic energy 42(5) (1977) 422-428.

[31] Y. Arai, Y. Suzuki, T. Iwai, A. Maeda, T. Sasayama, K.-i. Shiozawa, T. Ohmichi, Fabrication of uranium-plutonium mixed nitride fuel pins for irradiation tests in JMTR, J. Nucl. Sci.Tech 30(8) (1993) 824-830.

[32] H. Blank, H. Bokelund, Problems expected in the future fuel cycle development of dense fuels for LMFBRs, IAEA TECDOC 352 (1985) 189.

[33] N.G. Muralidharan, C.N. Venkiteswaran, V. Karthik, P.A. Manojkumar, S. Sosamma, C. Rao, V. Venugopal, K.V. Kasiviswanathan, Remote metallographic examination of mixed carbide fuel of fast breeder test reactor in radiometallurgy laboratory, Int. J. Nucl Eng Sci and Tech 1(2-3) (2005) 191-196.

[34] C.N. Venkiteswaran, N. Raghu, V. Karthik, A. Vijayaraghavan, V. Anandraj, T. Ulaganathan, T. Saravanan, V.V. Jayaraj, S. Kurien, J. Philip, Irradiation behavior of FBTR mixed carbide fuel at various burn-ups, Energy Procedia 7 (2011) 227-233.

[35] D.E. Burkes, R.S. Fielding, D.L. Porter, D.C. Crawford, M.K. Meyer, A US perspective on fast reactor fuel fabrication technology and experience part I: metal fuels and assembly design, J. Nucl. Mater. 389(3) (2009) 458-469.

[36] B.R.T. Frost, Nuclear fuel elements: design, fabrication and performance, Elsevier.

[37] D. Mohr, L.K. Chang, E.E. Feldman, P.R. Betten, H.P. Planchon, Loss-of-primary-flow-without-scram tests: Pretest predictions and preliminary results, Nucl. Eng. 101(1) (1987) 45-56.

[38] D.C. Crawford, D.L. Porter, S.L. Hayes, Fuels for sodium-cooled fast reactors, Trans. Am. Nucl. Soc 94 (2006) 791-792.

[39] M.T. Simnad, A brief history of power reactor fuels, J. Nucl. Mater. 100(1-3) (1981) 93-107.

[40] S.T. Zegler, M.V. Nevitt, Structures and Properties of Uranium-Fissium Alloys, Argonne National Laboratory1961.

[41] C.E. Lahm, J.F. Koenig, R.G. Pahl, D.L. Porter, D.C. Crawford, Experience with advanced driver fuels in EBR-II, J. Nucl. Mater. 204 (1993) 119-123.

[42] G.L. Hofman, L.C. Walters, T.H. Bauer, Metallic fast reactor fuels, Progr. in Nucl. Energy 31(1-2) (1997) 83-110.

[43] Konovalov, II, Survey on metal fuel on a base of uranium alloys, IAEA-TECDOC-970, 1997, p. 183.

[44] G.L. Hofman, L.C. Walters, Metallic fast reactor fuels, in: B.R.T. Frost (Ed.), Vol. 10A, Nuclear Materials, Materials Science and Technology, VCH Publishers Inc., New York, 1994, pp. 1–43.

[45] W.N. Beck, R.J. Fousek, J.H. Kittel, Irradiation behavior of high burnup Uranium-Plutonium alloy proto type fuel elements,, (1968).

[46] Y.I. Chang, The integral fast reactor, Nucl. Tech. 88(2) (1989) 129-138.

[47] Y. Sakamura, T. Inoue, O. Shirai, T. Iwai, Y. Arai, Y. Suzuki, Studies on pyrochemical reprocessing for metallic and nitride fuels: behaviour of transuranium elements in LiCl-KCl/liquid metal systems, Proceedings of the International Conference on Future Nuclear Systems, GLOBALâ€™99, 1999.

[48] J.D.B. Lambert, R. Strain, Oxide fuels, Wiley Online Library1994.

[49] R.V. Strain, J.H. Bottcher, S. Ukai, Y. Arii, Fuel-sodium reaction product and its influence on breached mixed-oxide fuel pins, J. Nucl. Mater. 204 (1993) 252-260.

[50] C. Ganguly, P.V. Hegde, G.C. Jain, Fabrication of (Pu0. 55U0. 45) C fuel pellets for the second core of the fast breeder test reactor in India, Nucl. Tech. 105(3) (1994) 346-354.

[51] C. Ganguly, A.K. Sengupta, Out-of-pile chemical compatibility of hyperstoichiometric (Pu0. 7U0. 3) C with stainless steel cladding and sodium coolant, J.Nuc. Mater 158 (1988) 159-165.

[52] D.E. Burkes, R.S. Fielding, D.L. Porter, Metallic fast reactor fuel fabrication for the global nuclear energy partnership, J. Nucl. Mater. 392(2) (2009) 158-163.

[53] V. Troyanov, V. Popov, I. Baranaev, Cermet fuel in a light water reactor: a possible way to improve safety. Part I. Fabrication and characterization, J. Nucl. Mater. 38(3-4) (2001) 267-270.

[54] G.L. Hofman, L.C. Walters, B.R.T. Frost, Dispersion Fuels, in: B.T. Frost (Ed.), Vol. 10A, Nuclear Materials, Materials Science and Technology, VCH Publishers Inc., New York, 1994.

[55] A.M. Savchenko, I. Konovalov, A.V. Vatulin, E.M. Glagovsky, New concept of designing Pu and MA containing fuel for fast reactors, J Nucl. Mater. 385(1) (2009) 148-152.

[56] D.S. Setty, K. Kapoor, N. Saibaba, Nuclear fuel cycle-developments and challenges in fuel fabrication technology in India, Progr. in Nucl. Energy 101 (2017) 100-117.

[57] H.S. Kamath, K. Anantharaman, D.S.C. Purushotham, A. Kakodkar, MOX fuel for the Indian nuclear power programme, MOX fuel cycle technologies for medium and long term deployment (Proc Symp Vienna, 1999), C&S Paper Series No, IAEA Vienna, 2000, pp. 190-199.

[58] S.C. Chetal, P. Chellapandi, Indian fast reactor technology: Current status and future programme, Sadhana 38(5) (2013) 795-815.

[59] T. Rajkumar, R. Clement, P. Puthiyavinayagam, P. Chellapandi, Influence of number of grooves in a mechanically bonded metallic fuel pin, Proceedings of the international conference on characterization and quality control of nuclear fuels, Hyderabad, 2012.

[60] C. Perumal, V. Balasubramaniyan, P. Puthiyavinayagam, R. Sundararajan, M. Kanakkil, P. Selvaraj, P.R.V. Rao, Design of 500 MWe Metal Fuel Demonstration Fast Reactor, 22nd International Conference on Nuclear Engineering, American Society of Mechanical Engineers, 2014 pp. V003T05A020-V003T05A020.

[61] J. Porta, C. Aillaud, S. Baldi, Core severe accidents with cermet fuels-A specific study for pressurized water reactors, 274(1-2) (1999) 174-180.

[62] A.A. Solomon, S.M. McDeavitt, V. Chandramouli, S. Anthonysamy, S. Kuchibhotla, T.J. Downar, Thoria-based cermet nuclear fuel: sintered microsphere fabrication by spray

drying, 10th International Conference on Nuclear Engineering, American Society of Mechanical Engineers, 2002, pp. 111-118.

[63] M. Bonnet, S. Baldi, J. Porta, Progress in core and cermet fuel modelling to calculate severe accidents, Progr. in Nucl. Energy 38(3-4) (2001) 387-390.

[64] Y.D. Baranaev, V.V. Popov, V.N. Sharapov, V.M. Troyanov, The feasibility of employing inert matrix ceramic fuels in a Russian light water reactor, J. Nucl. Mater. 319 (2003) 154-158.

[65] Vatulin A.V, Konovalov I.I, Advances in Powder Materials Processing, Powder Metallurgy Association of India 26 (1999) 32-39.

[66] IAEA Tecdoc1374, IAEA, September 2003.

[67] C. Haertling, R.J. Hanrahan Jr, Literature review of thermal and radiation performance parameters for high-temperature, uranium dioxide fueled cermet materials, J. Nucl. Mater. 366(3) (2007) 317-335.

[68] A.M. Savchenko, A.V. Vatulin, A.V. Morozov, I.V. Dobrikova, S.A. Ershov, S.V. Maranchak, Z.N. Petrova, Y.V. Konovalov, Inert matrix fuel with low melting point zirconium brazing alloys, J. Nucl. Mater. 352(1-3) (2006) 334-340.

[69] A. Savchenko, I. Konovalov, A. Vatulin, A. Morozov, V. Orlov, O. Uferov, S. Ershov, A. Laushkin, G. Kulakov, S. Maranchak, Dispersion type zirconium matrix fuels fabricated by capillary impregnation method, J. Nucl. Mater. 362(2-3) (2007) 356-363.

[70] A. Stanculescu, U. Kasemeyer, J.M. Paratte, R. Chawla, Conceptual studies for pressurised water reactor cores employing plutonium -erbium-zirconium oxide inert matrix fuel assemblies, J. Nucl. Mater. 274(1-2) (1999) 146-152.

[71] C. Degueldre, J.M. Paratte, Concepts for an inert matrix fuel, an overview, J. Nucl. Mater. 274(1-2) (1999) 1-6.

[72] Porta J., Dehaudt Ph, Aillaud C, “Inert Matrix Fuels: CERMET, Toward an Optimized Utilization of Pu in PWRs – Neutronic Studies and TANOX Experiment, TCM Fuel Cycle Options for LWR and HWR, IAEA, Victoria (Canada) 28 April-01 May 1999.

[73] C. Degueldre, Zirconia inert matrix for plutonium utilisation and minor actinides disposition in reactors, J. Allloys and Compds 444 (2007) 36-41.

[74] D. Haas, A. Fernandez, C. NÃ¤stren, D. Staicu, J. Somers, W. Maschek, X. Chen, Properties of cermet fuels for minor actinides transmutation in ADS, Energy Conv. and Manag. 47(17) (2006) 2724-2731.

[75] E. D'Agata, S. Knol, A.V. Fedorov, A. Fernandez, J. Somers, F. Klaassen, The behaviour under irradiation of molybdenum matrix for inert matrix fuel containing americium oxide (CerMet concept), J Nucl. Mater. 465 (2015) 820-834.

[76] S. Miwa, M. Osaka, T. Nozaki, T. Arima, K. Idemitsu, Oxygen potential of a prototypic Mo-cermet fuel containing plutonium oxide, J Nucl. Mater. 465 (2015) 840-842.

[77] J.O. Barrier, E.P. Coomes, P.E. Willi ford, L.A. Neimark, Cermet Fuels for space power systems, Symposium on Space Nuclear Power Systems, Albuquerque, New Mexico, January 13-16, 1986.

[78] S. Baldi, J. Porta, L. Zanotti, G. Rouvière, Advanced Reactors with Innovative Fuels Work shop Villigen, Switzerland 21-23 October 1998.

[79] V.P. Sinha, P.V. Hegde, G.J. Prasad, S. Pal, G.P. Mishra, Development of UO2/PuO2 dispersed in uranium matrix CERMET fuel system for fast reactors, J Nucl. Mater. 427(1-3) (2012) 12-17.

[80] D.D. Keiser Jr., M.A. Dayananda, Interdiffusion between U-Zr fuel and selected Fe-Ni-Cr alloys, Journal of Nuclear materials 200(2) (1993) 229-243.

[81] D.D. Keiser Jr., M.A. Dayananda, Interdiffusion between U-Zr fuel vs selected cladding steels, Metall. Mater.Trans. 25A(8) (1994) 1649-1653.

[82] D.D. Keiser Jr., M.C. Petri, Interdiffusion behavior in U-Pu-Zr fuel versus stainless steel couples, J.Nuc. Mater. 240(1) (1996) 51-61.

[83] R.L. Klueh, A.T. Nelson, Ferritic/martensitic steels for next-generation reactors, J. Nucl. Mater. 371(1-3) (2007) 37-52.

[84] D.R. Pedersen, L.C. Walters, ANL/CP-75696, Proc. Am. Power Conference, 1992.

[85] K. Huang, Y. Park, L. Zhou, K.R. Coffey, Y.H. Sohn, B.H. Sencer, J.R. Kennedy, Effects of Cr and Ni on interdiffusion and reaction between U and Fe-Cr-Ni alloys, J. Nucl. Mater. 451(1-3) (2014) 372-378.

[86] D.J. Hill, D.R. Pedersen, J.F. Marchaterre, Proceedings of the 23rd Intersociety Energy Conversion Engineering Conference,ASME, Denver, CO, 1988, p. p. 473.

[87] J.E. Cahalan, J.M. Kramer, J.F. Marchaterre, C.J. Mueller, D.R. Pedersen, R.H. Sevy, D.C. Wade, T.C.Y. Wei, Proceedings of International Topical Meeting on the Safety of Next Generation Power Reactors, ANS, Seattle, WA, 1988, p. p. 103.

[88] J.M. Kramer, Y.Y. Liu, M.C. Billone, H.C. Tsai, Modeling the behavior of metallic fast reactor fuels during extended transients, J Nucl. Mater. 204 (1993) 203-211.

[89] J.M. Kramer, Y.Y. Liu, M.C. Billone, H.C. Tsai, ANL/RE/CP-77809,1992.

[90] S. Kaity, T.R.G. Kutty, R. Agarwal, A. Laik, A. Kumar, Chemical compatibility of uranium based metallic fuels with T91 cladding, Nucl. Eng. Desg. 250 (2012) 267-276.

[91] T. Ogata, M. Kurata, K. Nakamura, A. Itoh, M. Akabori, Reactions between U-Zr alloys and Fe at 923 K, J. Nucl. Mater. 250(2-3) (1997) 171-175.

[92] T. Ogata, K. Nakamura, M. Kurata, T. Yokoo, M.A. Mignanelli, Reactions between U-Pu-Zr alloys and Fe at 923 K, J. Nucl. Sci.Tech 37(3) (2000) 244-252.

[93] A.B. Cohen, H. Tsai, L.A. Neimark, Fuel/cladding compatibility in U-19Pu-10Zr/HT9-clad fuel at elevated temperatures, J. Nucl. Mater. 204 (1993) 244-251.

[94] K. Nakamura, T. Ogata, M. Kurata, A. Itoh, M. Akabori, Reactions of U–Zr alloy with Fe and Fe–Cr alloy, J. Nucl. Mater. 275(3) (1999) 246-254.

[95] K. Nakamura, T. Ogata, M. Kurata, T. Yokoo, M.A. Mignanelli, Reactions of uranium-plutonium alloys with iron, J. Nucl. Sci.Tech 38(2) (2001) 112-119.

[96] C.T. Lee, H. Kim, T.K. Kim, C.B. Lee, Diffusion behavior in an interface between U–10Zr alloy and HT-9 steel, J Nucl. Mater. 395(1) (2009) 140-144.

[97] H.J. Ryu, B.O. Lee, S.J. Oh, J.H. Kim, C.B. Lee, Performance of FCCI barrier foils for U–Zr–X metallic fuel, J Nucl. Mater. 392(2) (2009) 206-212.

[98] C.W. Jacob, B.E. Warren, The crystalline structure of uranium, J. Am. Chem. Soc. 59(12) (1937) 2588-2591.

[99] D.L. Clark, S.S. Hecker, G.D. Jarvinen, M.P. Neu, Plutonium, The chemistry of the actinide and transactinide elements, Springer2008, pp. 813-1264.

[100] I.S. Golovnin, Properties of plutonium dioxide as nuclear fuel, Atomic Energy 89(2) (2000) 627-637.

[101] V.S. Yemel'Yanov, A.I. Yevstyukhin, The metallurgy of nuclear fuel: properties and principles of the technology of uranium, thorium and plutonium, Elsevier.

[102] H. Okamoto, L. Kacprzak, P.R. Subramanian, Binary alloy phase diagrams, ASM international1996.

[103] E.K. Storms, The refractory carbides Academic Press Inc1967, p. 171.

[104] R.N.R. Mulford, F.H. Ellinger, G.S. Hendrix, E.D. Albrecht, The plutonium-carbon system, Plutonium 1960, Proc. Int. Conf. on Plutonium Metal, E. Grison, WBH Lord and RD Fowler, 1960, pp. 301-11.

[105] M.G.A. Storms, E. K.. GRand,M .G., IAEA panel on Thermodynamic Properties of U-C, Pu-C and (U,Pu)-C Systems, Grenoble 1974.

[106] H. MATZKE, Science of Advanced LMFBR Fuels, Physics Publishing, North Holland, Amsterdam, 1986.

[107] H.A. Wriedt, The Pu-N (Plutonium-Nitrogen) System, Bull. Alloy Phase Diagrams 10(5) (1989) 593-602.

[108] F.H. Driggs, W.C. Lilliendahl, Preparation of Metal Powders by Electrolysis of Fused Salts, 22(5) (1930) 516-519.

[109] C.R. Clark, M.K. Meyer, Fuel powder production from ductile uranium alloys, 2lst International Conference on Reduced Enrichment for Research and Test Reactors, 1998.

[110] C.L. Trybus, M.K. Meyer, C.R. Clark, T.C. Wlencek, D.J. McGann, Design and fabrication of high density uranium dispersion fuels, Proc. 20th International Meeting on Reduced Enrichment for Research and Test Reactors Argonne National Lab., IL (United States), Jackson Hole, Wyoming, USA 1997.

[111] P. Chiotti, B.A. Rogers, The Production of Uranium and Thorium in the Powder Form, US Atomic Energy Commission, Technical Information Division1950.

[112] A. Lawley, Atomization: the production of metal powders, MPIF, 1992.

[113] W.D. Wilkinson, Uranium metallurgy, Interscience1962.

[114] P. Balakrishna, C.K. Asnani, R.M. Kartha, K. Ramachandran, K.S. Babu, V. Ravichandran, B.N. Murty, C. Ganguly, Uranium dioxide powder preparation, pressing, and sintering for optimum yield, J Nucl. Techn. 127(3) (1999) 375-381.

[115] M. Becker, Manufacture of uranium dioxide powder, Siemens AG, 1976.

[116] S.G. Brandberg, The conversion of uranium hexafluoride to uranium dioxide, Nucl. Tech. 18(2) (1973) 177-184.

[117] E.R. Irish, W.H. Reas, The Purex process-A solvent extraction reprocessing method for irradiated uranium, General Electric Co. Hanford Atomic Products Operation, Richland, Wash., 1957.

[118] O.L. Kruger, Preparation of PuC Pellets by Vacuum Sintering, Nucl. Appli. 1(4) (1965) 348-355.

[119] F. Anselin, G. Dean, R. Lorenzelli, R. Pascard, Carbides in nuclear energy, MacMillan, London, 1964, p. 113.

[120] F. Brown, P. Denard, P. Ellis, P.T. Good, L. R., Carbides in nuclear energy, MacMillan, London, 1964, p. 693.

[121] W.G. Tope, Production of plutonium mono carbide by reaction of elemental plutonium and carbon. ANL6969, 1965, p. 28.

[122] W.M. Pardue, V.W. Storhok, R.A. Smith, Properties of Plutonium mononitride and its alloys, pp 721-38 of Plutonium 1965. Proceedings of the Third International Conference on Plutonium, London, November 22--26, 1965. Kay, AE Waldron, MB (eds.). New York, Barnes and Noble, Inc., 1, Battelle Memorial Inst., Columbus, Ohio, 1967.

[123] Y. Suzuki, Y. Aral, T. Sasayama, Carbothermic synthesis of plutonium mononitride from the dioxide, J . Nucl. Mater. 115(2-3) (1983) 331-333.

[124] J.K. Tuli, Nuclear data sheets 103(3) (2004) 389-514.

[125] W.J. Maraman, W.D. McNeese, R.G. Stafford, Confinement Facilities for Handling Plutonium, Health Physics 29(4) (1975) 469-480.

[126] S.N. Dmitriev, Y.T. Oganessian, G.Y. Starodub, S.V. Shishkin, G.V. Buklanov, Y.P. Kharitonov, A.F. Novgorodov, Y.V. Yushkevich, D. Newton, R.J. Talbot, Ultra-pure 236Pu and 237Pu for environmental and biomedical research, Appl Radia & Istop 46(5) (1995) 307-309.

[127] J.G. Yevick, A. Amorosi, Fast reactor technology: plant design, MIT Press-The Massachusetts Institute of Technology1966.

[128] L.W. Brackenbush, K.R. Heid, W.N. Herrington, J.L. Kenoyer, L.F. Munson, L.H. Munson, J.M. Selby, K.L. Soldat, G.A. Stoetzel, R.J. Traub, Health physics manual of good practices for plutonium facilities., Pacific Northwest Lab., Richland, WA (USA), 1988.

[129] H.J. Ryu, S.Y. Lee, J.H. Kim, Y.M. Woo, Y.M. Ko, K.H. Kim, J.M. Park, C.B. Lee, Fabrication of particulate metal fuel for fast burner reactors, IAEA.INIS, 2012.

[130] W.C. Bell, R.D. Dillender, H.R. Lominac, E.G. Manning, Vibratory compacting of metal and ceramic powders, J.Am.Cer.Soc. 38(11) (1955) 396-403.

[131] R.K. McGeary, Mechanical packing of spherical particles, J.Am.Cer.Soc. 44(10) (1961) 513-522.

[132] W.M. Pardue, F.A. Rough, R.A. Smith, Nuclear Metallurgy, American Institute of Mining, Metallurgy and Petroleum Engineers, New York, 1969.

[133] B.D. Zope, V.K. Moorthy, GOVERNMENT OF INDIA ATOMIC ENERGY COMMISSION, BARC, Bombay, 1970.

[134] D. Olander, Nuclear fuels-present and future, J.Nucl.Mater. 389(1) (2009) 1-22.

[135] O.J. Wick, Plutonium handbook: a guide to the technology, Gordon and Breach1967.

[136] P.A.F. White, S.E. Smith, Inert Atmosphere in Chemical, Metallurgical and Atomic Energy Industries, Butterworths, London, 1962.

[137] C.Y. Ho, R.E. Taylor, Thermal expansion of solids, Vol. 4, ASM international1998.

[138] J.D. James, J.A. Spittle, S.G.R. Brown, R.W. Evans, A review of measurement techniques for the thermal expansion coefficient of metals and alloys at elevated temperatures, Measurement Scie. and Tech. 12(3) (2001) R1.

[139] D. Zhao, X. Qian, X. Gu, S.A. Jajja, R. Yang, Measurement techniques for thermal conductivity and interfacial thermal conductance of bulk and thin film materials, J.Electronic Packaging 138(4) (2016) 040802.

[140] M. Gustavsson, E. Karawacki, S.E. Gustafsson, Thermal conductivity, thermal diffusivity, and specific heat of thin samples from transient measurements with hot disk sensors, AIP1994.

[141] H. Disk, Instruction manual, hot disk thermal constants analyser,Software Version 5.9. p 42, 2007.

[142] W.J. Parker, R.J. Jenkins, C.P. Butler, G.L. Abbott, Flash method of determining thermal diffusivity, heat capacity, and thermal conductivity, J.App.Physics 32(9) (1961) 1679-1684.

[143] A.K. Sengupta, S. Majumdar, C. Ganguly, D.S.C. Purushotham, P.R. Roy, Determination of some important thermophysical properties of (U/sub 0.3/Pu/sub 0.7/) C fuel, American Ceram.Societ.Bulliten 65(7) (1986) 1057-1059.

[144] H.J. Lee, R.E. Taylor, Thermal diffusivity of dispersed composites, J.App.Physics 47(1) (1976) 148-151.

[145] T.Y.R. Lee, R.E. Taylor, Thermal diffusivity of dispersed materials, J. Heat Transfer 100(4) (1978) 720-724.

[146] A.R. West, Solid state chemistry and its applications, John Wiley & Sons2007.

[147] B.D. Cullity, Answers to problems: elements of X-ray diffraction, Addison-Wesley Publishing Company1978.

[148] H. Hausner, J. Zambrow, Powder metallurgy of uranium, Nuclear engineering and Science Congress, American Institute of Chemical Engineers, Cleveland, 1955.

[149] A. Taskinen, Dislocation density in carbonyl nickel during sintering, 15(9) (1980) 2253-2257.

[150] D.C. Crawford, S.L. Hayes, M.K. Meyer, Current US plans for development of fuels for accelerator transmutation of waste, IAEA TECDOC 1356, 2003, p. 151.

[151] W.J. Carmack, D.L. Porter, Y.I. Chang, S.L. Hayes, M.K. Meyer, D.E. Burkes, C.B. Lee, T. Mizuno, F. Delage, J. Somers, Metallic fuels for advanced reactors, J.Nuc. Mater 392(2) (2009) 139-150.

[152] International Atomic Energy Agency, IAEA TECDOC 1496, 2006.

[153] S. Kaity, J. Banerjee, M.R. Nair, K. Ravi, S. Dash, T.R.G. Kutty, A. Kumar, R.P. Singh, Microstructural and thermophysical properties of U–6wt.% Zr alloy for fast reactor application, Journal of Nuclear Materials 427(1) (2012) 1-11.

[154] V.P. Sinha, P.V. Hegde, G.J. Prasad, S. Pal, G.P. Mishra, Development of UO_2/PuO_2 dispersed in uranium matrix CERMET fuel system for fast reactors, J.Nuc. Mater 427(1-3) (2012) 12-17.

[155] C. Ganguly, D. Vollath, KFK-2049, Sept. 1974.

[156] A.T. Chapman, R.E. Meadows, Contract No. W-7405-eng-26, ORNL-3587, 1964.

[157] IAEA, Research Reactor Core Conversion Guidebook, Volume 4: Fuels (Appendices I-K), IAEA TECDOC-643, 1992.

[158] R.D. Cowan, Pulse method of measuring thermal diffusivity at high temperatures, J.Appl.Phys. 34(4) (1963) 926-927.

[159] I. Barin, Thermo chemical data of pure substances, VCH Verlagsgesellschaft mbh., D-69451 Weinheim, Federal Republic of Germany, 1995.

[160] M.V. Krishnaiah, G. Seenivasan, P.S. Murti, C.K. Mathews, Thermal conductivity of selected cermet materials, J. Allloys and Compds 353(1-2) (2003) 315-321.

[161] Irish E.R., Read W.H., The PUREX PROCESS,HW-49483, 1957.

[162] Powder Metal Technologies and Applications, ASM International Ohio Metals Handbook, 1998.

[163] R.N.R. Mulford, F.H. Ellinger, G.S. Hendrix, E.D.Albrecht, Plutonium 1960, Cleaver-Hume Press, London, 1961.

[164] T. Matsui, R.W. Ohse, EUR 10858 EN, Commissions of European Union Communities, Luxembourg, 1986.

[165] I. Casas, J. de Pablo, Contract No. 295722, FIRST-Nuclides, European Commission Community Research., 2013.

[166] D.E. Peterson, E.M. Foltyn, The Pu-U (Plutonium-Uranium) system, Bull. Alloy Phase Diagram 10(2) (1989) 160-164.

[167] D. C. Crawford, S. L.Hayes, M. K.Meyer, IAEA TECDOC-1356, 2003, pp. 151-163.

[168] T. Nishi, Y. Arai, M. Takano, M. Kurata JAEA-Data/Code -001, 2014, pp. 1-56

[169] H. Okamoto, P.R. Subramanian, L. Kacprzak, Binary Alloy Phase Diagrams, Second Edition ASM International,1990.

[170] L. Leibowitz, R.A. Blomquist, A.D. Pelton, Thermodynamics of the uranium-zirconium system, J.Nuc. Mater. 167 (1989) 76-81.

[171] T.B. Massalasksi, Binary phase Diagrams, 2nd edition, American Society of Metals,1990

[172] K. Nakamura, T. Ogata, M. Kurata, A. Itoh, M. Akabori, Reactions of U-Zr alloy with Fe and Fe-Cr alloy, J.Nuc. Mater. 275(3) (1999) 246-254.

[173] H. Okamoto, Cr-U (Chromium-Uranium), J. of Phase Equilibria Diffusion 33 (2012) 495.

[174] R.W. Cahn, P. Hassen, E.J. Kramer, Materials Science Technology,Vol. 10 A,VCH (1993) 32.

[175] A.K. Sengupta, R.K. Bhagat, A. Laik, G.B. Kale, T. Jarvis, S. Majumdar, H.S. Kamath, Out-of-pile chemical compatibility of Pb-Bi eutectic alloy with Graphite, Int. J. Mater. Res. 97(6) (2006) 834-837.

[176] K. Huang, Y. Park, A. Ewh, B.H. Sencer, J.R. Kennedy, K.R. Coffey, Y.H. Sohn, Interdiffusion and reaction between uranium and iron, J.Nuc. Mater. 424(1-3) (2012) 82-88.

[177] J.R. McLaren, M.C. Regan, H.J. Hedger, Carbides in Nuclear Energy, Macmillan and Co. Ltd., London, 1963.